A Study of Edge-Localized Mode Control with Resonant Magnetic Perturbation Fields

Inaugural-Dissertation

zur

Erlangung des Doktorgrades der
Mathematisch-Naturwissenschaftlichen Fakultät
der Heinrich-Heine-Universität Düsseldorf

vorgelegt von
Jonathan Robert Pearson
aus Huddersfield, England

August 2013

Aus dem Institut für Energie- und Klimaforschung - Plasmaphysik (IEK-4)
des Forschungszentrum Jülich GmbH

Gedruckt mit der Genehmigung der
Mathematisch-Naturwissenschaftlichen Fakultät der
Heinrich-Heine-Universität Düsseldorf

Referent: Prof. Dr. U. Samm
Korreferent: Prof. Dr. K.-H. Spatschek

Tag der mündlichen Prüfung: 21-10-2013

Contents

1 Introduction

Magnetically Confined Nuclear Fusion

Research into efficient but environmentally low impact power sources is essential to keep up with the increasing demand for energy and decreasing fossil fuel supplies. Extracting energy from fusion reactions has many advantages as a future energy source over the current methods. The energy density is extremely high in the fusion fuel; in fact for each kilogram of Deuterium-Tritium, 3×10^8MJ of energy is available (1 kg of coal $\sim$ 30 MJ). The reactants are abundant; Deuterium can be extracted from many sources such as electrolysis of sea water, and Tritium can be produced from neutron bombardment of Lithium, which could take place as a secondary reaction in the wall of a fusion device. The reaction is inherently safe as there is no possibility of chain reactions occurring and the waste produced is inert. The device which contains the reaction will become radioactive over the course of its lifetime due to highly energetic neutrons, but the isotopes created have a relatively small half-life compared to the current waste created by Fission reactors.

Thermonuclear fusion is the process of fusing light nuclei together under high temperature conditions to form heavier nuclei. Large amounts of excess energy are produced from this reaction as the heavier nuclei have a higher binding energy. This is the same process which occurs in the sun, where it is primarily a slow reaction between protons [1]. However, in the laboratory, the fusion of deuterium and tritium is a more practical reaction with a high energy yield and large cross section.

$$D^2 + T^3 \rightarrow He^5 \rightarrow He^4 + n^1 + 17.6\,\mathrm{MeV}, \tag{1.1}$$

where most of the energy ($\sim$ 14.1 MeV) is carried away by the neutron. It is very difficult to form a self-sustaining reaction under such high temperatures as the plasma naturally attempts to diffuse. The Lawson criterion [2] gives the conditions needed to create a self sustaining reaction, dubbed "ignition",

$$n\tau_E > \frac{12T}{\langle \sigma v \rangle \, \epsilon_\alpha}. \tag{1.2}$$

Here, τ_E is the confinement time, $\langle \sigma v \rangle = 1.1 \times 10^{-24}\mathrm{T}^2\mathrm{m}^2\mathrm{s}^{-1}$ is the reaction cross section averaged over a Maxwellian distribution of the positive ions in the plasma, ϵ_α is the energy of an alpha particle, and n and T are the density and temperature of the plasma, respectively. This criterion predicts that, for a temperature $\approx 20keV$ ($\sim 200 \times 10^6$K), ignition occurs when

$$n\tau_E T > 3 \times 10^{21} sm^{-3} keV. \quad (1.3)$$

This is called the fusion triple product.

In the laboratory, either an extremely high density or a long confinement time is required to meet this condition. Inertial confined fusion (ICF) compresses a high density fuel to a few thousand times the density of liquid hydrogen, in order to create the required conditions for fusion. This process is then repeated for a large number of very short reactions, analogous to a combustion engine. Alternatively, magnetic confinement fusion (MCF) meets this condition by forming a moderate density stable plasma, allowing for longer confinement times. However, for moderate density plasmas, the mean free path of the particles will be relatively long and most of the energy will be lost to the walls of the containing device in which the reaction occurs. Therefore, the main challenge is to create a device which can confine the high temperature plasma for long enough and then extract the useful energy.

In a magnetic field, charged particles have a gyro-orbit around the magnetic field lines. A magnetic bottle uses this principle to confine the plasma by creating a linear magnetic field produced by a set of coils with a much stronger field at each end (so the magnetic field lines converge at either end like a bottle), causing the particles to "bounce" between the two ends. At high energies, such as needed in thermonuclear fusion plasmas, particles will leak from each end of the bottle. By wrapping the linear field into a torus, so the two ends connect creating a continuous loop, leakage from the ends is no longer a problem. The geometry of the magnetic field in the torus can be described in terms of toroidal (long way around the torus), poloidal (short way around), and finally radial components.

Unfortunately, particles in this configuration will be prone to curvature effects and an $\mathbf{E} \times \mathbf{B}$ drift of the guiding centre, i.e. the point which the particles oscillate around. This drift occurs when an electric field is perpendicular to a magnetic field and the resultant drift is perpendicular to both of these fields. The electric field is created by the net charge difference due to the separation of ions and electrons within the changing magnetic field. If the particles are given a rotational transform, through the combination of poloidal and toroidal fields, then a helical path is created around the torus as seen in figure 1.1, so that the drifts and effects of curvature are averaged out. This is the fundamental idea behind most magnetic confinement devices.

The tokamak is one such MCF device, first suggested by Tamm and Sakharov [3] in the early 1950s. A toroidal field is produced by a set of external poloidal coils placed uniformly around the torus. A poloidal field is created by inducing a current in the plasma through a transformer, using the plasma like a secondary winding. This field, when superimposed upon the existing toroidal field, will create the required helical path, figure 1.2 (left). Consequently, the basic design and construction is relatively simple,

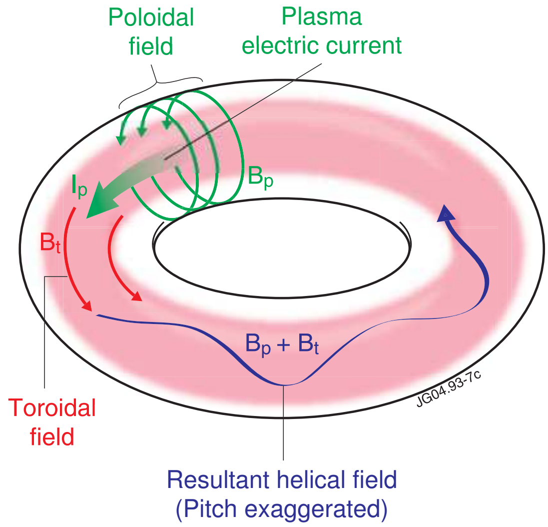

Figure 1.1: *The resultant helical path in a torus can be created by a combination of poloidal and toroidal fields. Diagram courtesy of JET-EFDA.*

although the physical understanding becomes complex as additional instabilities are driven by the plasma reluctance to the helical structure and the current induced in the plasma from the transformer.

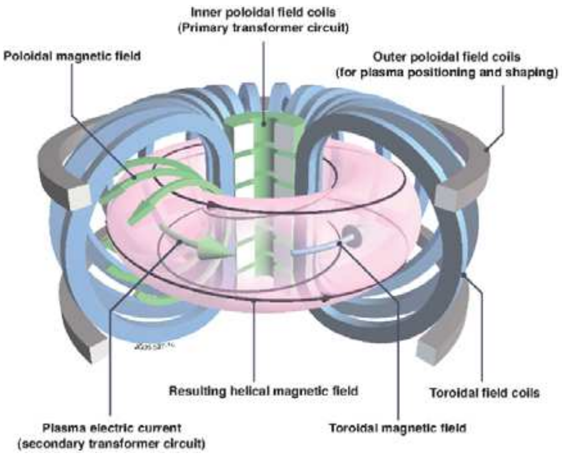

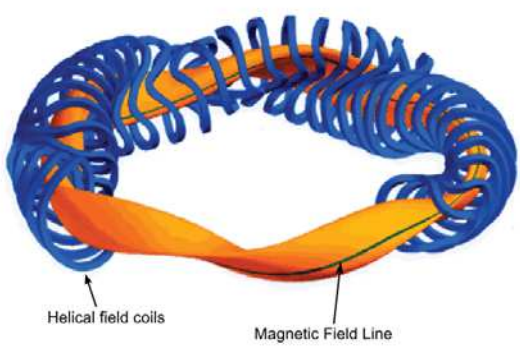

Figure 1.2: *Two schematics showing the principal idea behind a tokamak (left) and a stellarator (right). The tokamak is a simpler construction as the magnetic coils have a uniform design, but the stellarator is a more natural configuration for the plasma and so has less instabilities. Diagram courtesy of JET-EFDA.*

A common alternative is the stellarator, also suggested in the early 1950s [4], but this has had considerable less research conducted on it due to the difficulty of the engineering, figure 1.2 (right). Unlike the tokamak, the stellarator does not induce a current in the plasma, instead it generates the rotational transform purely through currents in the external coils. This requires that either the torus itself be deformed into a figure of eight or the confining coils be designed as twisting helical coils.

Here, the focus of the work is on the tokamak design.

The Bootstrap Current and Confinement

For a stable equilibrium, any confinement losses in a tokamak will be due to Coulomb collisions which are easily calculated and mainly depend on the mean free time between collisions called the "collisionality". However, the actual particle transport from the confined region is approximately double of that calculated from Coulomb collisions alone. This is due in part to neoclassical transport caused by "trapped" particles in the plasma, and instabilities.

Trapped particles have a relatively low energy and thus can become stuck in regions of low magnetic field. As the helical path traverses in both toroidal and poloidal directions the particles will encounter a higher field on the inboard side than the outboard side of the torus, due to the magnetic field produced by the transformer current having an inverse dependence to the radius. Thus, the inboard and outboard sides are called the high field side (HFS) and low field side (LFS), respectively. Particles with a high enough energy not to become stuck are called passing particles. The trapped particles will then bounce in the low magnetic field region, similar to the magnetic bottle effect. These are said to have "banana" orbits due to the particle having alternative displacements depending on the direction of the $\nabla\mathbf{B}$ drift relative to the particle velocity, as seen in figure 1.3.

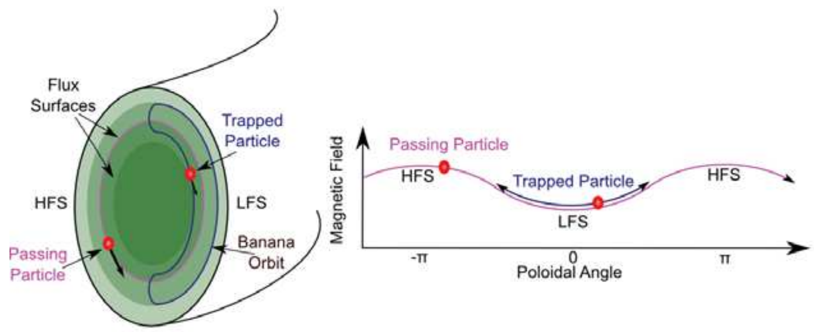

Figure 1.3: *The trapped particle is forced to stay on the low field side (blue orbit), with similar principles as the magnetic bottle, whilst the passing particles can follow the magnetic field lines all the way round (pink orbit).*

The interaction of the passing and trapped particles, and the interaction of the trapped particles in different banana orbits, produce an additional current called the "bootstrap" current [5, 6]. This is created in low collsionalities as the formation of banana orbits is reduced as particle collisions increase. The bootstrap current arises through a transfer of momentum from the passing particles to the trapped ones, especially between the passing electrons and trapped electrons and ions. Widely used expressions for the bootstrap current and neoclassical resistivity can be found in reference [7] which will be used later in chapter 5.

Plasma instabilities often cause transient breaches of the confinement, increasing the radial transport out of the plasma and thus degrade the confinement. Any magnetic confinement device will have to deal with the problem of particles escaping confinement, whether through leakage or instabilities, and their interaction with the plasma facing components.

A confined plasma is prone to a large variety of instabilities; here the focus will be mostly on magneto-hydrodynamic (MHD) modes. These can be characterised by their poloidal, m, and toroidal, n mode numbers, where a mode with $m = 2$ and $n = 1$ goes round once in the poloidal direction and twice in the toroidal direction before meeting itself. A useful parameter to define here is the safety factor, q, which denotes the number of times a magnetic field line goes around toroidally for each time it goes around poloidally. This is the inverse of the rotational transform and is so called as at low values, there is a higher risk of current driven instabilities. Surfaces in the plasma where $q = m/n$ is an integer are called rational surfaces and will be widely discussed in this study as they often have the largest interactions. The value of q in a tokamak ranges from near unity in the core to between 2 and 6 at the edge, although theoretically q can go to ∞ for divertor configurations (see below).

The surface separating the confined plasma region, with closed magnetic field lines (i.e. ones which wrap around on themselves to form a continuous loop), from the unconfined region, with open field lines (i.e. ones which will meet the chamber wall before themselves), is the last closed flux surface (LCFS). Outside the LCFS is a region where particles are removed called the scrape off layer (SOL), figure 1.4. Since the first wall will incorporate various structures, including diagnostic ports and heating antenna, the escaping particles need to be focused into controlled areas which can manage the high heat and particle fluxes. Originally, a limiter device was used, which is basically a barrier inserted close to the plasma edge to catch the particles before they reach the wall. This has many disadvantages, as being so close to the plasma means interacting particles will have high temperatures and velocities causing erosion of the limiter surface allowing impurities to enter the plasma as ash.

An alternative to the limiter is to include a divertor [8]. The transport of particles along the field lines is much greater than the transport across them. This means that if the open field lines are redirected using additional magnetic fields to specialised plates some distance away from the plasma, the particles can be focused to specific regions. To do this the divertor creates a X-point in the magnetic field, separating the confined field lines and those which will leave the plasma. The field line that is the first radially to be redirected by the X-point is known as the separatrix. A divertor configuration has the main advantage that the particles have more time to cool; so the thermal loads on the divertor plates are greatly reduced compared to the limiter design. Other advantages include: impurity levels in the plasma are much lower than the limiter case, due to impurities becoming ionised and flowing back to the divertor before reaching the plasma; the particles can cool enough to recombine creating a neutral cloud above the divertor further protecting the materials; and vacuum pumping of the divertor can remove helium ash which would otherwise cool the plasma. The most successful divertor design is a toroidally symmetric divertor. More advanced configurations are also being researched such as the "snowflake" divertor [9] which uses a second order X-point to spread the heat load over a broad area of the divertor plates.

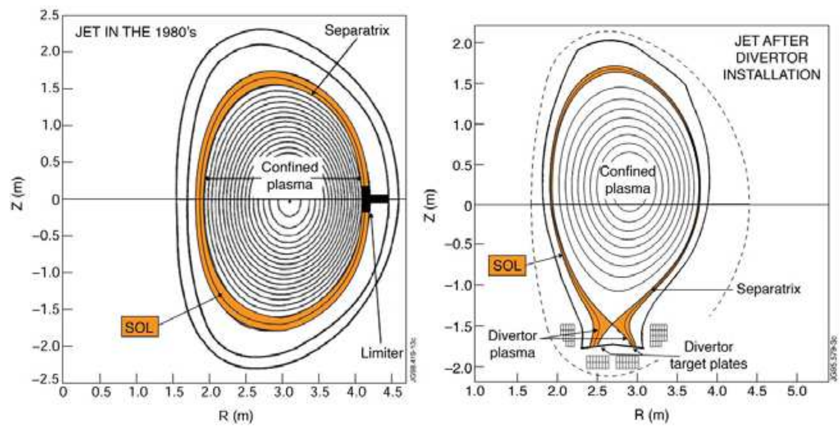

Figure 1.4: *Poloidal cross sections of the confined plasma in the joint European tokamak showing a limiter configuration (left) and a divertor configuration (right). The area affected by limiter and divertor is highlighted as the scrape off layer. Diagrams courtesy of JET-EFDA.*

The Appearance of Edge Localized Modes in the High Confinement Mode

In 1982 experiments on the ASDEX tokamak made a serendipitous discovery, that during the application of neutral beam injection heating, a transition to a high confinement mode (H-mode) was obtained under certain conditions [10]. The confinement time became approximately twice that of the normal low confinement mode (L-mode) and has since been confirmed on a large range of other devices. In the H-mode, steep gradients in the pressure, temperature and density are formed at the edge of the plasma, which are schematically shown compared against L-mode profiles in figure 1.5. The steep gradients in these profiles create a pedestal at the plasma edge, which can be thought of as a transport barrier, and is the reason for the increase in the confinement. Unfortunately, the formation of this barrier is still not fully understood; the leading theory suggests that an increase in the radial electric field shear decorrelates the plasma turbulence and thus reduces the particle diffusivities.

In addition to the increase in confinement, a new set of explosive instabilities called edge localized modes (ELMs) [11] appear, driven in the H-mode by the free energy stored in the high gradients at the plasma edge.

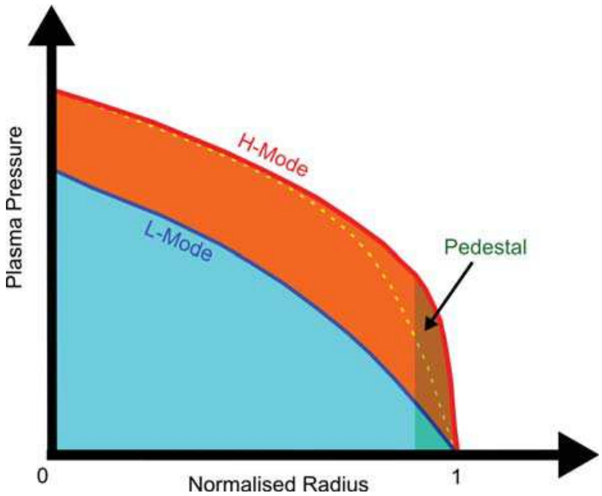

Figure 1.5: *Schematic example of the plasma pressure profile across the normalised minor radius for the high and low confinement modes. The highlighted region at the edge of the plasma is known as the pedestal and creates a transport barrier. Similar pedestals are created in the temperature and density profiles. After an ELM crash the plasma pressure will relax to the dotted yellow line releasing the difference in edge pressure as free energy.*

ELMs cause fast ($\sim 0.3 - 1\,\mathrm{ms}$) quasi-periodic collapses of the high confinement mode plasma pedestal, resulting in a loss of energy confinement and an increase in the radial transport across the plasma edge. Each ELM is characterised by an increase in the radiation shown in the D_α line emissions (interaction of the plasma with the surrounding neutrals creates radiation from the Balmer-Alpha series) and a burst of magnetic activity. The increase in D_α indicates an increase in edge recycling and can be used to give a measurement of the inward particle flux. These events can lead to large transient heat and particle loads on the plasma facing components as well as reducing the pedestal energy confinement by $\sim 10 - 20\%$. However, it should be noted that these events also act to clean the plasma of impurities. Hence a complete understanding of the mechanism behind the ELM and how to control such events is required for future magnetically confined fusion devices.

The research of ELMs is also of high interest generally, as it involves both linear and non-linear relaxations, requires knowledge of microscopic and macroscopic processes in a volatile plasma with a large magnetic field, and includes high dimensional effects such as turbulence and 3-dimensional distortions. This understanding enhances similar research into the mechanisms occurring at the edge of stars, for example solar flares.

Mitigation of Edge Localized Modes

Using results from various devices, an extrapolation of the heat and particles deposited on the wall components has been carried out for the next step fusion device, ITER [12]. Since the exact physics and scaling is unknown, the predicted ELM energy loss ranges from 5 to 22 MJ. It is expected that approximately half of this energy will reach the wall and be deposited over a region of $\sim 1\,\mathrm{m}^2$, known as the wetted area . Thus, the surface energy density is suggested to be $2.5 - 11\,\mathrm{MJm}^{-2}$ which is ~ 20 times higher than acceptable for the planned first wall components, primarily made of tungsten or carbon fibre composites, which can receive a maximum of $0.5\,\mathrm{MJm}^{-2}$. Therefore, it is important to find mitigation/suppression solutions for ELMs or develop materials for the plasma facing components which are better suited to withstand the high energy and particle loads.

Operational regimes which have naturally small or even no ELMs have been created by advanced plasma shaping and control of the edge stability. Unfortunately, these regimes differ between devices and are only found in small parameter spaces. A range of techniques to control the ELMs have been investigated, that either aim to control the triggering of the ELMs or attempt to remove the events completely. Pellet injection [13] and fast vertical kicks [14] to the plasma quickly destabilise ELMs in order to increase their frequency (assuming an inverse relation to energy loss per ELM). Alternatively, the application of non-axisymmetric external fields [15, 16, 17] or the induction of a toroidal ripple [18] to the plasma edge have been conducted, focusing on maintaining high confinement parameters while affecting the plasma stability continuously. A very good recent overview of the ELM control strategies can be found in reference [19].

In this study, the focus will be on resonant magnetic perturbations (RMPs) created through externally applied fields as an ELM control technique. It has been known for a long time that the edge of a tokamak plasma is highly sensitive to external magnetic fields. Some of the earliest work in this area was conducted to understand and compensate for “error fields” in a tokamak. All tokamaks are prone to error fields mainly due to imperfections and misalignment of the magnetic field coils. These static, helical fields, although only of the order $\boldsymbol{B_0}/\delta B \sim 10^{-4}$, can create non-rotating magnetic islands in the plasma called “locked modes”. Subsequently, this gives rise to the possibility of plasma disruptions, which will be extremely harmful for large plasma devices. The breaking of the coil current symmetry, caused by the error fields, creates low m, n modes. Therefore, additional magnetic coils are used to compensate the error fields by applying non-axisymmetric magnetic fields to the plasma. This research is the foundation required for the current understanding of controlling the plasma with additional magnetic fields.

RMPs are the resonant component of externally applied fields which induce perturbations on associated rational surfaces. When a perturbation is present with multiple helicities, then each equivalent rational surface will be affected forming a chain of magnetic islands through magnetic reconnection. This is a process where magnetic field lines break and immediately reconnect in a new configuration, as according to Gauss' law of magnetism, magnetic monopoles do not exist and so all field lines must be continuous. If the perturbation is large then these island chains will grow to a point where they interact with each other. In this case the magnetic field lines in the region of interaction become more random and have an increased radial deviation. A Poincaré plot of such a situation would show the field lines filling up the region rather than returning to one point as in the case within a laminar zone. This "filling" is called ergodization and will cause a large increase in the radial transport across the interaction region. Therefore the application of RMPs is expected to create a stochastic layer at the plasma boundary allowing the particles a short cut in radial transport through the parallel transport along the random field lines. However, it should be noted that in principle only special magnetostatic equilibria, such as Beltrami fields, have $\nabla \times \boldsymbol{B} = \mu \boldsymbol{B}$ with μ a uniform constant which would be a requirement for ergodic fields. Thus, the question of stochastization at the plasma edge is still being debated. RMPs are mainly applied through additional sets of magnetic coils although recently on the EAST tokamak a technique has been discovered that created RMPs through lower hybrid current drive [20].

The first observations of large ELM suppression were seen on the DIII-D tokamak [17, 21, 22] where RMPs were applied using a set of in-vessel coils, to a H-mode plasma, in order to create a stochastic boundary layer. This showed that a stochastic layer has a large effect on the ELMs but with little significant change in the radial transport barrier or the electron pedestal profile i.e. only moderate degradation in confinement observed. Many other devices have used in-vessel coils in attempts to control magnetohydrodynamic instabilities. Complete suppression of the largest ELMs was observed on KSTAR [23] while there was strong mitigation on AUG [24] and COMPASS-D [25]. Triggering of ELMs by RMPs has been reported on JFT-2M [26] and NSTX [27, 28]. A large advantage of using internal coils is that a higher localisation of the perturbation to the plasma can be achieved, allowing the perturbations to be more aligned with the resonant surfaces in the plasma. Also with the in-vessel coils being closer to the plasma larger near field effects are present as the magnetic fields decay at $1/r^{m+1}$. Additionally, if an alternating current (AC) RMP field is applied by external coils, the resistive wall time needs to be taken into account as the fields not only have further to travel, but also have more metallic structures to pass through before affecting the plasma.

Currently, it is thought that future fusion devices are unable to have in-vessel coils as these will not cope with the material stresses and create design difficulties for the vessel. The joint European tokamak (JET) applies RMPs through the external error field correction coils. Although full suppression was not observed, the feasibility of using external coils was proved as strong ELM mitigation was seen [29, 30, 31]. A drop in the edge density was observed simultaneously, the so-called "pump out" effect. Recently it has been shown that additional puffing of gas into the plasma edge can compensate for this effect [32]. The MAST tokamak has both internal and external coils and has also observed ELM mitigation [33, 34, 35, 36], making it a useful device for the comparison of these two application methods.

Even with so many experimental successes, the understanding of how the RMPs affect the ELMs is still far from complete. Observations vary strongly from one machine to another, so creating a universal theory is complicated. Considering the previous work, several questions arise concerning the application of RMPs to a plasma with ELMs, which this thesis will focus on:

- Do the resonant magnetic perturbations affect the edge localized modes through changes in the transport or stability?
- Which parameters are key for the ELM control?

The problem of ELMs in tokamaks is not only a highly important field to research but also immensely interesting. The extent of the complications in terms of experimental results and modelling will be outlined in chapter 2 along with a brief overview of the current research conducted into ELM control through RMPs. In this study, the concentration will be on attempting to understand a focused area in this field by looking to a current driven mode as the cause for some interesting features of the ELMs, and on how helical RMPs applied to the TEXTOR tokamak affect the plasma. The modelling tool used to achieve this is a peeling initiated current relaxation model, representing an ELM driven by peeling modes formulated and outlined in chapter 3. In chapter 4 the TEXTOR tokamak will be introduced as well as several of its features. The identification and interpretation of ELMs on TEXTOR will be described and then used to investigate the effect of applying rotating resonant magnetic perturbations. Chapter 5 then compares the current relaxation model to experimental results from the JET and TEXTOR tokamaks in order to explain a multi-resonant feature in the ELM frequency dependence on the edge safety factor observed in ELM control experiments on JET [37], and how that dependence appears on TEXTOR. Finally chapters 6 and 7 present a discussion and a summary of the main new findings, respectively.

2 The Problem of Edge-Localized Modes in Tokamaks

The study of ELMs is both a complex and wide area of research due to the large number of experimental results and theories in the field. This chapter gives an overview of the current understanding and on-going research into ELMs in order to allow the reader to set the work investigated in this thesis in the correct context.

Understanding Edge Localized Modes

Edge localized modes have been studied on a wide range of tokamaks including: Alcator C-MOD [38], ASDEX-U [39], COMPASS-D [40], DIII-D [41], EAST [42], JET [43], JFT-2M [44], JT-60U [45, 46], MAST[47], NSTX [48], TCV [49], and TEXTOR [50]. The magnetic fluctuations, short time scales of the ELM growth, and proximity of the plasma to an MHD stability limit when an ELM occurs, all point towards MHD being able to explain the ELM onset. The phenomenology varies depending on size and shape of the plasma making it necessary to distinguish between different types of ELM. Connor, Suttrop and Zohm [51, 52, 53] have summarised these observations and attempted to create a classification of which the main points will be outlined here.

Three main criteria are used to classify ELMs: the dependence of ELM repetition frequency on the heating power (the energy flux through the separatrix), occurrence of magnetic precursors, and MHD stability analysis, although reference [53] argues that this third criteria is insufficient across different machines. The largest and most dangerous ELMs are called type-I and appear as sharp bursts in the D_α signal seen in figure 2.1, labelled Large ELMs. These events occur in regimes which have good confinement but expel a large amount of energy. The repetition frequency of type-I ELMs is $\sim 10 - 100\,\mathrm{Hz}$ which increases with heating power. On the MAST tokamak a delay was found between the D_α signal and the ion saturation peaks associated with the type-I ELM events, measured using a reciprocating Langmuir probe. This delay time increases with the distance of the probe from the plasma allowing a calculation of the approximate speed of the released particles, $\sim 750\,\mathrm{ms}^{-1}$ [54, 55]. There is no clear magnetic precursor for type-I ELMs. An MHD stability analysis shows that these events fall on a constant pressure as seen in figure 2.1; this suggests a pressure driven instability being dominantly responsible.

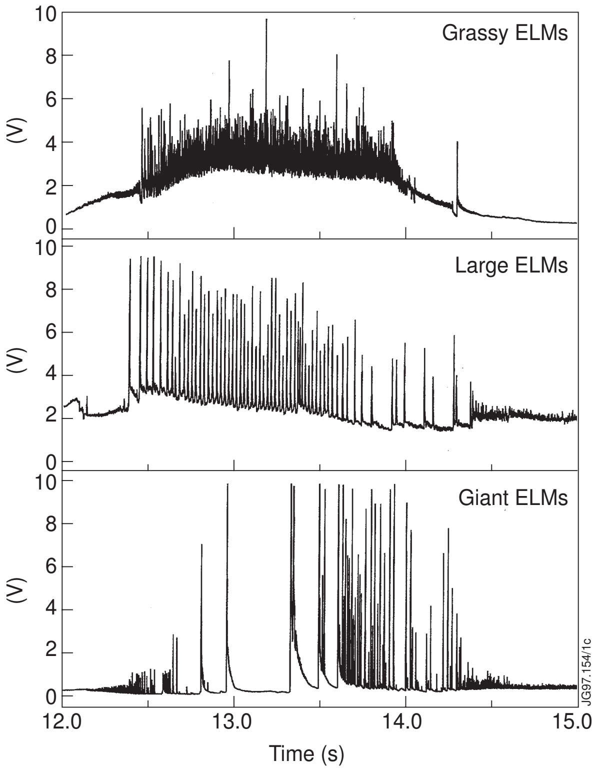

Figure 2.1: *Three different types of ELMs observed on the JET tokamak measured by the voltage increase on the divertor plates. Grassy ELMs or type-II ELMs have a noisy behaviour and so are difficult to analyse. The large ELMs shown are likely to be type-I with regular crashes. The giant ELMs are usually due to ELM free periods just before an ELM crash allowing the pedestal to build substantially and are often seen to have multiple crashes. Diagram courtesy of JET-EFDA.*

Another common type of ELM is the type-III group which are associated in plasmas with a lower confinement than the type-I ELMs. These appear in two areas of figure 2.2, one at high density and low temperature, the other at low density and high temperature. In general type-III ELMs appear just after the L-H transition and then disappear as the confinement increases until type-I ELMs appear. The repetition frequency of type-III ELMs decreases with increased heating power and these often have a clear magnetic precursor with $n \sim 5 - 10$, $m \sim 10 - 15$ and a frequency much higher than type-I.

Other ELM types are less common. Type-II or “grassy” ELMs were observed on ASDEX and JT-60U [46] with a repetition frequency up to 15 times higher than type-I ELMs but with similar pedestal characteristics. Overall these events release a much smaller amount of energy making them suitable for steady state operation. However, the parameter space for these ELMs is very small, associated with strong plasma shaping, a high edge safety factor, and high rotation. The MHD stability analysis shows these ELMs to occur between the first and second stable regions (see ballooning section below)

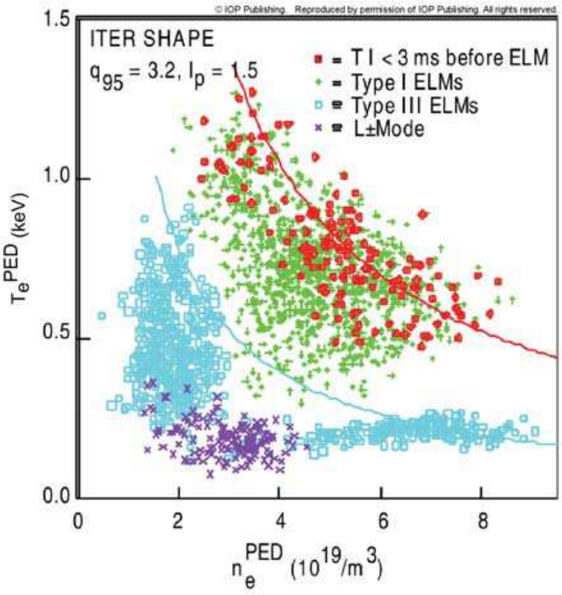

Figure 2.2: *Pedestal characteristics of different types of ELMs. Two regions of type-III ELMs can be seen at high and low density. Approximate boundary conditions for type-I and type-III ELMs have also been plotted [52].*

explaining the small parameter window. Dithering ELMs occur when the plasma is close to the L-H transition and thus the plasma is able to have a back transition to the L-mode after the ELM event before rebuilding and redeveloping the H-mode. Compound ELMs have also been observed where a larger ELM occurs immediately followed by a smaller one, hinting at multiple relaxation processes of the boundary conditions as for the Giant ELMs in figure 2.1.

The number of particle losses per ELM has been seen to depend on the collisionality [12]. At low collisionality the thermal energy lost during an ELM, is much greater than what would be expected for the amount of particles lost. These ELMs are labelled as "conductive". On the other hand at high collisionality, the energy lost per ELM decreases rapidly and can even become lower than the average particle losses, at which point the ELMs are labelled as "convective".

In ideal MHD, which does not include resistivity, the steep gradients created in the pedestal region will drive two types of instability, the ballooning mode [56] driven by the edge pressure gradient and the peeling mode [57] driven by the edge current density gradient. These modes are widely thought to be responsible for driving the ELMs [58, 56] and thus a variety of models exists to investigate their stability [59]. Similar non-linear MHD analysis [60] has been previously used to model astrophysical phenomenon like magnetosphere sub-storms and solar flares but has also been shown to be suitable in toroidal geometry [61].

The Ballooning Mode

The ballooning mode arises from the curvature of the tokamak geometry. High n modes, localised around their resonant surfaces, feel different curvature effects as they follow the helical field lines. On the high field side the curvature effect is stabilising, whereas for the low field side the curvature is seen to have a destabilising effect. The average of these effects is found to be stabilising for a plasma with a low pressure gradient. However, if the pressure gradient becomes too high, then the average of the curvature becomes a destabilising drive leading to ballooning modes. The stability of ballooning modes can be approximated from a balance of the driving term from the pressure gradient and the stabilising effect of the energy required for field line bending, shown here in terms of their potential energy [62];

$$\delta W_{\Delta P} \sim \frac{-dp/dr}{R_c}\xi^2, \qquad \delta W_{FLB} \sim k_{\|}^2 \left(\frac{B_\phi^2}{\mu_0}\right)\xi^2, \tag{2.1}$$

where p is the plasma pressure, R_c is the radius of curvature $\sim R_0$, the major radius of the torus, ξ is the radial displacement, B_ϕ is the magnetic field in the toroidal direction, and $k_{\|}$ is the parallel length to the magnetic field over which the displacement varies. Subsequently, a ballooning stability parameter can be introduced by equating the above two expressions, to characterise the ballooning mode

$$\alpha = -\frac{2\mu_0 q^2 R_0}{B^2}\frac{dp}{dr}. \tag{2.2}$$

This is a widely used parameter and will be seen later when discussing coupled peeling-ballooning modes.

The value of the magnetic shear is also important for the ballooning mode stability. At values of high magnetic shear the mode is stabilised. On the other hand, at very low values of shear "second stability access" is granted as seen in figure 2.3.

This additional region of stability is not an obvious result, as a higher pressure would increase the drive of the ballooning modes. However, at high pressure a strong distortion of the equilibrium magnetic flux surfaces occurs, which increases the local pitch and decreases the shear at the LFS. The increase in the local pitch causes the plasma to spend more time in the good curvature region, which as stated is stabilising. The decrease of the shear creates a large negative region of shear, which apart from being stabilising itself, also pushes the zero shear point away from the LFS to a more stable part of the plasma. The combination of these effects is responsible for the second stability access. This is advantageous not only due to the extra stability granted but also produces significant reductions in the required toroidal field and plasma current.

As this work is focusing on edge instabilities, it should be noted that the formulation of the ballooning stability criteria at the edge of a plasma is a little more complex than the conventional method [64]. At the edge of the plasma an extra boundary condition must

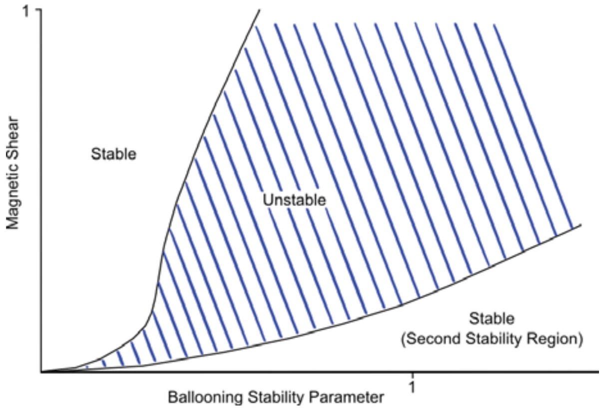

Figure 2.3: *The stability of the ballooning mode showing two stable regions at high and low magnetic shear. Reconstructed from reference [63].*

be in place as the ballooning mode can not extend into the vacuum region. This breaks the symmetry of the envelope of influence of the mode on the surrounding surfaces and creates a more localised perturbation.

Non-linear ballooning theory [61] suggests that the mode will be broad along the field line but narrow perpendicular to it. As a result the ejected particles will have a filament structure which will narrow and twist to squeeze between adjacent magnetic field lines. This filament is then predicted to have a radially explosive behaviour but could remain partially connected to the plasma core acting as a conduit for further particles to flow along. Multiple peaks were observed in the ion saturation current, measured using the reciprocating Langmuir probe on MAST [65], suggesting more than one structure rotating around the plasma. The energy of these structures, calculated from the change of the density profiles, would only contain a small amount ($\sim < 10\,\mathrm{J}$) and in total would only account for a fraction of the total ELM energy loss. Thus, these structures must not be isolated blobs but remain partially connected to the plasma and act as a particle conduit, i.e. a filament from core to SOL.

These predictions have been verified experimentally on the MAST tokamak [54, 55]. This was found when comparing high resolution Thomson scattering density profiles over an ELM event shows that ELMs have little effect on the inboard side but a large reduction of the density gradient on the outboard side. Immediately following this density gradient drop, poloidally localised density structures, moving radially away from the plasma, were seen, indicating propagating structures rather than a diffusion of particles. A high speed visible camera backs up these observations showing clear elongated structures along the field lines. Filament structures associated with ELMs have also been observed on ASDEX Upgrade [66].

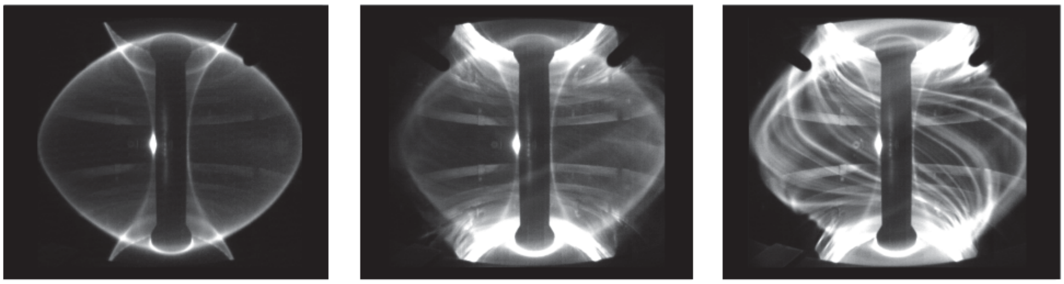

Figure 2.4: *Three snapshots taken directly from the fast visible camera on MAST showing an ELM event. Clear filament structures can be seen in the third image following the pitch of the magnetic field lines [67].*

The Peeling Mode

The term "peeling" in literature is first mentioned by Frieman [57] as a test function for the radial displacement which describes an instability to occur when a resonant condition is met, $m - nq_a^{(0)} = 0$ for $m > 1$. This requires the use of a cylindrical approximation and a large aspect ratio expansion. The peeling mode is only found in a cylindrical configuration, whereas the ballooning mode is non-cylindrical in nature.

The peeling mode is destabilised by the finite edge current density and is dependent on the location of the closest rational surface to the plasma edge in the vacuum. The pressure gradient gives both a stabilising effect through the magnetic shear and a destabilising effect through the bootstrap current. This is essentially the same as the well-known external kink mode. The difference is that the kink mode is driven by the derivative of the parallel current density, whilst the peeling mode is driven by the torque created by a finite value of the current density at the plasma edge and no current in the vacuum region. In addition, the peeling mode has a higher localisation than the external kink due to its sensitivity on the outer rational surface as seen in figure 2.5.

The effect of the distance of the plasma edge to the rational surface leads to strong dependencies on the q profile and the tokamak geometry. A stability criteria for the peeling mode in a toroidal MHD equilibrium surrounded by a vacuum with a continuous pressure profile is formed in reference [56] and will be used in chapter 3. This showed that the peeling modes would theoretically be unstable when the ELMs occur. Also Manickam [68] argues that the external kink and the more localized peeling mode are strong candidates for driving ELMs. In terms of experimental evidence, the PBX-M machine observed a MHD precursor to an ELM, identified as an ideal external kink mode [69]. Since then MHD analysis of the ELM crashes clearly states that for cases such as type-III ELMs the plasma would be peeling unstable and that sufficient levels of current to drive the peeling mode are present.

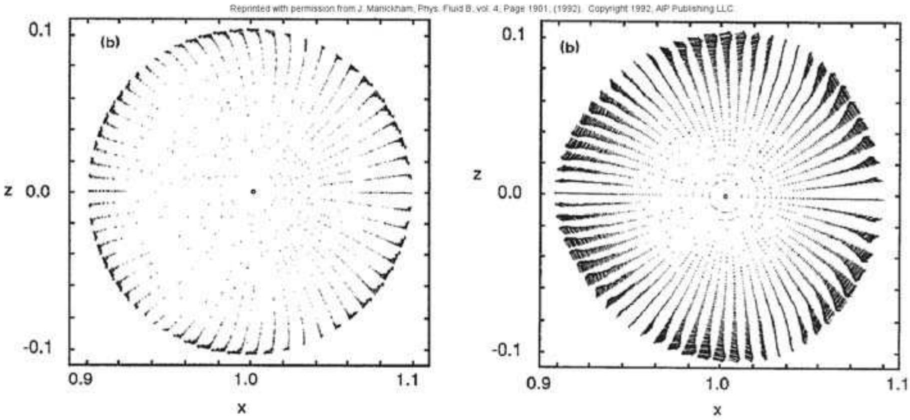

Figure 2.5: *The poloidal perturbations caused to the plasma by a peeling mode (left) and a kink mode (right). The peeling mode has a higher radial localisation affecting less of the plasma core [68].*

Due to the fact that the peeling mode stability has such a high dependence on the value of the current density at the edge, it is essential to have good measurements of both the finite value and the profile of the current density. This is therefore, a current hot topic for plasma diagnostics research [70, 71, 72, 73].

Finally the effect of a divertor on the peeling stability needs to be briefly considered. Theoretically at the separatrix, created by the divertor magnetic topology, $q \to \infty$. This will have a large effect on the peeling stability as multiple resonant q will be covered by the peeling mode and within the peeling stability a changing q profile needs to be considered. The behaviour of the unstable peeling mode growth rate at the last closed flux surface of the plasma was examined analytically [74, 75]. Modelling focusing on the X-point region is also being conducted [76, 77]. It was found that although the peeling drive was always present, the growth rate tended to zero and the mode became marginal by the presence of the separatrix. However, It is still unclear how the q profile acts in a real world situation and so this thesis will proceed using the value of the effective edge safety factor at 95% of the normalised poloidal flux, q_{95}, for tokamaks with a divertor configuration.

Coupled Peeling-Ballooning Modes

It has been put forward that a spectrum of peeling modes are unstable in the L-mode creating a large amount of anomalous transport [78]. As the plasma enters H-mode the collisionality increases stabilising the majority of the peeling modes, thus reducing anomalous transport; although a few peeling modes may remain marginally unstable. The transport barrier is now formed allowing the pedestal pressure to increase which in turn increases the ballooning stability parameter. When this reaches the ballooning stability limit it can either cause the onset of a ballooning mode, or the plasma can stay on the ballooning stability threshold whilst on a slower diffusive time scale the bootstrap current increases, due to the increasing pressure and decreasing collisionality which would allow a greater trapped particle fraction. When the bootstrap current has risen sufficiently to reach the peeling mode stability threshold, there is a possibility that the harmonics of the unstable peeling and ballooning modes couple, creating a large crash in the pedestal as seen for the type-I ELMs, schematically shown in figure 2.6 (left). Stability analysis of the coupled peeling-ballooning modes has shown the plasma to indeed reach the ballooning boundary and hold there until the peeling instability condition is met before the ELM crash occurs with intermediate toroidal mode numbers [79]. These coupled peeling-ballooning modes are complex and interesting phenomena as the bootstrap current, shear and pressure all play dual roles of stabilising and destabilising. Thus a useful representation of these modes is their potential energy δW for a radial displacement ξ [64],

$$\begin{aligned}\delta W =&\pi \int_0^{\psi_a} d\psi \oint d\theta \left\{ \frac{JB^2}{R^2 B_p^2} \left|k_\parallel \xi\right|^2 + \frac{R^2 B_p^2}{JB^2} \left| \frac{1}{n} \frac{\partial}{\partial \psi} (JBk_\parallel \xi) \right|^2 \right. \\ &- \frac{2J}{B^2} \frac{dp}{d\psi} \left[|\xi|^2 \frac{\partial}{\partial \psi} \left(p + \frac{B^2}{2} \right) - \frac{i}{2} \frac{I}{JB^2} \frac{\partial B^2}{\partial \theta} \frac{\xi^*}{n} \frac{\partial \xi}{\partial \psi} \right] \\ &\left. - \frac{\xi^*}{n} JBk_\parallel \left(\frac{\partial \sigma}{\partial \psi} \xi \right) + \frac{\partial}{\partial \psi} \left[\frac{\sigma}{n} \xi JBk_\parallel^* \xi^* \right] \right\}, \end{aligned} \tag{2.3}$$

where B_P is the poloidal component of the magnetic field, and θ, ϕ, and ψ are the toroidal coordinate system.

Here the equation has been written in a convenient form as it clearly states some of the underlying physics. The first line contains two terms associated with field line bending, the second line calculates the pressure gradient drive including curvature effects, and the last line gives the current density gradient drive where I is the plasma current, J is the current density, and $\sigma = \frac{I}{B^2} \frac{\partial p}{\partial \psi} + \frac{\partial I}{\partial \psi}$.

Considering each of the two modes individually, equation (2.3) states clearly the different terms involved. The peeling mode is highly localised at the plasma edge and has little coupling between its Fourier modes, so the field line bending effects disappear. The pressure gradient acts as a stabilising effect when the plasma experiences good curvature, whereas the current drive acts to destabilise the mode.
For a ballooning mode quite the opposite is true and it is found that the field line bending term is enhanced by multiple Fourier harmonics coupling over the rational surfaces and thus acts as a stabilising force. In this case the curvature is described as bad. The current gradient drive becomes less important at the large n associated with ballooning modes.

A final comment on the coupled peeling ballooning should be given to the shaping effects which are not obvious when just looking at equation (2.3). A large improvement has been seen in the performance of the H-mode with optimised shaping [80], figure 2.6 (right). Peeling-ballooning modes are decoupled when the triangularity is increased, since the magnetic shear depends highly on the shape of the plasma cross section, allowing access to second stability. Thus a "Bean" shape poloidal cross section would allow access to the second stability region [81].

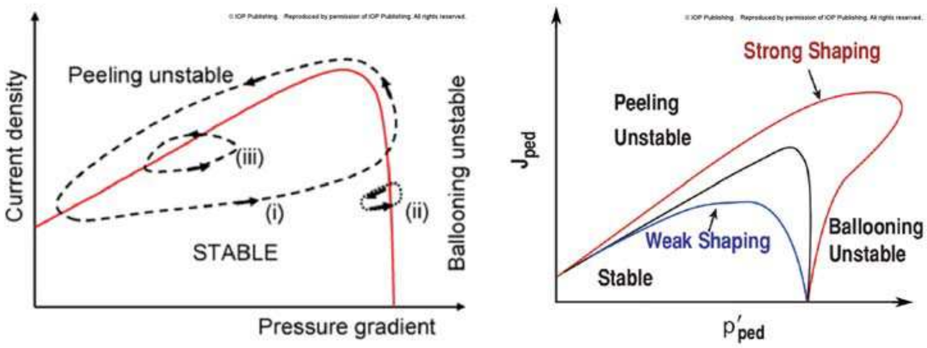

Figure 2.6: *(left) A schematic showing a simple peeling-ballooning stability boundary and possible ELM cycles labelled (i) to (iii). Each cycle crosses the stability boundary and then relaxes the plasma current and density [59]. (right) A schematic showing the effect of shaping on the peeling-ballooning stability diagram [82].*

Current Research in the Application of Resonant Magnetic Perturbations

A wide range of experiments focusing on the application of RMPs are currently ongoing in order to investigate how different fields affect the plasma and ELM stability and which of the design features of the RMPs coils are essential. A few key results are outlined here.

The RMP fields have the strongest interaction with the plasma at the rational surfaces and so the mode number of the applied field will have a high dependence on where in the plasma the perturbations take greatest effect and ultimately the ELM control. RMPs with toroidal mode numbers $n = 1, 2, 3, 4$ and 6 have been investigated across the range of machines, often showing different and sometimes opposite effects. For instance although DIII-D achieved suppression with $n = 3$, MAST, also using $n = 3$ in similar collisionalities, found large rotation braking which caused back transitions to the L-mode before the RMPs could have an effect on the ELMs [35]. This could be due to the DIII-D tokamak having a larger $n = 3$ intrinsic field or the different coil configurations which apply the RMP fields. Either way it becomes clear that n is not the only parameter which needs to be understood.

The toroidal phase and amplitude of the applied perturbation fields will also have a large effect on the ELM control. JET can apply four phases for DC $n = 1$ fields and two phases for DC $n = 2$ fields. All phases observe similar effects except for an artificial expansion of the plasma due to the action of the RMPs on the plasma control and position feedback i.e. the sensor measuring the plasma edge position sees the plasma shrink if the RMPs are applied at the same toroidal location, tricking the control system into allowing the plasma to expand causing large interactions of the plasma with the wall; this phase is called the "bad" phase and is no longer used. MAST sees much smaller effects on the ELMs and no pump-out effect when applying an odd parity through the RMP coils than an even parity. Simple vacuum modelling has shown this is due to a better alignment with the even parity case at the plasma edge.

As for the amplitude of the fields applied, a threshold in the RMP amplitude has been observed across all machines to be required before an effect on the ELMs is seen. This suggests a screening of the external fields until the threshold is reached when some form of penetration of the external fields into the plasma occurs.

The value of q_a has been seen to have a high effect on the ELM control and predicted in theory to be one of the key parameters. The original suppression experiments found that this was only achieved within a small resonant window of $q_{95} = 3.5 - 4.0$ and thus indicates a resonant nature [17]. An interesting feature occurred on JET where a multi-resonant nature was seen in the ELM frequency, f_{ELM}, dependence on the value of q_{95} [37, 83]. However, more recently ASDEX-U applied $n = 2$ perturbations to a range of q_{95} between 4.8 and 6.2 with similar collsionalities to those of the DIII-D suppression experiments observing mitigation of the ELMs by a factor of $6-8$ over a large q_{95} region, opposing the resonant nature observation [24].

Original observations on DIII-D suggested that the size of the stochastic region is an important parameter. However, an interesting result of these suppression experiments is that only the pedestal density drops. The electron temperature was seen to have only a little change implying that the RMP fields are not affecting the plasma edge exactly as expected. Since then the plasma edge density and temperature, when RMPs are applied, has been widely investigated, such as reference [84] for TEXTOR. On JET, the mitigation observed has been shown to be independent on the alignment of the magnetic field with the perturbation as the width of the stochastic layer increases linearly and then even saturates at a q_{95} value of 4.8. Results from MAST also suggest that the stochastic layer width is not the only criteria needed to be met for ELM mitigation/suppression as even with a larger stochastic layer than that of DIII-D, no effect was seen when applying $n = 3$ fields. Modification of the transport barrier by RMPs [85], the energy and particle transport change due to RMPs [86], and the effects on edge rotation [87] have all been intensively studied, although this is outside the remit of this study.

It was found on ASDEX-U that helical footprint patterns are created on the divertor plates during an ELM crash. This has been suggested to indicate different filaments impacting the plates [88]. Splitting of the main heat load deposited on the divertor plates has also been observed in both L-mode and H-mode [89, 90]. These two intriguing effects point towards changes occurring in the magnetic topology during the application of the RMP fields. On MAST, lobe structures in the plasma edge were detected to be created at the X-point, when the RMPs reached the threshold amplitude required to see an effect on the ELMs [91, 92]. Non-axisymmetric magnetic perturbations have been shown to split the separatrix into stable and unstable manifolds [93, 94, 95]. These manifolds interact with each other creating the lobes. These lobes have been shown analytically to intersect the divertor causing the observed strike point splitting [96, 97, 98].

Modelling of Resonant Magnetic Perturbation effects on the Plasma

Due to the interplay of pressure, current, plasma shape, magnetic shear, collisionality etc, large and complex modelling is often required to understand the physical mechanism behind the effect on the ELMs when external fields are applied.

Field line tracing codes, based on a description of divergent free magnetic field lines as a $1 + \frac{1}{2}$ degrees of freedom Hamiltonian system, offer simple, robust modelling of the plasma with no gyro or rotation effects. This technique has been widely used to model plasmas in equilibrium. To include perturbations into these models, the vacuum assumption is often used which is simply a superposition of the external field onto the plasma and hence does not take into account any response from the plasma. The standard map [99] is one such model and is valid for low collsionalities, although once the heating power increases to levels necessary for the H-mode, it becomes clear that additional effects need to be included, especially the collisions. The inclusion of weak collisions has been implemented [100] and more recently extended to include strong collisions [98].

An alternative approach is through the kinetic or fluid description of the plasma. These models reduce the MHD equations and attempt to solve the problem self consistently. Although more physical effects can be implemented in these codes, they are limited by the computational cost and often have to use questionable assumptions, such as unrealistic resistivity, to find a solution. A few examples of different implementations of fluid descriptions are now outlined.

The `EPED` model [101, 102] focuses on producing quantitative predictions of the pedestal characteristics, namely the height and width, through combining the stability constraint of the peeling-ballooning intermediate modes and the kinetic ballooning mode turbulence. This suggests that mitigation of ELMs is due to limiting the maximum pedestal height, whereas ELM suppression occurs due to a “wall” stopping the pedestal building further whilst maintaining the plasma edge stability below the peeling-ballooning unstable threshold. This wall would be a strong region of radial transport situated at the pedestal top such as the formation of a magnetic island at a resonant surface. The island position is dependent on the q profile and so explains why suppression has only been observed in a narrow q window.

The `ELITE` [103] and `MISHKA` codes [104], calculate the ideal MHD stability of a tokamak plasma edge, widely used to analyse MHD stability showing strong agreement between the onset of an ELM and the plasma crossing the stability boundary. `MARS-F` [105, 106, 107] is a single perturbed fluid solver in full toroidal geometry, which can model the linear response to RMP fields for realistic plasmas and has shown a high level of agreement with MAST results.

Larger codes such as `BOUT++` [108, 109, 110] and `JOREK` [111, 112, 113, 114] have been developed to create robust stability limit predictions, and to understand the full non-linear dynamics beyond MHD physics at the edge of a plasma during an ELM event. `BOUT++` simulations suggest that hyper-resistivity (electron viscosity) limits the radial broadening of the ELM by inducing magnetic reconnection at the steepest gradient in the pedestal. `JOREK` includes a full toroidal X-point geometry allowing it to accurately simulate the separatrix, which as pointed out has a large effect on the coupled peeling-ballooning modes.

None of these codes can fully simulate the problem yet and still many questions remain unanswered.

3 The Peeling Initiated Current Relaxation Model

In this chapter, the model used for this study is established. The main feature of the model is a calculation of the boundary conditions for the minimum potential energy state, after an ELM crash has occurred. Towards the end of the chapter the implementation of the model is explained and extensions of the model are considered.

A Relaxation Approach to Modelling Edge Localized Modes

High order complex models, such as outlined in the last chapter, are seeing good agreement with experimental results but are often time consuming, extremely focused and narrow in the conditions which can be modelled, and due to the large amount of effects being simulated self-consistently, it is often difficult to differentiate what is happening. Thus, the physical mechanisms and exact parameter dependencies are often still unclear. In this study, a model is created which focuses on peeling modes in a cylindrical approximation, giving clear indications of how the peeling mode driven ELMs depend on the plasma parameters, especially the plasma current and edge safety factor. This has the major advantage of being a quick and robust way to gain insight into the basic physical processes occurring, although it does not give exact predictions for real world experiments. Therefore, this should be thought of more as a guide to focus the direction of research rather than a final result.

Each ELM can be described as a collapse of the pedestal. In fact the most accurate way of evaluating the size of the ELM is to look at the difference in the temperature, density and pressure profiles at the plasma edge before and after an ELM event occurs. This means that there is a source of free energy in the pedestal which is released in each event allowing the plasma edge to drop to a lower energy state. Therefore, if ELMs are modelled as a series of isolated relaxations, with the pedestal rebuilding between ELMs until a crash condition is met, then a constrained minimisation of the magnetic energy can calculate the final state that the plasma will relax to. This is a Taylor relaxation in the current and here is hypothesised to be initiated by a set of peeling modes. The relaxation would start at the plasma edge and proceed radially inwards until a stable state is found to all ideal peeling modes. Following the relaxation process (identified with the ELM 'crash'), in the absence of any sustaining e.m.f., the current profile will diffuse away from the relaxed state and start to rebuild the pedestal, until a further peeling mode is triggered and the process repeats. There is thus a continual cycle of instability-relaxation-diffusion.

Similar analysis has been widely used in the past. Spies *et al* extended the Taylor relaxation to include a contribution from a vacuum, which separates the plasma from the conducting wall [115]. This has previously been utilised to explain the reversal in the amplitude of the magnetic field in a reversed field pinch [116], and on tokamaks, to explain magnetic reconnection [117, 118] and the sawtooth collapse process [119]. More recently it was applied to model MHD equilibria as a set of relaxed regions of pressure, in order to over come numerical irregularities [120].

To this end a one-dimensional current relaxation condition shall be formed, to describe the required circumstances for the peeling modes to drive an instability. Next, the final relaxed state will be investigated against the value of the safety factor and current density at the plasma edge. Extensions to investigate the current density profile are outlined at the end of this chapter. However, as the peeling mode depends mainly on the value of the edge current density rather than the profile, only the values of current and q_a at the edge need to be considered.

The current relaxation model was chosen for this study as it was suggested that the peeling mode dependence on the value of q_a could explain some interesting observations on JET. Thus an investigation focusing on the peeling mode stability, rather than a full equilibrium solution, should highlight if indeed the peeling mode could explain the experimental observations, or if other mechanisms were required. The analytical description of the peeling mode stability through the energy principle is already well established. However, modelling the ELM event as a current relaxation of the plasma edge is not commonly investigated, making this model unique in its focus and implementation. This allows us to look at the final state of the plasma without being concerned with the exact process occurring, which is currently unknown, and enables a quick and robust calculation of how the peeling stability is affected in a tokamak by changes in q_a. As this model is individual there are no other codes to benchmark against and the results will have to stand on their own against experimental observations. As previously stated the aim is not to give exact numerical answers but show dependencies in order to enhance understanding and focus future research.

The aim of the following analysis is to create boundary conditions for the final state of this relaxation, allowing predictions of the size of an ELM crash under different plasma conditions. These boundary conditions will then be implemented into a code with the objective of being able to compare with experimentally relevant quantities, especially the value of the edge safety factor, q_a. Firstly, the energy principle will be stated from the well known analysis found in [62]. Secondly, a peeling mode stability condition will be created following the original formulation found in [56]. Thirdly, the first two sections will be combined to create the necessary boundary conditions for the final relaxed state as originally proposed in [121, 122]. Finally, the obtained calculations are implemented into a new `fortran 90` code able to solve analytically the boundary conditions and investigate the dependencies of current and q_a on the model. This implementation of the current relaxation model and the discussions of the extensions presented towards the end of the chapter are unique to this study.

The Energy Principle

The energy principle, simply put, says that if a perturbation of an equilibrium lowers the potential energy then the original state is unstable. This can be used to calculate the stability of a magnetic configuration without having to solve complex partial differential equations. Instead, this method uses a variational formulation to give an integral description of the linearized MHD equations and then assumes conservation of total energy. This leads to the postulate that the most negative eigenvalue of the total energy gives the minimum in potential energy, W, which by definition will be a stable state. From this it is concluded that the plasma is only stable if the change in potential energy, $\delta W \geqslant 0$.

The formulation of the energy principle is well known and widely used [123, 124]. Here the principle is used for a toroidal plasma surrounded by a conducting wall with a vacuum separating the plasma from the wall where the equilibrium can be described by the single fluid ideal MHD equations,

$$\frac{d\rho}{dt} = -\rho\boldsymbol{\nabla}\cdot\mathbf{v}, \tag{3.1}$$

$$\rho\frac{d\mathbf{v}}{dt} = \mathbf{J}\times\mathbf{B} - \boldsymbol{\nabla}p - \rho\boldsymbol{\nabla}\phi, \tag{3.2}$$

$$\frac{dp}{dt} = -\gamma p\boldsymbol{\nabla}\mathbf{v}, \tag{3.3}$$

$$\boldsymbol{\nabla}\times\mathbf{E} = -\frac{\partial\mathbf{B}}{\partial t}, \tag{3.4}$$

$$\boldsymbol{\nabla}\times\mathbf{B} = \mu_0\mathbf{J}, \tag{3.5}$$

$$\boldsymbol{\nabla}\cdot\mathbf{B} = 0, \tag{3.6}$$

$$\mathbf{E} + \mathbf{v}\times\mathbf{B} = 0, \tag{3.7}$$

where ρ is the plasma mass density, $\mathbf{v}$ is the fluid velocity, $\mathbf{J}$ is the current density, $\mathbf{B}$ is the magnetic field, p is the plasma pressure, γ is the ratio of specific heats, $\mathbf{E}$ is the electric field, ϕ is the electric potential, and $\frac{d}{dt} = \frac{\partial}{\partial t} + \mathbf{v}\cdot\boldsymbol{\nabla}$.

Lortz [125] demonstrated that the vacuum and wall contributions could be neglected for the peeling mode due to the localisation of the mode at the surface and so only the energy change associated with the plasma needs to be considered. The result is shown in equation (3.8) in its "intuitive form" which gives greater insight into the physics contained [62],

$$\delta W = \frac{1}{2}\int_{Plasma} d\tau \left[|\mathbf{B}_{1\perp}|^2 + \mathbf{B}_0^2 |\boldsymbol{\nabla}\cdot\boldsymbol{\xi}_\perp + 2\boldsymbol{\xi}_\perp\cdot\boldsymbol{\kappa}|^2 + \gamma p_0 |\boldsymbol{\nabla}\cdot\boldsymbol{\xi}|^2 \right.$$
$$\left. -2(\boldsymbol{\xi}_\perp\cdot\boldsymbol{\nabla}p)(\boldsymbol{\kappa}\cdot\boldsymbol{\xi}_\perp^*) - \frac{\mathbf{J}_0\cdot\mathbf{B}_0}{\mathbf{B}_0^2}(\boldsymbol{\xi}_\perp^*\times\mathbf{B}_0)\cdot\mathbf{B}_{1\perp}\right], \tag{3.8}$$

where the magnetic field line curvature vector $\boldsymbol{\kappa} = \frac{\mathbf{B}_0}{B_0}\cdot\boldsymbol{\nabla}\frac{\mathbf{B}_0}{B_0}$, ξ is the radial displacement as before, and the $\perp$ subscript denotes the component in the direction perpendicular to the magnetic field lines. The first three terms are stabilising representing the energy required to bend magnetic field lines, the energy needed to compress the magnetic field and the energy necessary to compress the plasma, respectively. The last two terms can be stabilising or destabilising depending on their sign. These represent drives for pressure and current driven modes.

The Peeling Mode Energy Principle

To apply the energy principle to a peeling mode an orthogonal coordinate system which can describe the tokamak as a set of magnetic surfaces is required. Since a tokamak is an axisymmetric toroidal device the magnetic field is written as $\mathbf{B} = \boldsymbol{\nabla}\psi\times\boldsymbol{\nabla}\phi + \mathbf{I}(\phi)\boldsymbol{\nabla}\phi$ and the coordinate system (ψ, ϕ, θ) is created where ψ is the flux coordinate defining different toroidal magnetic surfaces, ϕ is the angle around the torus axis and θ is the poloidal angle. Now an individual Fourier mode $\boldsymbol{\xi} = \boldsymbol{\xi}(\psi,\theta)exp(in\phi)$ can be introduced allowing δW to be minimised with respect to the components of $\boldsymbol{\xi}$ parallel to $\mathbf{B}$ and lying in the magnetic surface thus reducing the potential energy to a quadratic form in ξ_ψ only [64].

From this an Euler equation can be created to minimise δW in terms of ξ_ψ,

$$\frac{d}{dx}\left(x^2\frac{d\xi_\psi}{dx}\right) - \frac{Q}{P}\xi_\psi = 0, \tag{3.9}$$

which when solved yields the solutions $\xi_\psi = a_+ x^{\lambda_+} + a_- x^{\lambda_-}$ where $\lambda_\pm = -\frac{1}{2} \pm \sqrt{\frac{1}{4} + \frac{Q}{P}}$. The flux surface average quantities P, Q and S are given in the appendix of reference [56]. It turns out that $Q/P = -D_M$ and thus the stability criterion is the well known Mercier criterion, $D_M - \frac{1}{4} < 0$ [126]. The Mercier criterion is a necessary condition for the stability of interchange modes localized around rational surfaces where the field line bending term is minimal. So D_M corresponds to the balance between the driving force of the interchange mode and the stabilising magnetic shear predicted by ideal magneto-hydrodynamics.

However, the peeling mode is dependent on a finite current at the plasma edge and also on the position of the rational surface. Therefore, a more stringent stability criterion is needed for the cases where the rational surface appears just inside or outside the plasma. These two stability conditions need to be matched and combined.
For the case where the rational surface is within the plasma, ξ_ψ should be zero outside the plasma and satisfy equation (3.9) for $x_a < x < 0$. This requires a_- to be 0 and so δW becomes

$$\delta W = -\frac{1}{2}P|x_a|^{2\lambda_+ +2}x_a\left[\frac{S}{P} + \lambda_+\right]. \tag{3.10}$$

The criteria for this case is then

$$\sqrt{1-4D_M} > 1 - 2\frac{S}{P}. \tag{3.11}$$

For the second case where the rational surface is just outside the plasma a_+ is set to 0 as only ξ_ψ inside the plasma is interesting. Thus δW is now

$$\delta W = -\frac{1}{2}Px_a^{2\lambda_- +3}\left[\frac{S}{P} + \lambda_-\right], \tag{3.12}$$

and the stability criteria is

$$\sqrt{1-4D_M} > 2\frac{S}{P} - 1. \tag{3.13}$$

Finally these two criteria are combined to give a final peeling mode stability condition for the usual tokamak case,

$$\sqrt{1-4D_M} > 1 + \frac{2}{2\pi q'}\oint \frac{j_\parallel B}{R^2 B_p^3}dl, \tag{3.14}$$

where the definitions for S and P have been substituted. The role of the edge current in the stability is now more apparent, showing it to have a destabilising nature. Finally, if plasma shaping effects are neglected, as this is a cylindrical model, but the Pfirsch-Schlüter current is included then the leading order stability condition can be written in terms of the radial derivative of the Shafranov shift, $\Delta_s^{'}$ [56]

$$\alpha\left\{\frac{r}{R}\left(1-\frac{1}{q^2}\right) + s\Delta_s^{'} - f_t\frac{Rs}{2r}\right\} > Rqs\left(\frac{j_\parallel^{driven}}{B}\right)_{edge}, \tag{3.15}$$

where the magnetic shear $s = \frac{r}{q}\frac{dq}{dr}$, f_t is the trapped particle fraction, $j_\parallel^{driven}$ is the driven current without the bootstrap or the Pfirsch-Schlüter contributions and α is the usual ballooning stability parameter defined in chapter 2. The terms on the left hand side of this formula are split into contributions from the stabilising Mercier criteria and Pfirsch-Schlüter current, and the destabilising bootstrap current. Each of these comes through the effects of toroidicity on the peeling mode which will disappear when only considering a cylindrical model. The right hand side gives information about the cylindrical effects on the peeling mode and are of the highest interest to this work. Here, the mode is set to be at the edge of the plasma and so the distance between the unstable rational surface and the plasma edge is zero. Later, the effect of having the rational surface a distance away from the edge will be shown to also have a destabilising effect on the peeling mode.

Relaxation Model for Peeling Initiated Edge Localized Modes

Now that a condition has be formulated that states when the peeling modes will become unstable, boundary conditions for the final relaxed state can be created. The actual relaxation process will not be investigated; (possibly a series of micro-tearing instabilities could be the physical process) rather the focus is on the final relaxed state. The current relaxation model says that after a peeling mode becomes unstable a relaxation of the plasma edge to a lower magnetic potential energy state occurs. This relaxation is formulated in a similar way to the original Taylor relaxation [116] which was used to explain the reversed toroidal field in a reversed field pinch device by calculating a set of final relaxed states characterised by $\boldsymbol{\nabla} \times \mathbf{B} = \mu\mathbf{B}$ where μ is an absolute constant. However, for the outlined case, the relaxation is restricted to places where MHD instabilities are present and so only the edge of the plasma is affected. The relaxation will start from the plasma edge and move radially inwards towards the core leaving in its wake a "Taylor" state. In a conventional tokamak ordering this will create a flattening of the toroidal current density, shown in the simple schematic figure 3.1 as the dashed line. Clearly, this creates larger gradients in the current density at the boundaries of the relaxed region i.e. at the plasma vacuum interface and at the point where the relaxation meets the unperturbed core. As the peeling mode is driven by the current density gradient, one would expect this to have a further destabilising effect completely collapsing the plasma edge. However, at the outer boundary a stabilising negative skin current forms due to the discontinuity in the q-profile. These skin currents or "sheets" will have the effect of screening the rest of the plasma from the perturbation. If then an equilibrium can be found of the destabilising current gradient drive and the stabilising skin currents, stable for all peeling modes, then the plasma will relax to this state. The boundary conditions describing this state will now be derived.

To calculate the final relaxed state a region is defined extending from the plasma edge at $r = a$ inwards to a radius r_E which is as yet to be determined. The distance $a - r_E$ will be the relaxation width, d_E. In this region the magnetic potential energy will be minimised subject to two invariants due to the annular topology of a tokamak edge. These are the global helicity, $K = \int_{r_E}^{a} (r/q)(r^2 - r_E^2)dr$, and the total poloidal flux, $\Psi_\theta = \int_{r_E}^{a} \frac{r}{q} dr$. The poloidal magnetic energy, $W_\theta = \frac{1}{2\mu_0} \int_V B_\theta^2 dV$, is now minimised subject to the conservation of the invariants. The solution

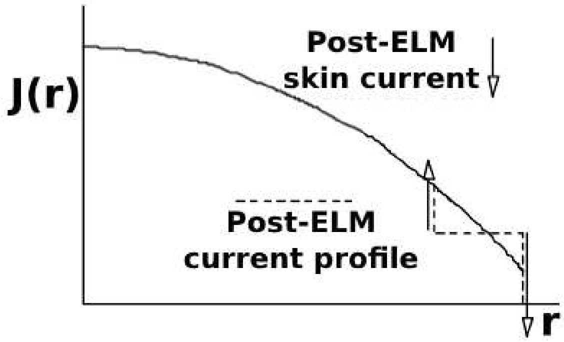

Figure 3.1: *A simple schematic of the radial profile for the toroidal current density. The profile before the relaxation (solid line) and an idealised case after the relaxation (dashed line) are shown. The skin currents are marked as arrows on the boundaries of the relaxed region. At the plasma vacuum boundary the skin current has a negative amplitude, whereas the skin current at the inner boundary will have a positive amplitude.*

$$q^f(r) = \frac{r}{Cr + \frac{D}{r}} \tag{3.16}$$

makes the Lagrangian multipliers stationary and solves the problem. Here the superscript f denotes the final state after the relaxation, C and D are constants determined by conservation of K and Ψ_θ between initial and final states.

A cylindrical approximation can be used for the relaxation of the plasma edge as the pressure is removed along with any toroidal coupling. This can be seen in equation (3.15) by setting α to 0. In this cylindrical geometry the marginal force balance is given by the well-known "tearing" equation ([127]) for the perturbed poloidal flux, $\psi = rb_r$,

$$\frac{d}{dr}\left(r\frac{d\psi}{dr}\right) - \frac{m^2\psi}{r} = \frac{m}{F}\mu_0\frac{dJ_z}{dr}\psi, \tag{3.17}$$

where the safety factor $q = rB_0/(R_0B_\theta)$ and

$$F = \mathbf{k}\cdot\mathbf{B} = \frac{B_\theta}{r}(m - nq) = m\frac{B_0}{R_0}\left(\frac{1}{q} - \frac{n}{m}\right). \tag{3.18}$$

This equation can now be used to describe the relaxed state stability although the jumps in F and the current at the two boundaries make the situation a little more complex. To deal with these discontinuities, boundary conditions on ψ need to be created which ensure the tangential stress is continuous across the boundaries and that the total magnetic field has no normal components on either of the perturbed boundaries. This second constraint means that the boundaries must remain as flux surfaces and can be written formally as $\hat{\mathbf{n}} \cdot \mathbf{b} = \hat{\mathbf{n}} \cdot \boldsymbol{\nabla} \times (\boldsymbol{\xi} \times \mathbf{B})$. This then requires that although ψ will be discountious, ψ/F will not.

Knowing that $\xi = \psi/(rF)$ is continuous, one can write down a boundary condition for $\psi^{'}(a)$. Start with the differential equation for this quantity created by substituting $\psi = rF\xi$ into equation (3.17)

$$\frac{d}{dr}\left(r^3 F^2 \frac{d\xi}{dr}\right) - (m^2-1)rF^2\xi = 0. \tag{3.19}$$

This is a marginal force balance equation with only finitely varying quantities and thus can be integrated across the P/V interface to give

$$\left[\left[F^2 \frac{d\xi}{dr}\right]\right]_P^V = 0, \tag{3.20}$$

which when using ψ as the independent variable leads to

$$\left[\left[F^2 \frac{d}{dr}\left(\frac{\psi}{rF}\right)\right]\right]_P^V = 0. \tag{3.21}$$

This jump condition for $d\psi/dr$ gives boundary conditions for both boundaries of the relaxed region. After some algebra it follows that the edge boundary condition between the plasma edge and the vacuum region ($r = a$) is

$$\Delta_a\left[\Delta_a\Delta_a^{'} + I_a\right] + \kappa_a\left[(\kappa_a - 2\Delta_a)(\Delta_a^{'} + m - 1) + 2\frac{n}{m} - I_a\right] = 0, \tag{3.22}$$

and the inner boundary condition between the relaxed region and the unperturbed core ($r = r_E$) is given by

$$\Delta_{E_-}\left[\Delta_{E_-}\Delta_E^{'} + I_{E_-} - I_{E_+}\right] + \kappa_E\left[(\kappa_E + 2\Delta_{E_-})(\Delta_E^{'} + m + 1) + 2\frac{n}{m} - I_{E_-}\right] = 0. \tag{3.23}$$

Here several dimensionless quantities have been introduced which represent equilibrium and perturbation properties in a more physical context. These are: the distance between a radial position j and the resonance where $n = mq$

$$\Delta_j = \left(\frac{1}{q_j} - \frac{n}{m}\right); \tag{3.24}$$

a relation of the toroidal current density to the safety factor

$$I = R_0\mu_0 J/B_0 = \frac{1}{r}\frac{d}{dr}\left(\frac{r^2}{q}\right); \tag{3.25}$$

the equation for the safety factor radial jump across the boundaries where the surface skin current density is I_{js}

$$\kappa_j = \frac{R_0}{aB_0}\mu_0 I_{js} = \left[\left[\frac{1}{q}\right]\right]_{j_-}^{j_+}; \tag{3.26}$$

and the jump in the perturbed poloidal flux radial derivative which is a well known quantity from tearing mode analysis

$$\Delta_j^{'} = \left[\left[\left(\frac{r}{\psi}\frac{d\psi}{dr}\right)\right]\right]_{j_-}^{j_+}. \tag{3.27}$$

The two boundary conditions required are now fully formed and so the relaxed state condition is found by linking these conditions through connecting $\Delta_a^{'}$ and $\Delta_E^{'}$ and assuming that the relaxed current will be uniform as stated by equation (3.16). In the region $r_E < r < a$ equation (3.17) gives $\Psi \approx r^{\pm m}$ and thus Ψ can be taken as $\psi = Ar^m + Br^{-m}$, therefore $\Delta_E^{'}$ is related to $\Delta_a^{'}$ by

$$\Delta_E^{'} = -2m\frac{\Delta_a^{'} + 2m}{g\Delta_a^{'} + 2m}, \tag{3.28}$$

where $g = 1 - (r_E/a)^{2m}$.

Our peeling driven relaxation problem is now fully formalised and a peeling instability is found to occur whenever the solution of equations (3.23) and (3.28) for $\Delta_a^{'}$ is greater than zero,

$$\Delta_a\left[\Delta_a\Delta_a^{'} + I_a\right] + \kappa_a\left[(\kappa_a - 2\Delta_a)(\Delta_a^{'} + m - 1) + 2\frac{n}{m} - I_a\right] > 0. \tag{3.29}$$

The first term is the destabilising peeling drive where the I_a is the same as the right hand side of equation (3.15). The Δ_a term is then the contribution from the rational surface being a distance away from the edge. The second term is the stabilising contribution from the negative skin current. This equation can also be deduced from the MHD energy δW principle which shows the left-hand side of equation (3.29) is $\propto -\delta W$, demonstrated in appendix A of [122].

Application of Current Relaxation Model

This model was implemented into a `fortran 90` code with the aim of investigating the edge safety factor dependence on the f_{ELM} for different plasma profiles. The final stable solution for all peeling modes is given when equation (3.29) is equal to zero. This is very useful as for given initial plasma conditions where a peeling mode will be unstable equation (3.29) will give the final relaxed state i.e. the inner radius of the annular relaxed region, d_E. In other words, d_E is the largest value such that the final relaxed equilibrium configuration is stable to all peeling modes. From this the frequency of the relaxation can be predicted from the calculated relaxation widths using a diffusive model as the current diffuses away from the relaxed state

$$\frac{d}{dt} = D_\eta \frac{d^2}{dr^2} \quad \rightarrow f_{ELM} \approx \frac{D_\eta}{d_E^2}, \tag{3.30}$$

where D_η is a diffusion coefficient. For this investigation the interest is in the scaling which is independent of the value of D_η as this is not influenced by changes in q_a and so any effect would not change the understanding of the edge safety factor dependence.

The program calculates equation (3.29) with toroidal mode numbers from $n = 1 \rightarrow 10$ and poloidal mode numbers from $m = 1 \rightarrow q_a n$, filtering out the non-resonant modes, for a range of q_a. The relaxation width was scanned inwards from the plasma edge to 20% of the normalised radius until a new stable equilibrium is achieved. It is assumed that the plasma will always take the largest relaxation width as its lowest energy state. Thus, for each q_a a dominant relaxation width is predicted. Results from this model are shown and used in chapter 5.

Extension to Include the Current Density Profile

The bootstrap current, as pointed out, can form a significant component of the toroidal current in a tokamak, and is likely to be most significant in the pedestal region due to the strong density and temperature gradients there. Thus, the bootstrap current may have a significant effect on the stability of the plasma to peeling modes, and hence on ELMs.

The effect of adding a bootstrap current to the edge of the plasma is now investigated as a small ELM width expansion. This will build on the previous formulation found in reference [122] but with the addition of a bootstrap current J_B [P. Devoy, Private Communication 2010]. For the purpose of simplification, it is assumed that the bootstrap current is distributed as a δ-function at some point inside the plasma, r_B, and that the initial current profile containing this bootstrap is in an unstable state. The current density is expanded from the edge inwards to give

$$J_Z = J_a - x(aJ_a^{'}) + \frac{x^2(a^2 J_a^{''})}{2} + J_B \delta(r - r_B), \tag{3.31}$$

where x is the normalised distance from the edge of the plasma given by $r = a(1-x)$, and J_a is the current at $r = a$. The poloidal magnetic field is related to this current by the expression

$$rB_\theta = -a^2 \mu_0 \int (1-x) J_Z dx. \tag{3.32}$$

Using small value approximations for x and substituting the expression for J_Z into the above equation it is obtained that

$$B_\theta = -a\mu_0 \left(J_a \left(x + \frac{x^2}{2} \right) - \frac{ax^2}{2} J_a^{'} \right) + \left[B_{\theta a} - a\mu_0 J_B (1 - x_B) \right] (1 + x + x^2), \tag{3.33}$$

where x_B is the distance of the bootstrap from the edge and $B_{\theta a}$ is the poloidal magnetic field at $r = a$. This leads to expressions for the expanded total poloidal flux and helicity for the initial state,

$$\Psi_\theta = a\left[B_{\theta a} - \mu_0 J_B(1-x_B)\right]\left(d_E^2 + \frac{d_E^2}{2}\right) - \mu_0 J_a\left(\frac{d_E^2}{2} - ...\right) + \mu_0(a^3 J_a^{'})\left(\frac{d_E^3}{6} + ...\right), \quad (3.34)$$

$$\frac{K}{a^4 B_\theta} = \left[\frac{B_{\theta a}}{a} - \mu_0 J_B(1-x_B)\right]\left(d_E^2 - \frac{d_E^3}{3}\right) - \mu_0 J_a\left(\frac{d_E^3}{3} - ...\right) + \mu_0(a J_a^{'})\left(\frac{d_E^4}{12} + ...\right). \quad (3.35)$$

The post relaxed q profile will have the form

$$q_f(r) = \frac{r}{Cr + D/r}, \quad (3.36)$$

thus it can be shown that the relaxed helicity and poloidal flux are

$$\Psi_\theta = a^2\left[C\left(d_E - \frac{d_E^2}{2} - ...\right) + D\left(d_E + \frac{d_E^2}{2} - ...\right)\right], \quad (3.37)$$

$$\frac{K}{a^4 B_0} = \left[C\left(d_E^2 - d_E^3 - ...\right) + D\left(d_E - \frac{d_E^3}{3} + ...\right)\right]. \quad (3.38)$$

It now proves convenient to define a new constant

$$C_0 = C + D - \left(\frac{B_{\theta a}}{a} - \mu_0 J_B(1-x_B)\right). \quad (3.39)$$

Using the invariant nature of the total helicity and the poloidal flux, simultaneous equations can be formed containing C_0,

$$\left(1 + \frac{d_E}{2} + \frac{d_E^2}{2}\right)C_0 - \left(d_E + \frac{d_E^2}{3}\right)C = -\mu_0 J_a \frac{d_E}{2}\left(1 + \frac{d_E}{3}\right) + \mu_0(a J_a^{'})\left(\frac{d_E^2}{6}\right), \quad (3.40)$$

$$\left(1 - \frac{d_E}{3} + \frac{d_E^2}{12}\right)C_0 - \left(\frac{2d_E}{3} - \frac{d_E^2}{3}\right)C = -\mu_0 J_a \frac{d_E}{3}\left(1 - \frac{d_E}{2}\right) + \mu_0(a J_a^{'})\left(\frac{d_E^2}{12}\right). \quad (3.41)$$

Solving for C_0 gives

$$C_0 = \frac{-\mu_0(a J_a^{'})}{12} d_E^2. \quad (3.42)$$

This is equal to the previous calculation of C_0 from reference [122] equation (C8), even though the starting definition included the bootstrap term. The surface skin current formed in the relaxation process at the edge of the plasma is now introduced

$$\chi_a = \frac{R_0}{aB_0}(B_{\theta a+} - B_{\theta a-}), \tag{3.43}$$

where $B_{\theta a+} = a(C + D) + a\mu_0 J_B(1 - x_B) - aC_0$ and $B_{\theta a-} = a(C + D)$. Therefore equation (3.43) can be rewritten as

$$\chi_a = \frac{R_0}{aB_0}\left(a\mu_0 J_B(1 - x_B) + \frac{\mu_0 a^2 J_a'}{12} d_E^2\right). \tag{3.44}$$

This implies that J_B must be of order d_E^2 in order for this expansion to be valid. From here it can be shown from looking at the ordering of the stability balance of the plasma that the largest ELM width will occur when

$$\chi_a(max) = -\frac{I_a^2}{16n}, \tag{3.45}$$

where I_a is the toroidal current density at $r = a$ and n is the toroidal mode number of the peeling instability. Equations (3.44) and (3.45) are solved leading to an expression for the maximum ELM width in relation to the toroidal current

$$d_{E,max}^2 = \frac{-3I_a^2}{4n(aI_a')} - \frac{12I_B(1 - x_B)}{aI_a'}. \tag{3.46}$$

Finally, this can be compared with the case without bootstrap current

$$d_{E,max}^2 = \begin{cases} \frac{-3I_a^2}{4naI_a'} & \text{if } r_{E,0} > r_B, \\ \frac{-3I_a^2}{4n(aI_a')} - \frac{12I_B(1-x_B)}{aI_a'} & \text{if } r_{E,0} < r_B. \end{cases} \tag{3.47}$$

where $r_{E,0}$ is the location of the inner boundary of the relaxed region in the case of zero bootstrap and I_B is the bootstrap current density. It can easily be seen from equation (3.47) that the ELM width splits, according to whether the location of the bootstrap current (r_B) is reached by the relaxation process or not.

As for the case without the additional bootstrap current, the distribution shows deterministic scatter, with the ELM width depending on the proximity of q_a to a rational value. The bifurcation which appears in the ELM widths when a bootstrap current is present becomes larger as the magnitude of the bootstrap current increases. A physical interpretation is that the ELM size in the presence of bootstrap can be determined from considering the bootstrap-absent case: if the ELM width in the latter situation is large enough to encompass the bootstrap current, then the ELM increases to incorporate the bootstrap current region, while if the ELM width is small, the bootstrap current is not encountered and the ELM width is unaffected by its presence. In other words, the first case for $d_{E,max}$ in equation (3.47) is basically independent of the bootstrap, whereas the second case is increased by an amount dependent on the bootstrap current magnitude.

In mathematical terms, the bifurcation can be understood from consideration of the dependence of the perturbed energy, δW, on the relaxation radius, d_E, for a given q profile (see figure 3.2). It can be seen that δW takes a double-peaked form (unlike the bootstrap-absent case, in which it is a simple monotonic dependence).

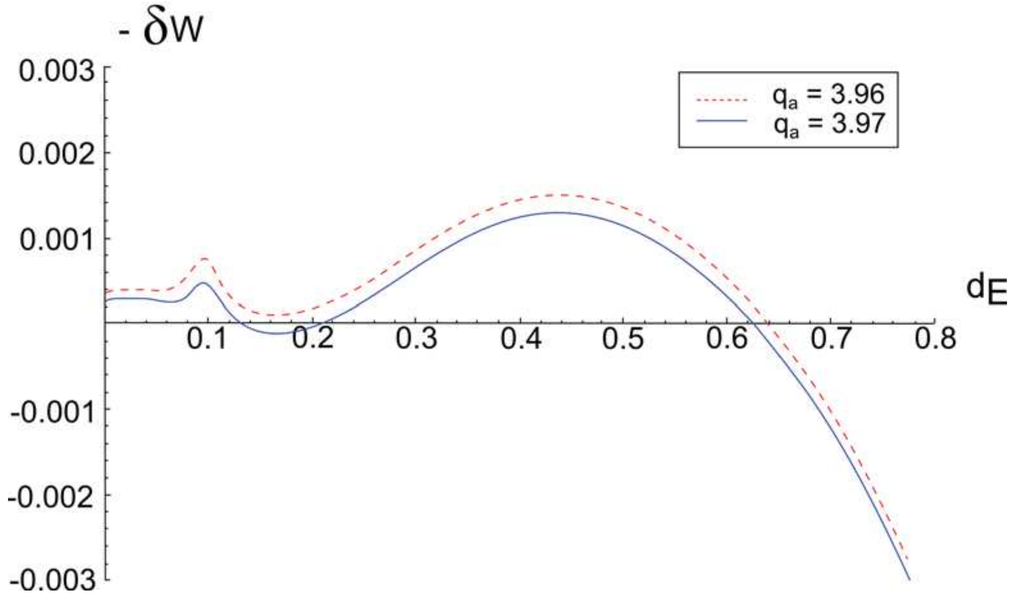

Figure 3.2: *The stability of the dominant mode, calculated by the current relaxation model, over the normalised radius of the plasma. When $-\delta W$ becomes negative the mode becomes unstable. Two cases are presented with different q_a showing different relaxation widths required for the mode to be unstable.*

Thus, a small change in the edge q can cause the relaxation radius to 'jump' discontinuously due to the contribution of the bootstrap overcoming the first unstable point. The actual values of the ELM width ($d_{E,max}$) are unrealistically large but this is a consequence of the rather idealised cylindrical model, δ function approximation of the bootstrap current, and other limitations.

This bifurcation of relaxation widths could help to understand the occurrence of small and large ELMs appearing under the same plasma conditions. The larger ELMs are interpreted as dominant low n modes with radial widths extending past the bootstrap current region, thus placing them on the upper band of the bifurcation. The loss of pressure gradient caused by these larger relaxations will greatly decrease the bootstrap current, whereupon higher n modes are predicted to become active. These then produce smaller higher frequency relaxations which do not involve the equilibrium bootstrap contribution, placing them on the lower bifurcation band. Over a subsequent time, scale that increases with collisionality, the bootstrap equilibrium current rebuilds and the process starts again.

The inclusion of RMP fields into the current relaxation model could not describe the important three-dimensional effects and coupling of the RMP fields. However, a recent suggestion based on previous stellarator work [C. J. Ham, Private Communication 2013], indicates that a possible approximation can be made through including the RMP fields as an additional q profile. This could be a future extension of the model and discussions are underway to assess the validity of the results obtained.

4 Identification and Investigation of ELMs with rotating Resonant Magnetic Perturbations

In this chapter, the ELMs occurring on the TEXTOR tokamak and the effect of applying a rotating RMP field to the TEXTOR ELMs will be investigated. The TEXTOR tokamak has unique features making it an ideal candidate for peeling dominated ELMs and also fits closely to the model assumptions due to its size and configuration. Thus the main experimental investigation in this study will be focused on TEXTOR and its unique application of RMPs through an in-vessel helical coil system presented below. Additionally, two probe heads are described which are used to make measurements on TEXTOR of the fast ion losses and localized edge currents, both of which give indications of the edge dynamics and thus the ELM behaviour. The analysis of f_{ELM} will be outlined and validated as this is a key parameter investigated in this study. The second half of the chapter will study the effect of applying a rotating RMP on the f_{ELM}, specifically looking at changes to the L/H power threshold and which of the phase and amplitude of the applied RMPs is having the greater influence. Finally, the plasma response to the externally applied fields will be investigated for different applied phases.

The TEXTOR Tokamak

The tokamak experiment for technology orientated research (TEXTOR) [128], was designed to test new concepts and materials focusing on plasma-wall interactions. To this end TEXTOR was built with easily accessible large ports and to be able to completely separate into two halves, allowing access to change the liner. The machine has a circular poloidal cross section with major radius 1.75 m and minor radius 0.47 m. The maximum toroidal field and plasma current which can be achieved are 3.0 T and 0.8 MA, respectively. It has a fully toroidal bumper limiter on the HFS, remotely movable main limiters mounted at the LFS at certain toroidal positions and a full toroidal belt limiter called the advanced limiter test II (ALT-II). Portions of all these limiters can be seen in figure 4.1 (right). TEXTOR can apply a heating power up to ~ 5.5 MW by radio frequency heating, ion and electron cyclotron resonance heating and two neutral beam injection systems which have the unique feature that they point in opposite toroidal directions allowing control of the power balance and plasma rotation. Overviews of the installed diagnostics can be found in references [129] and [130].

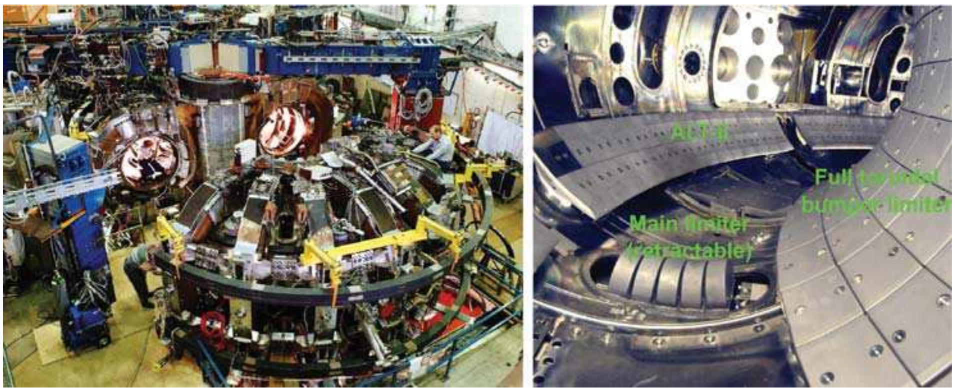

Figure 4.1: *Photographs of TEXTOR showing the tokamak separated into two halves in the reactor hall (left) and the main limiters inside the plasma chamber (right).*

The limiter H-mode

A limiter H-mode was first achieved on TEXTOR in 2006 [50]. The input power required was found to be twice that of what would of be expected for a similar sized tokamak with a poloidal divertor. The total neutral beam heating power available on TEXTOR is currently $< 3\,\mathrm{MW}$ which is sufficient to reach the L/H threshold although does not go far beyond this threshold, and so a TEXTOR limiter H-mode can be prone to regular back transitions. Typically, a low toroidal field is required between 1.3 and 1.6 T to have a sufficiently high value of beta. The plasma current is restricted between 190 and 250 kA due to operational limits, which results in a $\Delta q_a \approx 1$. Recently, the actual value of q_a is difficult to measure to a high enough degree of accuracy due to limited edge diagnostics as TEXTOR approaches its end. However the change of q_a can be approximated accurately so all dependencies stated are valid although the exact q_a value is debatable. The poloidal rotation, in the electron diamagnetic drift direction, increases across the L-H transition. A shift of the plasma position to the HFS is required for the limiter H-mode as this decreases the size of the plasma and thus increases the power density and decreases interactions with the LFS limiters. The target plasma of a limiter H-mode has a relatively low energy confinement and high levels of recycling, compared to divertor H-modes, due to the interactions with the limiters close to the plasma edge, however, an increase in the particle confinement is present.

Over the course of this study 143 separate TEXTOR shots were observed to have regions of limiter H-mode, in addition to ~ 100 previous cases. Thus, TEXTOR does indeed have relaxations of the edge caused by ELMs, although with a lower pressure drive than divertor devices indicating the ELMs are mainly current driven. No toroidal dependence in the D_α signals located at different toroidal locations has been observed for the ELM events. The ELMs observed on the TEXTOR tokamak are difficult to characterise using the standard types as set out in the second chapter. The ELMs have a high frequency $\sim$ 300-1000 Hz and have been mostly seen to have a type-III

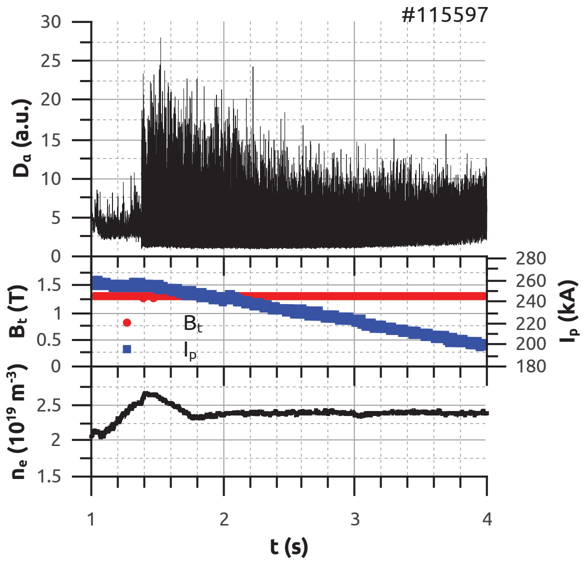

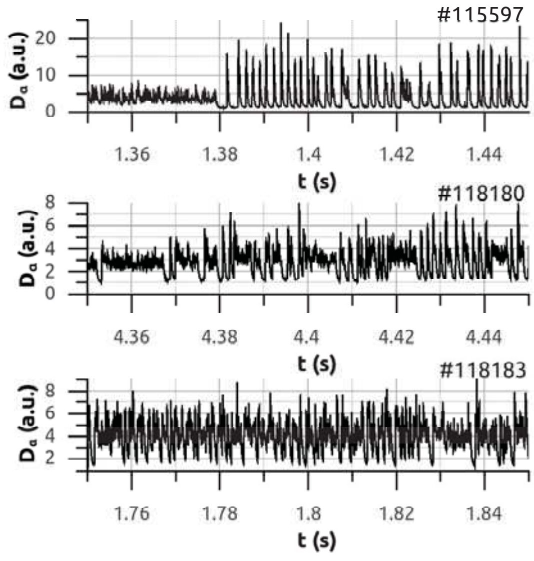

Figure 4.2: (*a*) *From top to bottom:* D_α *signal, toroidal magnetic field and plasma current, and density time traces for a typical TEXTOR H-mode shot* #115597. *The L-H transition occurs at* $\sim$ 1.4 s *seen as a large increase in the amplitude and a drop in the baseline of the* D_α *signal as well as a sharp increase in the density. The* B_{t} *is held constant as was usual for the experiments conducted, whilst the* I_{p} *is scanned across the full range available showing a large effect on the* D_α *signal.* (*b*) *Three examples of different kinds of ELMs observed in different shots making the identification of TEXTOR ELMs difficult.*

power dependence (i.e. higher heating power decreases the f_{ELM}) although type-I power dependence has been witnessed. The limiter interaction acts similarly to a large gas puffing at the plasma edge which has been seen to change the type-I ELMs to type-III ELMs on divertor devices, and so it is reasonable to compare against type-III ELMs. Type-III ELMs have also been observed when a divertor plasma is positioned in such a way so the plasma is touching a wall component which then acts as a limiter.

A typical H-mode on TEXTOR, and the D_α signals for a few different types of ELMs observed, are shown in figure 4.2. Examples of limiter H-mode ELMs observed in the D_α traces are shown in figure 4.2 (b). The top trace shows clearly defined ELMs, whereas the other two traces show examples of when the ELM identification is difficult; this issue will be discussed later. The middle trace shows a dithering H-mode due to the plasma conditions being very close to the L/H power threshold as this has a lower heating power. The bottom trace is also due to the plasma being close to the L/H power threshold as the B_{t} is higher here, producing a very noisy signal.

The quality of H-mode can be found when looking at profiles of density, temperature and pressure. On a TEXTOR limiter H-mode, these show a global increase across the profile and a small pedestal in the density although only small pedestals can be found for the temperature and pressure.

Probe Measurements of the Plasma Edge on TEXTOR

Fast Ion Losses Measured by the Directional Probe

The rotating directional probe (DP) [131] measures the ion saturation current at nine radial positions using two arrays of Langmuir pins along the probe. The first array is observable whilst the second array lies 180° round the probe hidden from view in figure 4.3. The probe is mounted on the fast reciprocating arm [132] and inserted into the plasma for a total duration of 570 ms. In this time the probe does a full rotation at a maximum speed of 4 Hz, which not only gives information about the pitch of ion losses but also distributes the heat load uniformly on the probe head.

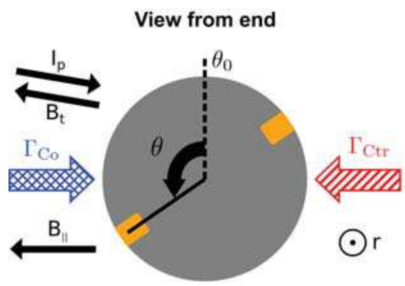

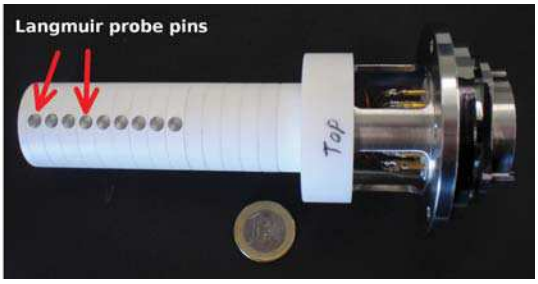

Figure 4.3: (*a*) *A schematic showing the fast ion losses measurement during a rotation of the probe.* (*b*) *Photo of the directional probe head showing one array of Langmuir probes and compared against a* 1 *euro coin for a size reference.*

The following new results are taken when the probe is plunged into a limiter H-mode with full NBI 1 and partial NBI 2 heating up to a radial position of $R_0 = 228$ cm, so that the probe is outside the last closed flux surface but beyond the limiter. As the directional probe rotates each array will pick up the co-current and the counter-current ion losses with peak measurements 180° apart. Figure 4.4 shows one example of the up-stream ion saturation current measurements for two time intervals in the same shot.

When comparing the ion saturation current with the D_α signal it is clear that during an ELM event there is a large increase in the ion losses from the plasma to the scrape off layer where the probe is situated. The data from two of the Langmuir pins on the directional probe at different radial positions, shows a radial decrease in the ion losses as would be expected for any ejection of particles from the plasma edge. Towards the

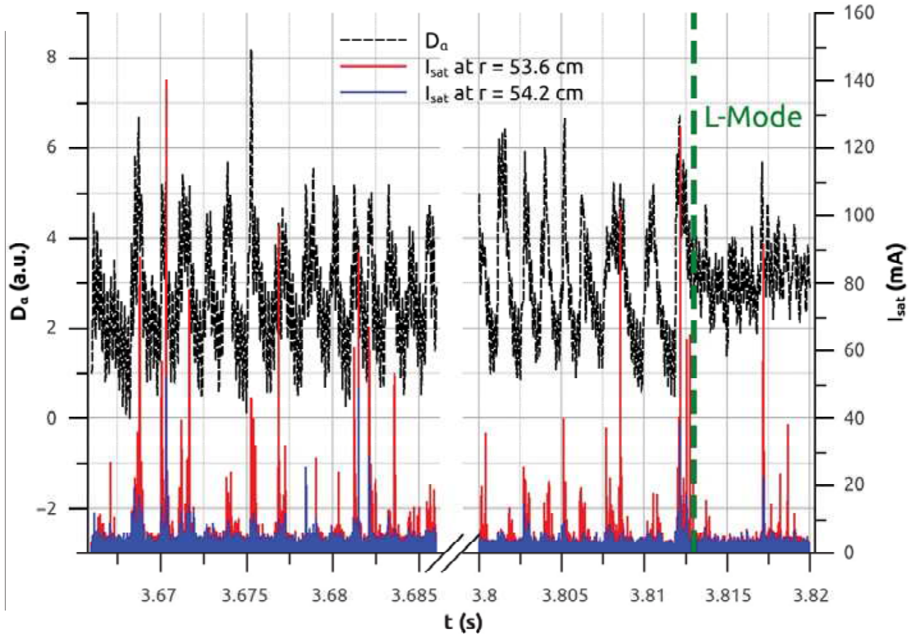

Figure 4.4: *The ion saturation current from two of the probe pins is compared to the D_α signal (black dashed) for two different time intervals from the TEXTOR shot* #119329. *The first measurement occurs when the top array of pins on the directional probe are aligned with the up-stream flow during a H-mode phase. As the probe rotates the bottom array becomes aligned with the up-stream flow at a later time interval during which a L-H transition occurs at* 3.813 s.

end of the second interval a back transition to the L-mode is seen although large spikes in the ion saturation current are still seen. The inner most Langmuir pin measurement is focused upon over one ELM period in figure 4.5, to demonstrate the nature of the fast ion losses over an ELM.

Multiple peaks in the ion saturation current can be seen which do not correlate with the applied RMP frequency observable in the D_α trace. The first peak occurs at the same time that the peak in the D_α signal occurs. The rise and fall time of the peaks in I_{sat} have the same rate and between each peak the signal goes back down to zero. This indicates a structure moving radially outwards rather than a burst which would have different rise and fall times of I_{sat}. The number of peaks varies between zero and 5 for different ELMs, although three peaks is the most common case observed to date. If this is indeed a radially moving structure, then the radial propagation speed can be calculated from the time difference between the Langmuir pins. Figure 4.6 shows a cross correlation from the first three top pins.

The difference in the peak points gives the lag of the data and thus the drift is found as the radial propagation speed. This turns out to be $1200\,\mathrm{ms}^{-1}$ compared to the usual

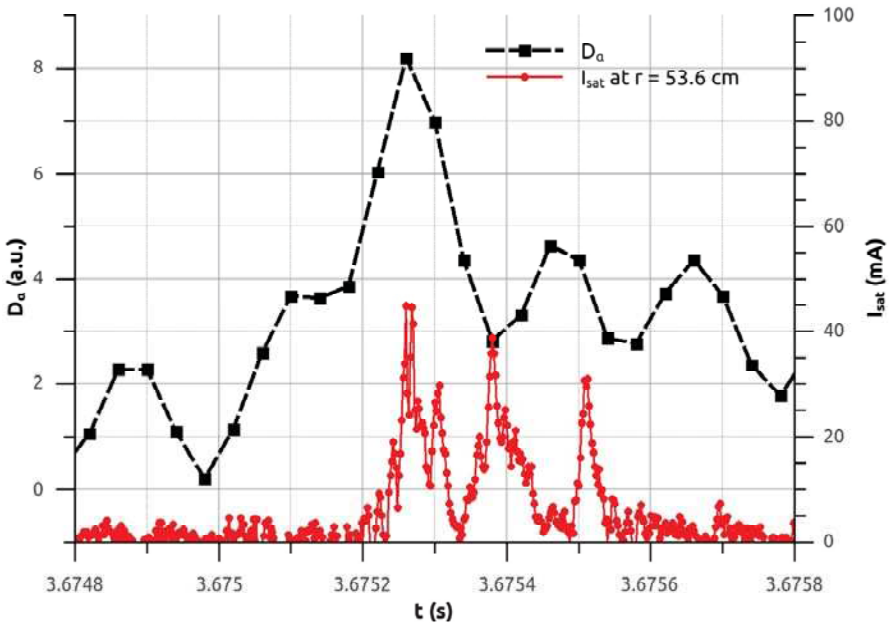

Figure 4.5: *The ion saturation current measured by the inner most Langmuir pin on the directional probe for one ELM event represented by the increase in the D_α signal. The oscillations in the D_α signal are due to the applied RMP field.*

ohmic case on TEXTOR where the ion losses are thought to have a radial propagation speed of 200 ms^{-1}. This figure is close to the radial ELM filament speed calculated using the rise of the saturation current on MAST where filaments were seen to travel with radial velocities ranging from 500 to 2 kms^{-1} [133]. One question which arises is, if these are ELM filaments then why are they observed to coincide with the D_α peak, the inward particle flux from the wall, which should only occur once the ELM filament has already passed the probe head. This could be a discrepancy in the timings of the signals although a more likely explanation is that these peaks are caused by a secondary structure rather than the main ELM filament. Similar multiple bursts in the fast ion losses when an ELM event occurs have been reported on the ASDEX-U tokamak although over a much longer period of time due to different types of ELMs being measured.

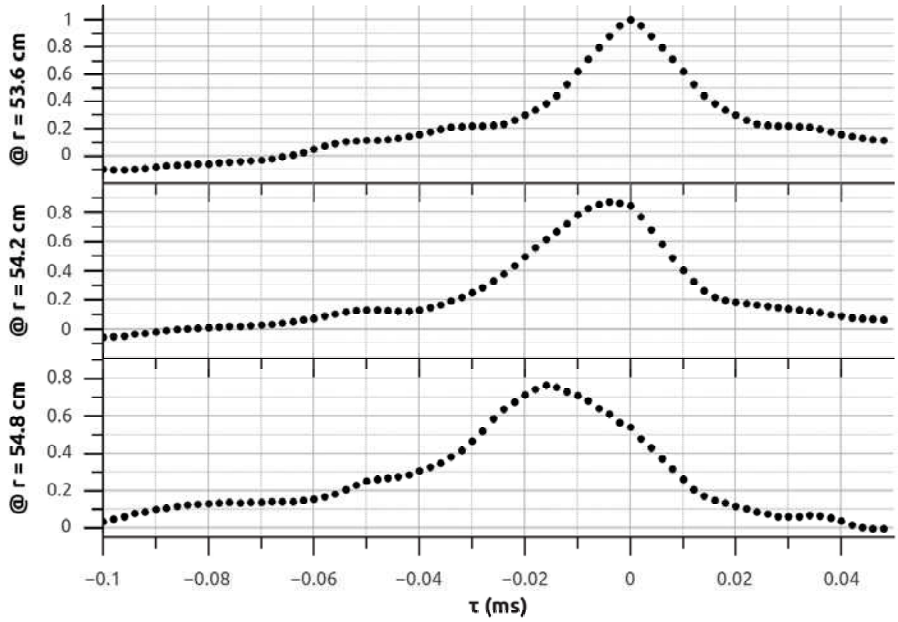

Figure 4.6: *Cross Correlation of the three inner most pins on the directional probe head showing a time difference in the measurements caused by a radial propagation of ions.*

Plasma Response Measured by the Magnetic Probe

The fast moveable magnetic probe (FMMP) was designed to measure the plasma response to an AC DED perturbation. The probe head has three sets of three pick up coils measuring the toroidal, poloidal and radial magnetic signals at different radial positions 5 mm apart. Similar to the directional probe, the FMMP can be fixed onto the fast reciprocating arm and inserted into the low field side of a TEXTOR plasma up to $R_0 = 213\,\mathrm{cm}$. As the magnetic probe is built as one unit, it can tolerate higher mechanical stresses and so can be inserted into the plasma with a higher speed than the directional probe, $\sim 0.8\,\mathrm{ms}^{-1}$.

In this investigation the FMMP was inserted into the edge of a H-mode plasma up to $R_0 = 217\,\mathrm{cm}$. The presence of the probe would alter the edge topology, as this would act as a small limiter, and so only measurements on the way into the plasma are considered here in order to avoid invalid results. For this study the probe was used to measure the plasma response from the plasma by measuring the total local perturbed magnetic field in toroidal, poloidal, and radial directions, and then subtracting the vacuum contribution through a cross correlation with a calibration shot.

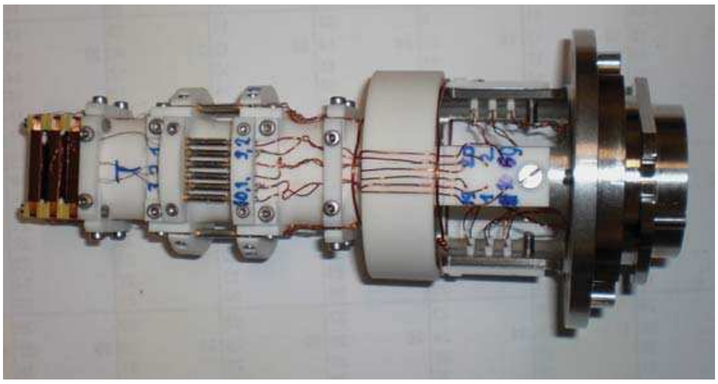

Figure 4.7: *Photo of the uncovered magnetic probe head. The three sets of copper windings observable are the pick up coils, allowing for a small radial profile measurement. A Boron Nitrate cover protects the probe from the plasma although this is not shown here.*

Identification of Edge Localized Mode Frequency on TEXTOR.

Recently, on TEXTOR the identification of the ELMs and their effect on the plasma has been difficult due to a lack of edge diagnostics as the machine approached its finish. Without a temperature profile measurement the size of the ELMs is unknown, however, the frequency of the ELMs can be identified through either D_α emissions, hydrogen cyanide (HCN) interferometer density measurements, or the Mirnov coil signals. Here, the D_α signal is utilised as it has a high frequency of 100 kHz and is reliable for the entire shot time. For each ELM event the D_α signal increases by a factor of $10-30$ depending on the type of ELMs present seen in figure 4.2 (b). Care has to be taken to distinguish ELM events from the background noise and also from any double signals created by wall recycling or faults in the data acquisition. The signal is therefore processed with a cut-off of $a \times \sigma_c$, where σ_c is the r.m.s of the D_α signal and a is a constant that is optimised to keep the cut-off above the noise level of the shot. Before and after each ELM the signal will be below the cut-off value and so defines an inter ELM region.
In this region the maximum value gives the highest value of emissions which, although this does not define the ELM size or precise time, still can be used to identify a single ELM event and so can be used for this frequency calculation. An example trace is shown in figure 4.8 (top) where each star denotes an identified ELM.

The middle trace in figure 4.8 is useful to see the general trend of the f_{ELM} during the shot, although an averaging is required to get a reasonable value. The distribution of the ELM frequencies calculated is shown in the bottom trace of figure 4.8.

Over the course of the measured results the f_{ELM} calculation has been verified several times using both the HCN and Mirnov data as well as utilising a fast infra-red (IR)

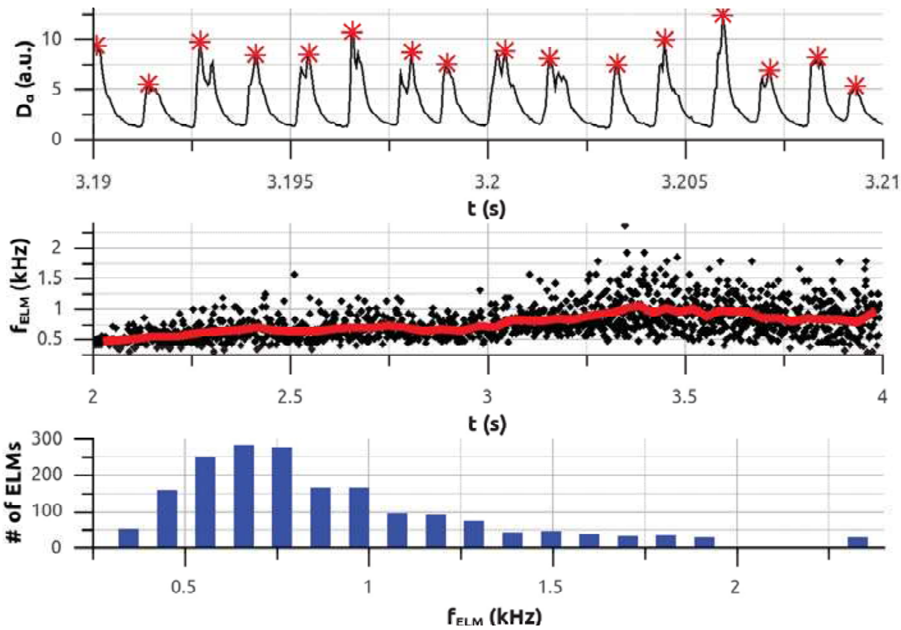

Figure 4.8: *(top) A section of the D_α trace showing a series of ELMs. Each identified ELM is highlighted with a star whilst ignoring double peaks which are not additional ELM events. (middle) A plot of the varying trend of ELM frequencies observed across the shot, with a simple mean value plotted as the red line. (bottom) The distribution of ELM frequencies for the entire shot shows a Maxwellian distribution.*

camera. The camera is a FLIR $SC7500MB$ with a frame rate of 14 kHz measuring light with $\lambda = 2 - 5\,\mu$m, directed at the insertion depth of the FMMP, which when applied into the plasma acts as a limiter. The increase in temperature for each ELM event can be seen in figure 4.9 giving an $\sim f_{ELM}$ of 430 Hz and average temperature rise of ~ 200 K.

Unfortunately, this could only be used for one set of results as the majority of the H-mode experiments on TEXTOR use Deuterium in both beams into a Deuterium plasma causing a large amount of neutrons which are harmful to the camera. Thus when installed the beams were applied with hydrogen although this was found to give a weaker H-mode due to the acceleration of the neutrals in the beams being smaller.

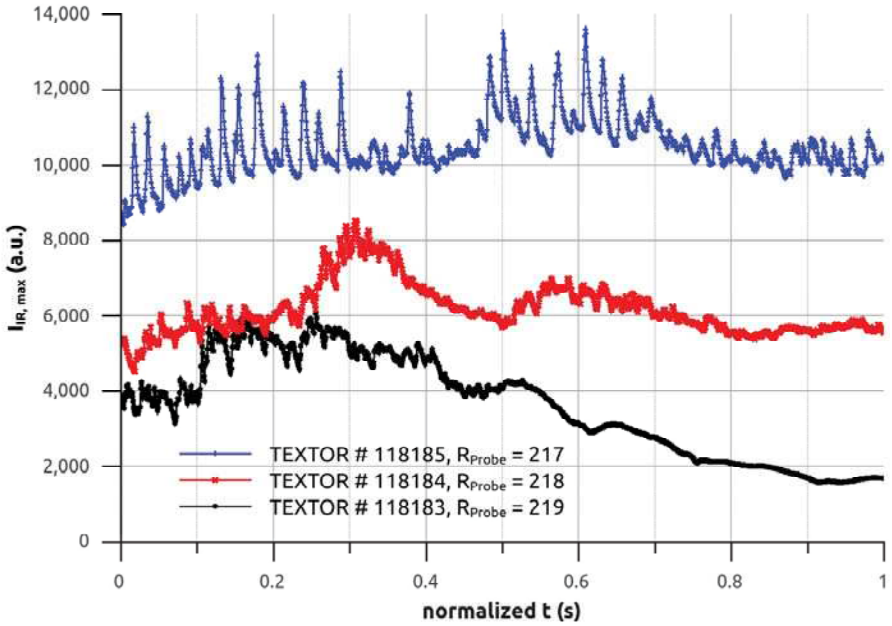

Figure 4.9: *Emission intensities from the IR camera for three consecutive shots, #118183, #118184, and #118185, with the FMMP inserted into the plasma at 219 , 218 and 217 cm, respectively. As the camera is not calibrated for the probe head material the exact temperatures are not shown here but the approximate change in temperature can be calculated. As the probe is inserted deeper towards the plasma edge the temperature increases. For the insertion depth of 217 cm a noticeable increase in the density is seen and the ELM behaviour changes indicating the probe is touching the plasma i.e. is in the last closed flux surface. At this point the temperature on the probe head can be seen to increase rapidly and the ELM structures can be observed in the sudden temperature spikes.*

Effect of Rotating Resonant Magnetic Perturbations on ELMs

So far the focus has been on the natural ELMs on TEXTOR and how to identify them. This section will investigate the effect of rotating RMPs applied through the unique dynamic ergodic divertor on TEXTOR.

The Dynamic Ergodic Divertor

In 2003, the dynamic ergodic divertor (DED) [135] was installed on TEXTOR in order to investigate the effects on the heat exhaust, plasma confinement and impurity screening, when the transport parameters are influenced by helical magnetic fields. This consists of 16 helical coils wrapped around the central column on the HFS (which therefore stops TEXTOR from separating into two halves as before). Either static DC or up to 5 kHz

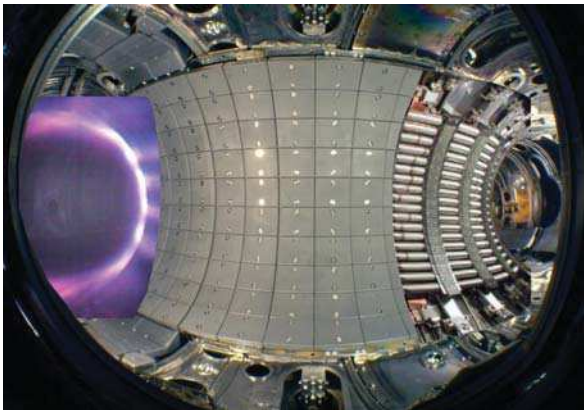

(a)

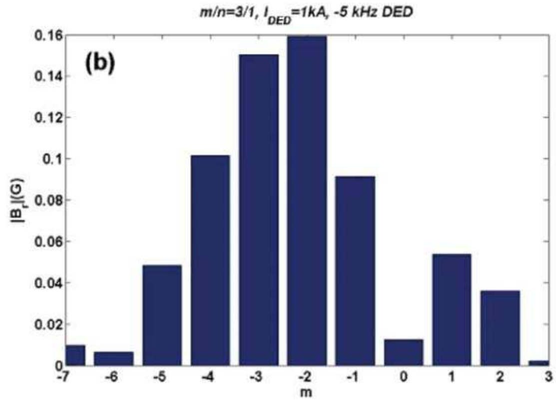

(b)

Figure 4.10: (*a*) *A wide angle view of the inside of TEXTOR showing the DED coils uncovered at the right side, the limiter shielding in the middle, and the effect on the plasma in the left of the image.* (*b*) *The radial components of the Fourier spectrum for the* $3/1$ *DED measured at the LFS [134].*

rotating helical fields can be induced into the edge of the plasma using the DED coils which are aligned with the $q = 3$ surface. The rotation direction of the rotating fields has the convention of being positive for the counter-current direction which is also the electron diamagnetic drift direction.

The effect of the DED on the plasma can be seen by looking at the HFS of the part of the photo including the plasma in figure 4.10. Clear striated structures are formed with regions of high and low interaction deep into the plasma, especially in the 3/1 configuration. This creates a helical divertor and an ergodized region but also tearing modes have been seen to be excited [136].

Observations of the Effect when Rotating Fields are Applied to a Limiter H-mode

The DED on TEXTOR has the unique capability to apply rotating perturbation fields in both co- (-) and counter (+) current directions. As the DED is wrapped around the centre column of TEXTOR the perturbation fields applied are helical in nature. Over the course of this study the DED is set in the 3/1 configuration so that the fields are aligned with the $q = 3$ surface. The alignment of the helical fields has the advantage of greater near field effects than experiments with external perturbation coils. Thus, it is useful to fully investigate the unique features of the DED and assess if major advantages are present when using such a system for future control schemes, before the shut down of TEXTOR at the end of 2013.

Previous studies of the effect of the DED on a limiter H-mode in TEXTOR have concentrated on the impact of the applied perturbation mode spectrum on the transport and formation of structures in the edge of the plasma. The 6/2 configuration has been focused upon, as this has been seen to have the largest operational region with a significant impact on the D_α bursts associated with the ELM events when a DC field was applied with an increasing amplitude (see figure 8 of reference [136] and figures 2 and 3 of reference [137]). A decrease in the pedestal pressure height was also seen as the I_{DED} increased, found to be mainly due to a drop in the temperature rather than in the density, as it would be for a back transition from H- to L-mode, (see figure 3 of reference [138]). The density pump-out effect has been shown on TEXTOR only when the DED is applied with high amplitudes [86], suggesting a triggered mechanism such as magnetic reconnection becoming apparent at a perturbation threshold. In the L-mode plasmas investigated, an improvement of the plasma confinement (increase of 20%) was seen when applying the DED due to a density barrier forming depending on the value of q_a [139].

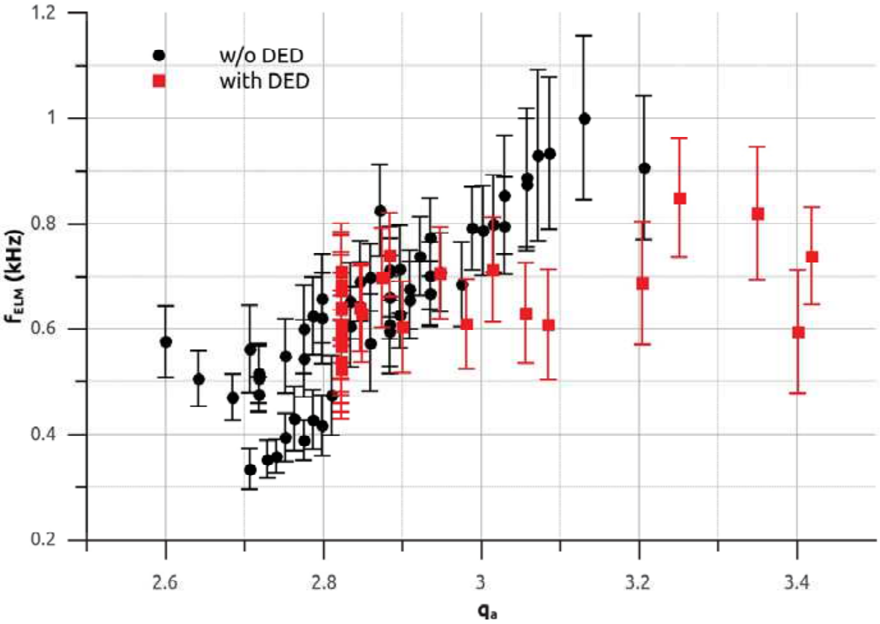

Figure 4.11: *Comparison of scanning the edge safety factor with (red squares) and without (black circles) the* -5 kHz *DED applied at a density of* $2.4 \times 10^{19}\,\mathrm{m}^{-3}$.

Here the DED was applied with ± 1 kHz, ± 5 kHz rotating and static fields with a maximum $I_{DED} = 0.8$ kA, as this is the operation limit for the 5 kHz case. The 3/1 mode has a deeper penetration into the plasma and can easily excite 2/1 tearing modes, possibly causing disruptions, and so has a much smaller operational region than the 6/2 configuration. Figure 4.11 shows a q_a scan including data with and without a -5 kHz DED applied at the same plasma density.

The change in the q_a dependence is striking and unexpected. Previous results from other tokamaks show the application of RMPs to increase the f_{ELM} or completely suppress the ELMs, but rarely decreases the frequency. Even results on TEXTOR in the 6/2 configuration, show a strong increase in the f_{ELM} when the DED is applied as already mentioned. Unfortunately, due to the appearance of low q instabilities killing the plasma, it is unclear if the results are showing a constant f_{ELM} with no dependence on q_a or whether the dependence has only been lowered after $q_a = 3$. An interesting point is made when looking at the q_a range available. It seems that the range has been shifted to higher values of q_a when the DED is applied. A possible explanation is due to the high dependence of the q_a on the value of the minor radius, defined up to the last closed flux surface, which would be decreased when the edge of the plasma is ergodized, thus increasing the calculated value of q_a.

In figure 4.12, two time segments showing the D_α signal from the same shot are shown; one without the DED, and one with. The D_α bursts have a greater level of noise, partly from near field oscillations changing the inward particle flux due to the DED, and partly due to an increase in the emissions between ELMs. Although the D_α baseline appears to decrease, this is due to the DED vibrating the plasma which would directly effect the inward particle flux, and so the average baseline is actually still at the same level as the case without DED. The height of the bursts has decreased when the DED is applied although the frequency remains constant at $\sim 650\,\mathrm{Hz}$, which is to be expected at this value of q_a when comparing with figure 4.11.

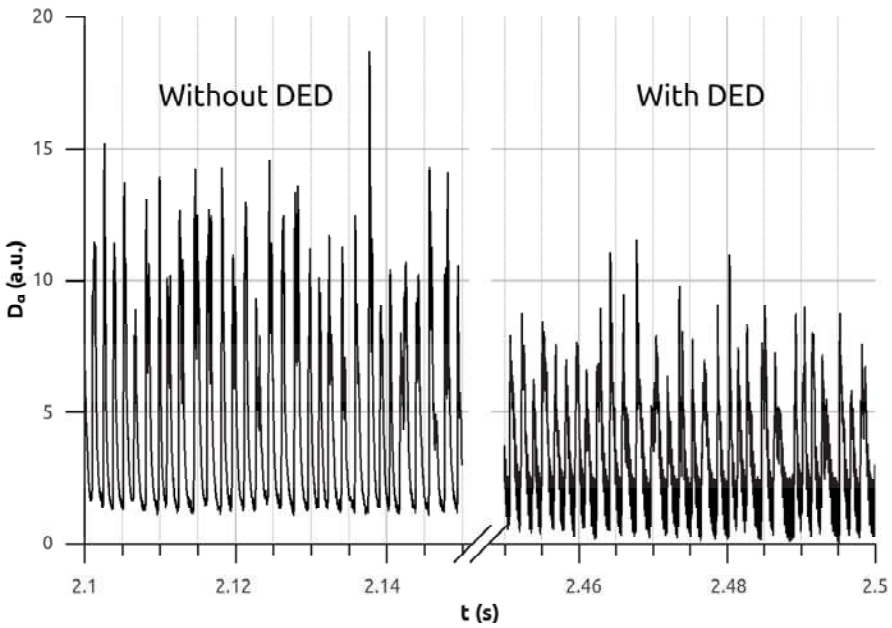

Figure 4.12: *Two time periods from TEXTOR shot* $\#119837$ *without (left) and with (right) the DED applied at* $-5\,\mathrm{kHz}$ *at* $q_a = 2.76$.

Effect of Rotating Fields on the L/H Power Threshold

The phase and frequency of the applied perturbations is expected to have an effect on the plasma and ELM behaviour, due to the interaction with the plasma rotation and resonances to different frequencies. Firstly, the effect of the different rotating fields on the L/H transition was investigated by looking at the density threshold required to enter the H-mode, observed as a sudden jump in the density and a large drop in the emissions picked up by the D_α signal. Figure 4.13 presents data of the line averaged density dependence on the plasma current, with a -5 kHz DED field applied, and on the DED phase at the first L/H transition of the plasma.

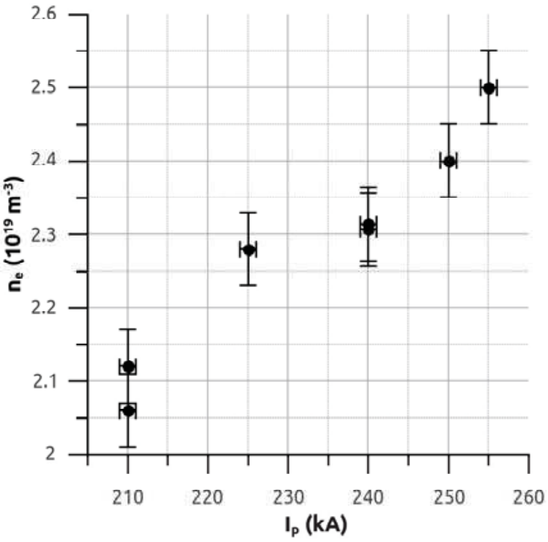

(a)

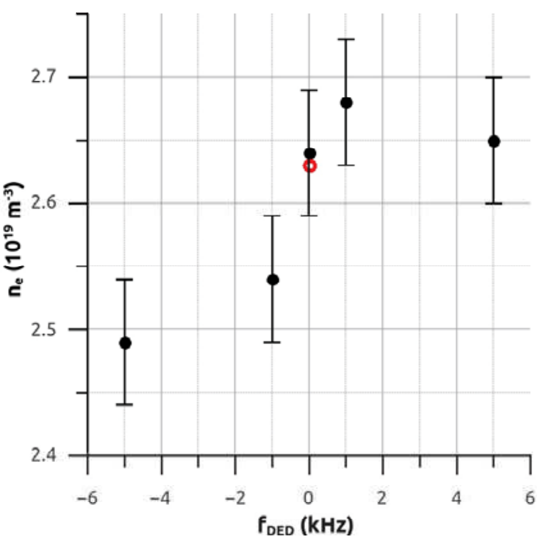

(b)

Figure 4.13: The density at the point where the plasma goes into the H-mode for the first time for (*a*) *a plasma current scan with a* -5 kHz *DED field* and (*b*) *for different DED phases at the same* I_p. *The red hollow circle gives a typical transition density threshold without any DED applied.*

The access to the H-mode is commonly characterised by the L/H power threshold. This is mainly dependent on the plasma density, showing a linear increase for medium to high densities across a range of tokamaks [140]. At low densities the power threshold has an inverse linear dependence, meaning that the power threshold has a minimum value of density where it is easiest to enter the H-mode [141]. Interestingly, figure 4.13 (a) shows a linear dependence of the density threshold on the plasma current which is not seen for plasmas without the DED applied. This is a new result and difficult to understand as previous scaling for the L/H transition has only taken the plasma density, magnetic field and size of the confined plasma into account [142]. As on TEXTOR the power available is quite low, the limiter H-modes created have to be as close to this minimum density threshold as possible which the I_p may be affecting.

Figure 4.13 (b) shows that the L/H density threshold depends on the phase of the DED suggesting that the -5 kHz case allows easier H-mode access. Previously it has been seen that the presence of static RMPs hinders the formation of the H-mode through increasing the edge transport. This result shows one possible advantage of using rotating RMP fields instead.

Rotating Field Amplitude and Phase Dependence on Edge Localized Modes

The effect of the different DED phases and frequencies on the ELM behaviour in TEXTOR was investigated. The I_{DED} was slowly increased during a limiter H-mode while monitoring the ELM frequency. Figure 4.14 (a) shows two sets of data from this scan at different densities. A separate scan was made, during a DED flat-top, of the q_a dependence for each of the four different DED cases, seen in figure 4.14 (b).

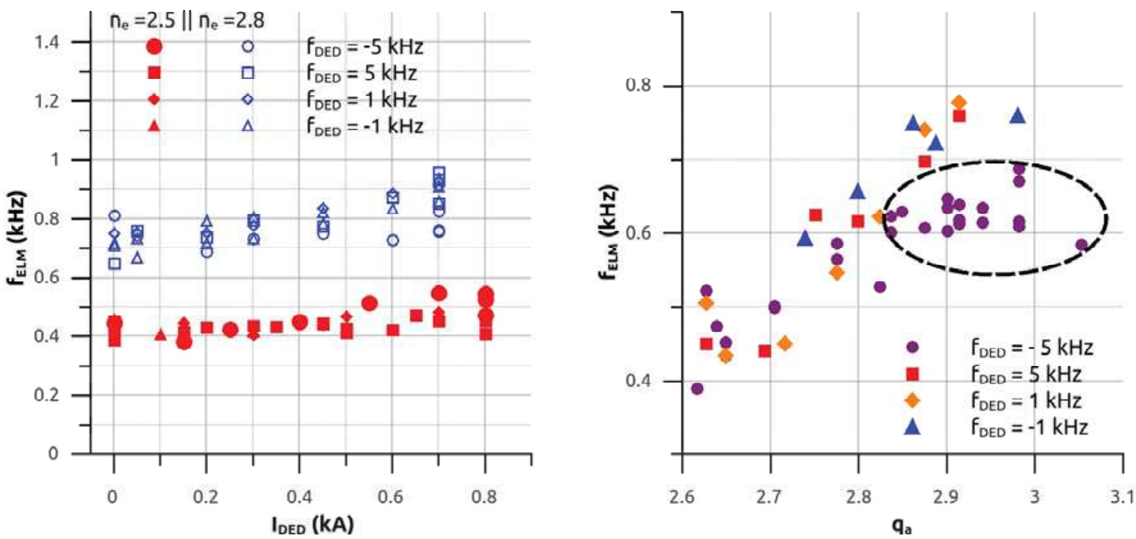

(a) (b)

Figure 4.14: *(a) Different DED phases are represented by different symbols but all have a similar trend. The open symbols have a higher density than the closed symbols agreeing with the density dependence observed in figure 5.11. (b) The q_a dependence on f_{ELM} with DED for the four different phases. Highlighted is a region where the -5 kHz case shows a different dependence.*

For a single value of q_a, the dependence of I_{DED} for all four phases, at both densities, shows little effect on the f_{ELM}. This indicates that the effect of the DED seen in figure 4.11, is not dependent on the I_{DED}, at least not up to the maximum applied here of 0.8 kA. As stated in experiments on other machines which apply RMPs, a threshold of I_{DED} was always found, also seen before on TEXTOR with the 6/2 configuration although at a much higher I_{DED}.

So the focus shifts to the q_a scan for different applied fields whilst holding I_{DED} at the maximum available. This shows several interesting features, firstly, this data seems to go against that previously shown in figure 4.11 as the plasma current dependency is present and low q_a values are calculated for all four cases. As figure 4.11 focused on a comparison with the -5 kHz DED this suggests that the other three phases have little effect on the q_a dependence and that the plasma current effect seen without the DED remains dominant. As for the -5 kHz case, the density was lower and this shot was not repeated so the data could not be plotted in figure 4.11. However, it does show the same constant f_{ELM} from $q_a = 2.8$ onwards and therefore suggests that the observations made earlier are due to an effect of the interaction of the -5 kHz DED field with the $q = 3$ surface. The idea of a coupling between the $q = 3$ surface and the -5 kHz RMP fields is backed up when looking at the magnetic frequency spectrum's from the Mirnov coils. It can be seen that 3/1 mode locking occurs at the point when the -5 kHz DED case starts to have a different nature from the other three DED fields applied. Thus the effect of the DED on f_{ELM} in this study depends more on the plasma response, which depends on the q profile, than on the strength of the applied field.

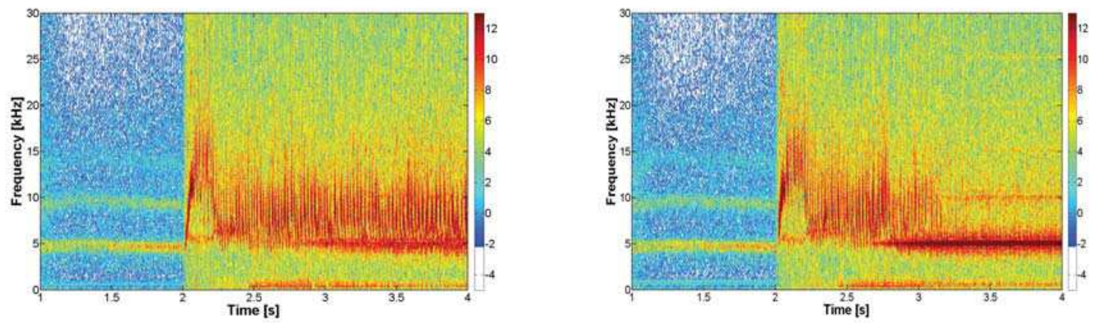

(a) (b)

Figure 4.15: Magnetic frequency spectrum's calculated on TEXTOR using the Mirnov coils for (*a*) *shot* #118441 *with* +5 kHz and (*b*) *shot* #118441 *with* -5 kHz. *Notice the mode locking to the DED frequency for the* -5 kHz *case. This occurs at the point that the* $q_a = 3$ *surface enters the plasma.*

This effect was not always observed when a different NBI ratio (i.e. an increased NBI 2 and decreased NBI 1) was applied. The ratio of NBI powers has a high effect on the toroidal rotation due to the opposing directions of the beams. This has been previously reported to have a large effect on the 2/1 tearing mode threshold [143] as this depends on the frequency shift between the MHD frequency and the external magnetic perturbations.

Plasma Response to Externally Applied Fields in the Limiter H-mode

When discussing the effects of any external field on a magnetically confined plasma, the response of the plasma to that field needs to be considered. It is well known that a "screening" effect exists whereby the plasma partially or fully shields external magnetic fields on the rational surfaces, and that this is essential for a stable tokamak operation as it acts as a damping mechanism.
The screening current is produced by the motion of the electron fluid across field lines, inducing eddy currents localized on the rational surfaces perturbed by the external field. These currents oppose and compensate the applied fields, hindering magnetic reconnection. The level of screening is highly dependent on the difference between the rotation frequency of the applied RMPs, Δf_{DED}, and the electron perpendicular rotation, $\nu_{\perp}^{e}$, called the slip frequency. $\nu_{\perp}^{e}$ has two components: the electromagnetic torque, produced by an $\boldsymbol{E} \times \boldsymbol{B}$ force at the plasma edge; and the electron diamagnetic drift, dependent on the gradient of the pressure. The neoclassical toroidal viscosity torque, due to the braking of the toroidal magnetic symmetry by the RMPs [144, 145] should be considered as this also has a large effect on the plasma rotation.

If the external fields overcome the screening effects then partial or full magnetic reconnection occurs on the resonant rational surface leading to "field penetration", observed through a dramatic braking of the plasma. Alternatively, an indication of whether the fields have penetrated into the plasma can be found when looking at the phase and amplitude of the magnetic signals at the plasma edge. Using the fast moveable magnetic probe, a measurement of the response of the plasma to the external fields can be calculated. Screening is observed as a current with a single peak at the surfaces due to the eddy currents. When penetration occurs, the formation of static (relative to the RMPs) magnetic islands on the rational surfaces creates a zero point in the perpendicular magnetic field, and so radially this is seen as a current consisting of two peaks with opposing amplitudes $\pi/2$ out of phase with each other. This is due to the reversed gradient of the magnetic field either side of the island. Pictorial representations of both currents are shown in figure 4.16 The change from one current to another will be seen as a phase change of $\pi/2$ at the resonant rational magnetic surface.

The plasma response was investigated when applying a ± 5 kHz DED field in both co and counter current phases, with a constant amplitude of 0.7 kA and applying a I_{p} scan from 255 to 195 kA. Figure 4.17 shows the results comparing the two phases. The

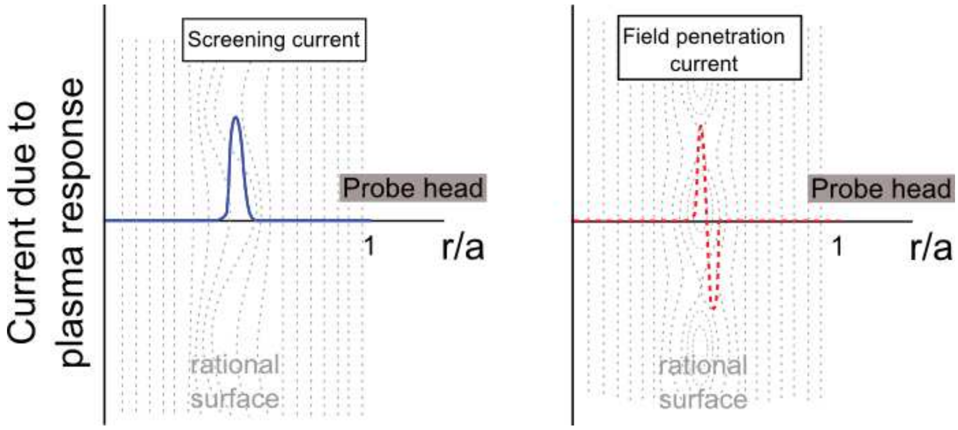

Figure 4.16: *Schematics of a partial screening current (left) and the current produced by the formation of islands when field penetration occurs (right). The probe is shown to illustrate that the observed current the probe measures has a $\pi/2$ phase shift between the two cases.*

calculation consists of a cross correlation between the measured signal from the FMMP, B_{total}, and the applied DED current in order to extract the component of B_{total} which fluctuates with f_{DED} called δB_{total}. The plasma response B_{plasma} is found when taking away the vacuum field B_{vacuum} found through the measured signal when applying DED without plasma.

The plasma responses from both DED phases, show a large dependence on I_p due to the resonant surface closest to the edge of the plasma, which would have the largest measured component of plasma response, moving away from the probe head as q_a increases. Also, as the I_p increases the β_N also decreases, affecting the torques in the plasma and allowing resonant field amplification effects to grow (see next chapter). However, as seen by the plateau in the +5 kHz case, this dependence is not always linear.

An interesting feature is seen for the +5 kHz case at ~ 2.85 s when a phase jump is observed as the plasma moves from L- to H-mode. This suggests that the screening is stronger in the H-mode region, although only a small change is seen in δB_{plasma} where the measurement seems to saturate for a period of time creating the previously mentioned plateau. The change in screening over the L/H transition comes through the E_r at the edge of the plasma increasing in the ion diamagnetic drift direction and thus altering the $\boldsymbol{E} \times \boldsymbol{B}$ force. The increase in pressure that comes along with the H-mode formation, would also change the screening through the electron diamagnetic drift term in $\nu_\perp^e$. After the sudden phase jump there is a smooth change in the phase, characterising the screening evolving slowly towards field penetration which is a much more common observation. This phase sensitivity maybe being enhanced by the low value of q, allowing disruptions to occur with the formation of small islands. A L/H transition can also be seen in the -5 kHz case with a possible change in the plasma

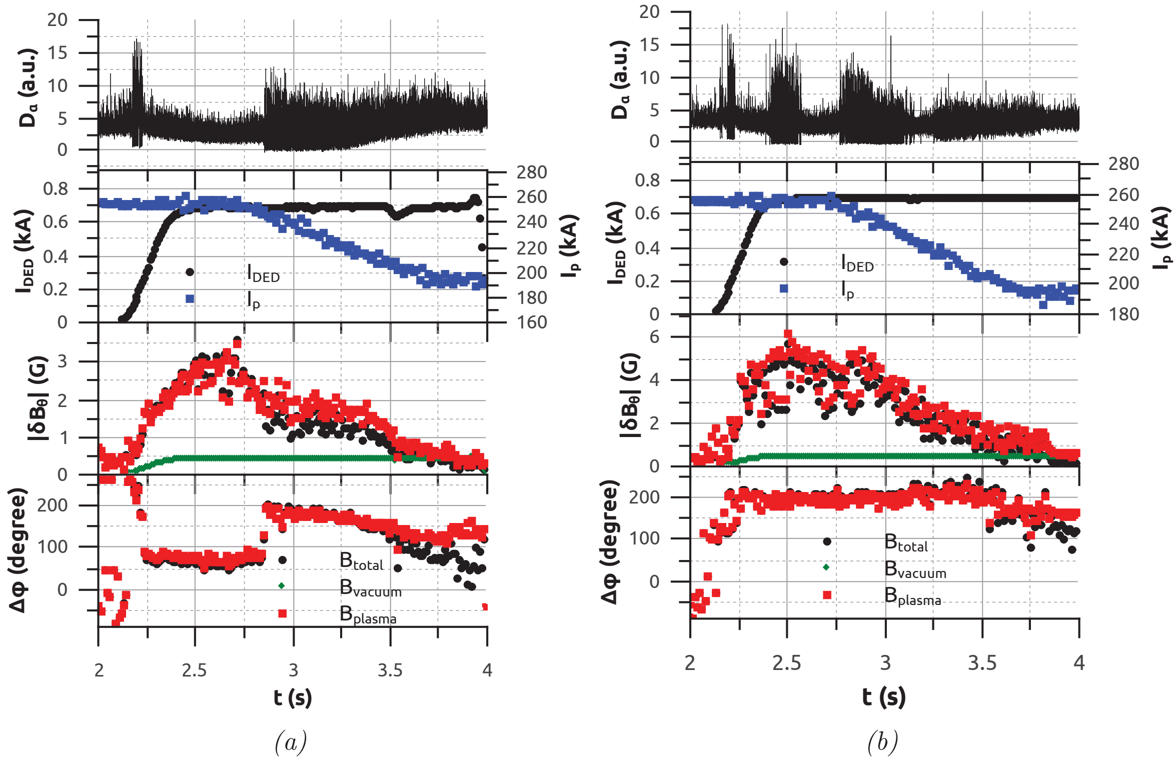

Figure 4.17: (Top) D_α signal, (middle upper) DED and plasma currents, (middle lower) magnetic signals for the total field measured from the FMMP (black circles), vacuum case without plasma (green diamonds) and the calculated magnetic response from the plasma (red squares), and (bottom) phase of δB_{total} (black) and δB_{plasma} (red) relative to the vacuum field. (*a*) +5 kHz *DED.* (*b*) −5 kHz *DED.*

response but no change in the phase.
The −5 kHz case has almost twice the amplitude of plasma response than the +5 kHz due to the difference in rotation. As the −5 kHz case rotates in the opposite direction to the electron fluid across the filed lines, the screening will be enhanced compared to the +5 kHz case where the rotation of the DED is in the same direction as the motion of the electron fluid and so relatively the velocity of the electron fluid is decreased.

Previous studies have been conducted on TEXTOR to investigate the plasma response in ohmic plasmas [134]. A direct comparison between the H-mode and ohmic scenarios is inadvisable due to higher β_N and increased rotation as the H-mode plasma has NBI beams applied and low B_t. However, it is still of interest to compare the main results and observations. Figure 4.18 shows the plasma response over an edge safety factor scan for both ±5 kHz DED phases.

The −5 kHz case saw no change in the plasma response across the $q_a = 3$ surface, whereas the +5 kHz case sees a large drop, as seen in figure 4.18. Both phases were

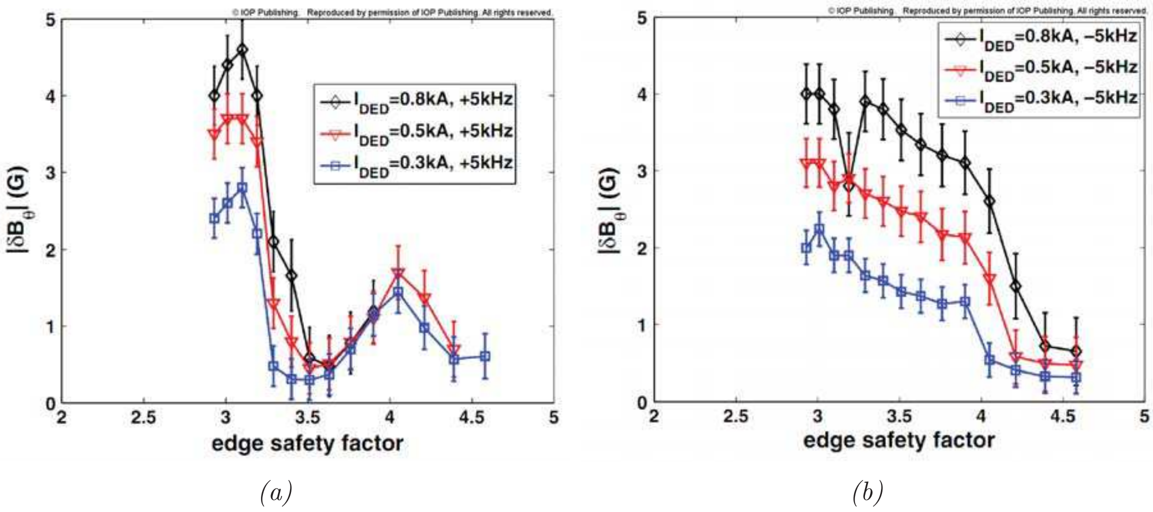

Figure 4.18: *Comparison of the plasma response over a q_a scan for (a) +5 kHz and (b) −5 kHz DED in L-mode plasmas on TEXTOR [134].*

seen to have a drop in the plasma response over the $q_a = 4$ surface. The lack of change over the $q_a = 3$ surface for the −5 kHz was explained due to the similar amplitudes of the $m = -2$ and $m = -3$ harmonics, shown in figure 4.10 (right), meaning that no significant difference would be seen when the 3/1 surface is introduced, compared to the 4/1 and 5/1 surfaces. It was also found that for the ohmic cases the +5 kHz rotates at a frequency closer to the MHD frequency [146] than for the −5 kHz case where the MHD frequency is defined as,

$$f_{MHD}(r_s) = \left[\frac{m}{2\pi r}\left(E_r + \frac{\nabla p_e}{en_e}/B_\phi\right)\right]_{r=r_s}, \tag{4.1}$$

and r_s denotes the position of the rational surface. This means that the formation of islands at the edge is more likely to occur for the +5 kHz phase and could explain the phase jump when entering H-mode for the +5 kHz case, as field penetration could be present in the L-mode and then as the plasma enters H-mode, the screening effect increases. This would be less likely to be seen in the −5 kHz case as the islands are more difficult to form.

Saturation of Plasma Response

The amplitude of the DED will have a large effect on the plasma response and may show a transition from screening to penetration as I_{DED} increases over a threshold value. This was investigated for the ± 5 kHz whilst holding I_p constant shown in figure 4.19.

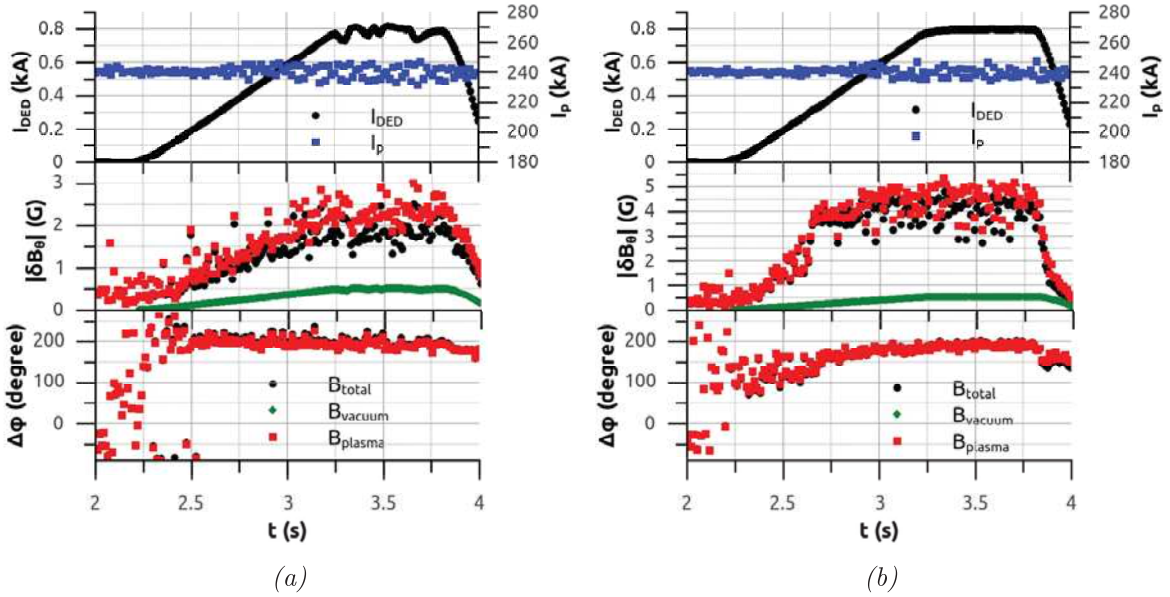

Figure 4.19: Same plots as figure 4.17 but without the D_α signal and this time scanning the DED amplitude whilst holding I_p at 240 kA. (*a*) +5 kHz *DED.* (*b*) −5 kHz *DED.*

Clearly, the plasma response increases as the DED amplitude increases as would be expected. However, a difference is seen between the two DED phases, when for the −5 kHz case the plasma response has a sudden increase to a saturated value, even though the I_{DED} continues to increase. This saturation of the plasma response has been further investigated by looking at when the saturation occurs for different plasma currents in figure 4.20.

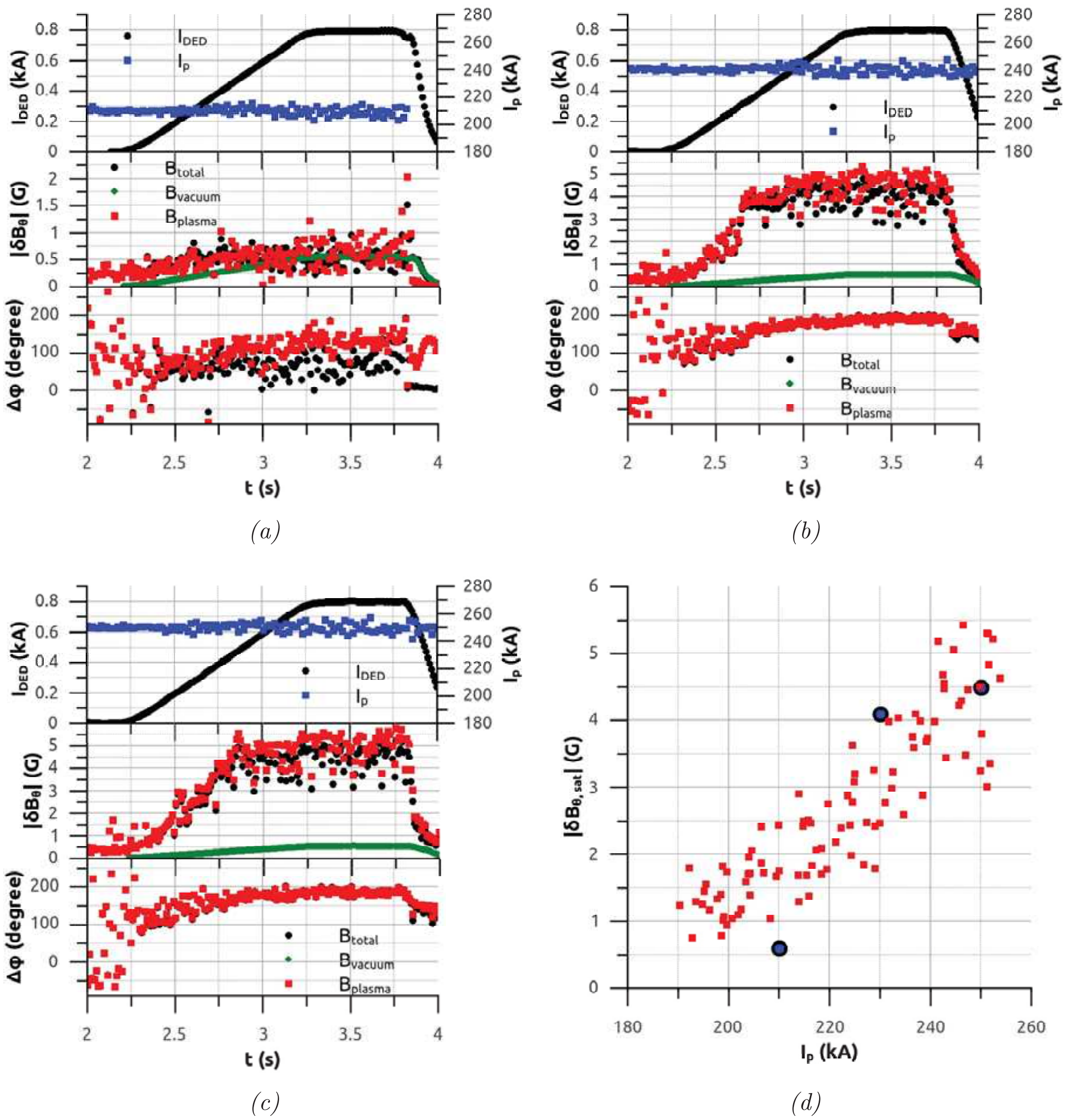

Figure 4.20: (*a*)(*b*)(*c*) *Same plots as figure 4.19 but only with* $-5\,\mathrm{kHz}$ *fields and constant* $I_\mathrm{p} = 210$, 240 *and* $250\,\mathrm{kA}$, *respectively.* (*d*) *The level that the plasma response saturates at for different values of plasma current. This scan includes the three points shown in figures 4.20(a), (b), and (c) shown as the highlighted blue circles, but also a full scan of the* I_p *dependence on the saturation level taken from figure 4.17.*

For each case in figure 4.20 the plasma response increases at a non-linear rate to the I_{DED} and saturates before the end of the DED ramp. The value that the plasma saturates at is dependent on the current and can be seen to be linear when a full I_{p} scan is conducted. As discussed the distance of the integer rational surface to the edge will be being decreased as I_{p} increases, allowing a larger response, although this explanation would expect to see a large drop in the response as an integer surface is crossed. As the Δq for the I_{p} scan is < 1 it is possible that no integer q_a has been crossed. This would seem to be at odds with the approximate value of q_a given in figure 4.11 which sees a $q_a = 3$ occurring for $I_P \sim 225\,\mathrm{kA}$ although it should be remembered that the q_a value is changed when the DED is applied, due to changing minor radius as the ergodized region increases. For all cases where saturation occurs there is no effect on the ELM behaviour or frequency.

In summary, the TEXTOR tokamak has been presented as a suitable device for ELM studies with a variety of techniques to measure the ELM frequency and several advantages which fit closer to the model presented in chapter 3. The ELMs are identified as type-III although have some different characteristics from larger divertor machines due to the high recycling and impurities caused by the presence of a limiter. Using magnetic probes inserted into the plasma edge several new observations have been made including multiple bursts of ion losses per ELM event indicating filament structures with a radial propagation of $1200\,\mathrm{ms}^{-1}$.

The application of the DED to the limiter H-mode has shown a remarkable decrease in the f_{ELM} when fields are applied with $-5\,\mathrm{kHz}$ frequency, but sees little effect when applying the $\pm 1\,\mathrm{kHz}$ or $+5\,\mathrm{kHz}$. A scan of the current applied through the DED up to $0.8\,\mathrm{kA}$, saw no change on the f_{ELM} but mode locking was observed for the $-5\,\mathrm{kHz}$, during a q_a scan, at the approximate point when the $q = 3$ surface enters the plasma. The density threshold required to enter the H-mode was seen to depend on the value of I_{p} and on the phase of the DED fields applied showing a lower threshold for the co-current applied fields. Both of theses results have not been previously observed.

The plasma response to the applied fields was seen to be dependent on the plasma current possibly due to the changing position of the rational surface in the plasma edge. Different behaviour was seen in the plasma response measurements between the co and counter current DED phases. The $+5\,\mathrm{kHz}$ case saw a phase change as the plasma entered the H-mode indicating a change from field penetration to screening. The $-5\,\mathrm{kHz}$ case has a much large plasma response to the applied fields and has even seen the response to saturate at an amplitude of DED which also depends on the plasma current.

5 Multi-Resonant Frequency Dependence of ELMs on the Edge Safety Factor

This chapter examines the interesting result observed on JET that a mixed dependence occurs between the ELM frequency and the value of q_{95} and investigates how this can be explained using the current relaxation model. This is an excellent tokamak to study ELM control as the size of the machine and type of ELMs observed give the best available indication of how larger future tokamaks will be affected. The implications of the agreement seen between the model and experimental results will be discussed and backed up by resonant field amplification measurements on JET. Finally, a similar q_a scan is conducted on TEXTOR as this machine is more suited to have the peeling driven ELMs on which the current relaxation model is based. The results are interpreted in terms of the relaxation model and compared to the JET observations. This is done in order to ascertain if the multi-resonance is also present on TEXTOR and what this means for the understanding of RMP effects on ELM control.

The JET Tokamak

The joint European tokamak (JET) is currently the largest tokamak in the world with its primary focus on being a test bed for ITER technologies and scenarios. It has a D-shaped poloidal cross section with major and minor radius 2.96 m and 1.0 m, respectively. A toroidal field of 4 T and plasma current of 7 MA have been reached. JET created its first plasma in 1983 and became the first machine to operate with deuterium-tritium plasma. Although originally run with a limiter device, the flexible design allowed JET to be upgraded in 1993 to a pumped divertor keeping it at the forefront of fusion research. JET can achieve long high power pulses with a total NBI heating power of ~ 23 MW, total ICRH heating of ~ 32 MW and LHCD of 12 MW. In 1997, JET successfully obtained the highest stored energy observed on any tokamak of 17 MJ for 1.5 s in a $D-T$ reaction [147]. In 2011, the first wall was upgraded to an "ITER-like" wall consisting of tungsten and beryllium seen in figure 5.1.

A large range of ELMs have been observed and investigated on the JET tokamak, including type-I, mixed type-I/II, type-III, and pure type-II or grassy ELMs. The naturally occurring ELMs are usually type-I although transitions to type-II ELMs is created by increasing the triangularity and type-III ELMs occur when a sufficiently

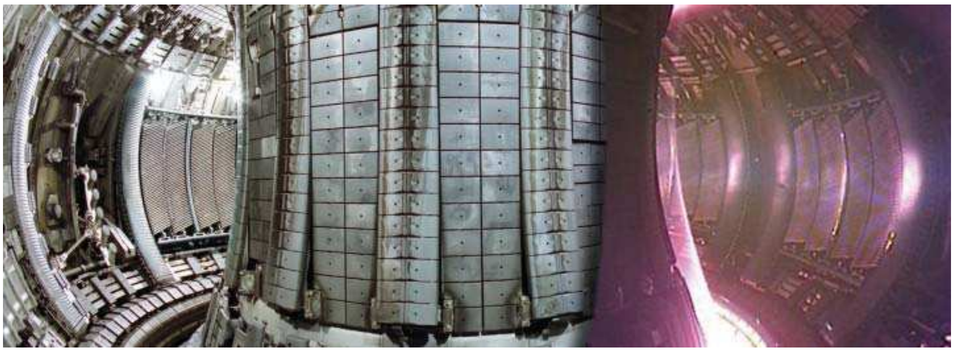

Figure 5.1: *The inside of the JET tokamak with (right) and without (left) plasma. Photo: EFDA-JET.*

high gas puffing is applied to a H-mode plasma. Large currents in the plasma edge seem to be favourable to maintaining the type-III ELM regime suggesting the current driven peeling mode is dominant here especially as the type-III ELMy plasmas are seen with a drop in the edge pressure, which is usually a stabilising effect for the peeling mode.

The Error Field Correction Coils

On JET, the error field correction coils (EFCCs) [148] attempt to compensate for the largest harmonic of the intrinsic error field in order to reduce the locking of modes. These are made up of four coils mounted outside the vessel designed with a four-fold symmetry, each covering an angle of 70 °. The coils have 16 turns and are approximately square with dimensions of 6 m. Either $n = 1$ or $n = 2$ fields can be applied although the $n = 1$ fields have a larger effective perturbation strength by two orders of magnitude. Through these coils static $n = 1$ and $n = 2$ RMP fields can be applied.

The original experiments using the EFCCs to attempt to control ELMs were undertaken when JET had a carbon fibre composite (CFC) wall. At this time, for low collisionality plasmas, ELM mitigation was observed by a factor of 4 increase in f_{ELM} when $n = 1$ fields were applied, and by a factor of 3.5 for $n = 2$ fields [29, 30]. The electron density was observed to decrease by $\sim 25\,\%$ during the application of the EFCCs, the previously mentioned pump-out effect. The fast ion losses were also seen to be reduced due to higher confinement. No obvious mitigation effects were seen in high collisionality plasmas.

The recent upgrade to an ITER-like wall consisting of a tungsten divertor and beryllium first wall shows some different characteristics. The EFCCs have been applied with $n = 2$ magnetic perturbations to the plasma aiming to investigate the difference in behaviour to previous experiments with the CFC wall [149]. A strong mitigation of ELMs in a high collisionality H-mode is observed, changing the type-I ELMs from their natural

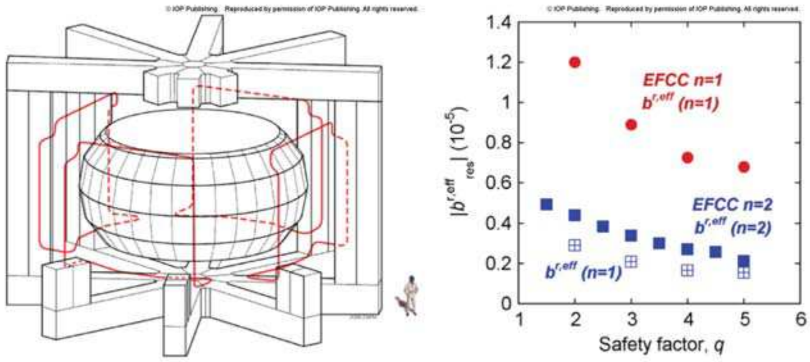

Figure 5.2: *(left) A sketch of the EFCCs installed on JET. The coils are located outside the plasma chamber some distance from the plasma. (right) The effective magnetic fields dependence on the edge safety factor for* $n = 1$ *and* $n = 2$. *The effective magnetic field applied drops as* q *increases. The* $n = 2$ *field has a large* $n = 1$ *side-band component which has almost the same amplitude at high* q *[30].*

frequency of $\sim 45\,\text{Hz}$ to much smaller ELMs with a higher frequency of approximately a few $100\,\text{Hz}$. No density pump-out was observed and the temperature variations on the outer divertor plate were minimal. This effect was seen only when the amplitude of the perturbation fields exceeded $44\,\text{kAt}$. For a low collisionality plasma the type-I ELMs persisted but with a frequency increased by a factor of 4 similar to the CFC wall experiments. Further investigations are planned to continue the low collisionality studies and apply $n = 1$ fields to the ITER-like wall scenario.

Current Relaxation Model Explanation of Multi-resonance on JET

In 2006, $n = 1$ and $n = 2$ perturbations, produced by the EFCC, were applied on JET in order to investigate the effect on ELM stability when applying low n static external magnetic perturbations. The f_{ELM} was observed to increase by between a factor of 4 and 5 times compared to without the EFCCs, with a subsequent decrease in the amplitude of each individual ELM. This raises several questions as to exactly how the perturbation fields are interacting with the plasma and if the ELMs are still the same type or whether the entire plasma edge stability has changed to a different regime. One interesting observation, which could give a great deal of insight into the underlying mechanism, was that a multi-resonant dependence was created in the f_{ELM} on the value of the effective edge safety factor, q_{95}, only when the RMPs were applied [37]. This was seen when either $n = 1$ or $n = 2$ fields were applied, figure 5.3.

Clearly, a strong dependence on the value of q_{95} has become dominant when the RMPs are applied. As the peeling mode is known to have a strong dependence on q_a, a possible

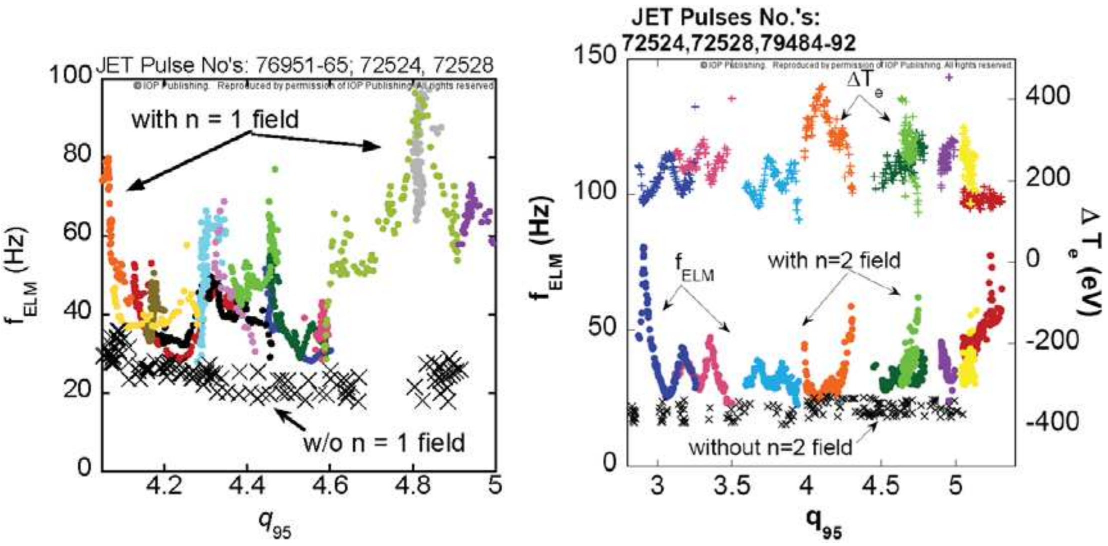

(a) *(b)*

Figure 5.3: The f_{ELM} dependence on the effective edge safety factor, q_{95}, for (*a*) $n = 1$ *and* (*b*) $n = 2$. The temperature change per ELM is also shown for the $n = 2$ case. The black crosses represent measurements without the RMP fields [83].

explanation was put forward using the peeling initiated current relaxation model from chapter 3. Figure 5.4 shows the dominant toroidal mode number and f_{ELM} predicted by the model against the q_a for high and low values of the normalised edge current density, $I_a = 2J_a/q_0J_0$ (found when substituting $q_0 = 2B_0/\mu_0 R_0 J_0$ into equation (3.25)).
It can be seen that the low I_a case has a high level of agreement with the multi-resonance effect observed on JET, whilst for the case with high I_a, an almost constant value of f_{ELM} within the broad range of q_a is seen. (It should be noted that quantitative agreement can hardly be expected given the idealised nature of the cylindrical model as previously discussed).

Looking back to equation (3.29) it is clear where the multi-resonant nature comes from. Before the relaxation is initiated there will only be the driving term from the peeling mode as no skin currents are formed yet. Thus the instability depends only on the condition

$$\left[\Delta_a \Delta_a^{'} + I_a\right] > 0. \tag{5.1}$$

As Δ_a is generally a small positive term for ideal peeling modes and $\Delta_a^{'} \sim O(m)$, the criteria mainly depends on the relative magnitude of I_a. This explains why in figure 5.4, it can be seen that the case with a high edge current density has very little dependence on q_a. However, if the value of I_a is decreased sufficiently, then the Δ_a term will start to dominate the criteria creating the resonant dependence on q_a as seen in the definition

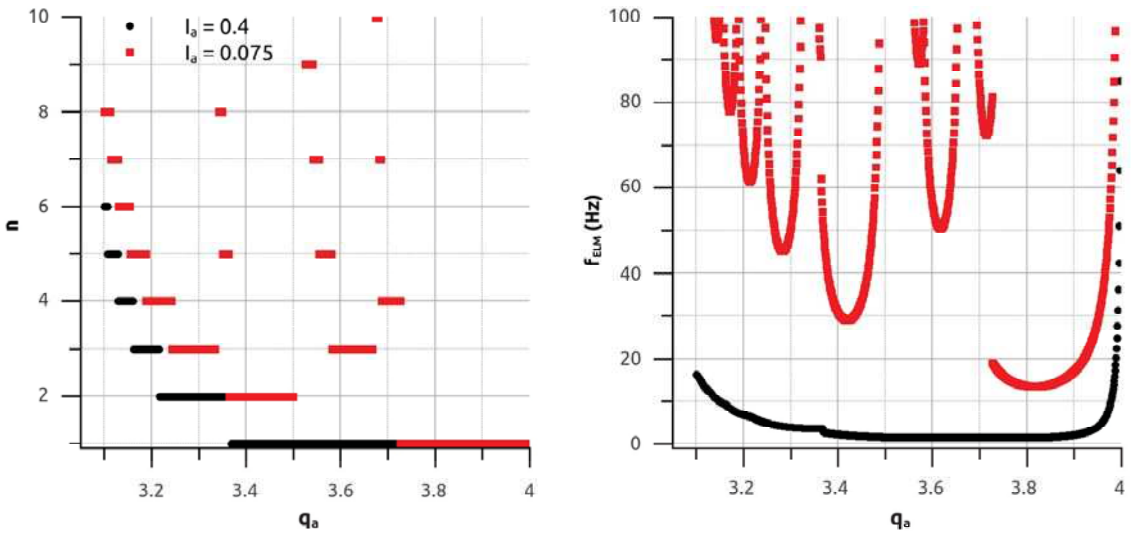

(a) *(b)*

Figure 5.4: The current relaxation modelled q_a dependence of the (*a*) *dominant toroidal mode number and* (*b*) f_{ELM}, for two normalised current density values of 0.4 (black circles) and 0.075 (red squares).

for Δ_a in equation (3.24).

This implies that either the I_a has been decreased or the effect of the Δ_a has been enhanced by the RMPs. A decreased I_a will mean a smaller peeling drive, but having a rational surface near the edge will make it more unstable. As for why the dominant n increases when Δ_a becomes more prominent, this is due to the lowest unstable n is often the dominant driving mode whilst higher mode numbers have less of an impact on the plasma. If the edge becomes more unstable due to the position of the rational surface then higher n have the possibility to couple with the surface allowing them to become the dominant driving mode, thus causing an earlier relaxation.

An inspection of a fine scan of the I_a value in the model, figure 5.5, sees that the multi-resonance structure is formed slowly and smoothly as I_a decreases, rather than appearing at a certain threshold. This indicates that a balance of effects is being altered rather than a sudden change in stability or an abrupt formation of a new driving mechanism. Also, as well as the multi-resonance changing the f_{ELM}, there is a general increase across the entire q_a range is seen as I_a decreases. This can be seen at $q_a = 3.8$ in figure 5.5 where all four cases have the same dominant toroidal mode number ($n = 1$) but different f_{ELM}. This then suggests that a decrease in I_p will increase the f_{ELM} which would be an unexpected result if one was not familiar with the Δ_a driving term.

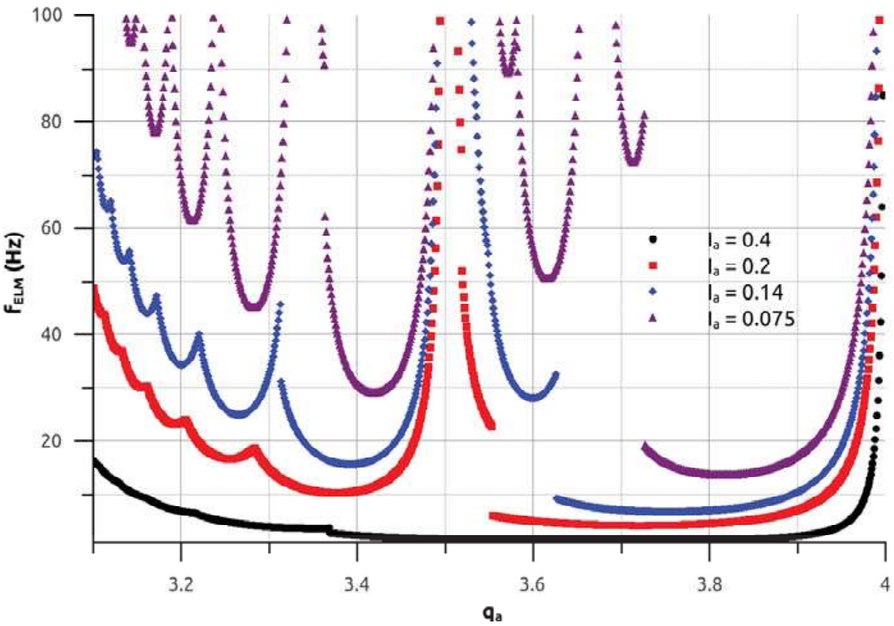

Figure 5.5: *Four plots from the model of f_{ELM} with varying I_a, showing the model predictions of gradual formation of the multi-resonance and overall increase of f_{ELM}.*

The arguments put forward so far assume that the ELMs on JET have a large peeling drive and that this is affected by the RMPs. As the observed ELMs on JET are known to be type-I, which is thought to have both peeling and ballooning drives, then it must be asked, can the peeling mode stability individually have such a large effect on the ELMs, and can $n = 1$ modes really be responsible for the ELM events? For answers to these questions analysis of resonant field amplification measurements, as an indication of the plasma stability, is used.

Resonant Field Amplification

On DIII-D, the plasma was observed to react significantly more to an $n = 1$ perturbation when the value of $\beta_N > \beta_N^{no-wall}$, where $\beta_N = \frac{2\mu_0 a<p>}{I_P B_t}$ and $\beta_N^{no-wall}$ is the stability limit for ideal MHD modes without the presence of a stabilising conducting wall. The toroidal rotation was also seen to be damped heavily as the plasma approached marginal stability. These results suggested that a weak magnetic perturbation could have a strong effect on the plasma stability, similar to a small error field creating locked modes, and so is of great interest when discussing RMP effects on a plasma. The observed effect was defined as resonant field amplification (RFA) [150], whereby low n, low frequency, meta stable modes (i.e. modes with their growth rates, $\gamma \sim 0$) in the plasma amplify externally applied magnetic fields through a resonant response. This can cause rapid damping of the toroidal rotation through a transfer of angular momentum from the plasma to the surrounding coils. This was originally discussed in terms of the circuit equations, although a more intuitive description is found in reference [151] where perturbed magnetic fields are calculated in the plasma, vacuum region and conducting shell. The amplitude of the perturbed magnetic field at the wall can be expressed in terms of the wall time, $\tau_w = \mu_0 \sigma r_w d$ and the external fields, B^{ext}

$$\tau_w \frac{\partial B}{\partial t} = \Gamma B + 2\mu B^{ext}, \tag{5.2}$$

where σ is the conductivity, μ_0 is magnetic permeability, r_w is the wall radius, and d is the wall thickness. The parameter Γ is an amplitude factor of the mode and gives an indication of the RFA.

The theory predicts that RFA will be largest when above the ideal $\beta_N^{no-wall}$ limit as the resistive wall mode (RWM) stability boundary is reached. Indeed, a significant enhancement of RFA has been observed as the plasma exceeds the no-wall stability limit [152, 153] due to the onset of RWMs. The onset of limiting modes in the plasma can also be predicted by looking at the sensitivity of the RFA which will increase as the plasma approaches a stability limit. Sudden increases in RFA have been observed at values of β_N below the RWM threshold, just before a fast rotating 5 kHz internal kink mode has been destabilised. Thus, the measurement of RFA is a useful tool for investigating the plasma stability.

Experimentally the amplitude of RFA can be approximated as the ratio of the plasma response to the plasma vacuum reference,

$$RFA = (B_r - B_r^{vac})/B_r^{vac}. \tag{5.3}$$

The plasma response from an oscillating $n = 1$ or $n = 2$ RMP field can be measured using in-vessel saddle coils. On JET, there is an array of poloidal saddle coils in each of the eight toroidal octants. For the following measurements an average of the mid-plane saddle coils on the low field side is required, labelled coils 1 and 14. Unfortunately, these are prone to faults and need careful calibration to ensure accurate results. For an $n = 1$ perturbation the EFCCs are applied at octants 3 and 7, $\pi/2$ out of phase with each other, alternatively an $n = 2$ perturbation is shown in figure 5.6.

The ratio of measured amplitudes from the difference of octants 3 and 7, versus the difference of octants 1 and 5, gives the RFA measurement from the $n = 1$ response. For the case where the perturbation applied is an $n = 2$, the EFCCs are applied at octants 3 and 7 with the same phase. To measure the RFA from just the $n = 2$ response, the ratio of amplitudes from octants 1 - 3 + 5 - 7 versus octants 2 - 4 + 6 - 8 is required. This assumes that the plasma response is much smaller than the vacuum perturbation and so can be neglected from the signals with the applied EFCCs and that there will be a 90 ° phase shift between the applied field and the plasma response. When applying

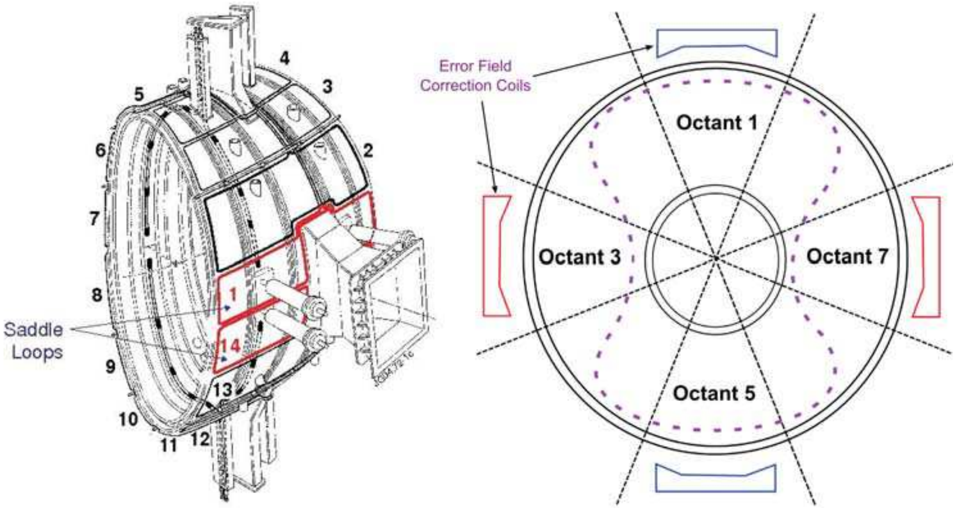

Figure 5.6: *(left) A schematic of a poloidal cross section on JET showing one octant. A poloidal array of saddle coils is observable with two mid-plane coils highlighted. An average from these coils gives the mid-plane magnetic signal required and can be found in each of the eight octants, giving a complete toroidal measurement. Diagram courtesy of JET-EFDA. (right) A birds eye view of the position of the EFCC coils with an $n = 2$ shape drawn as the dashed line.*

an AC field to the plasma the ratio of amplitudes from these saddle coils yields a good result but phase should be considered when applying a stationary oscillating field.

The threshold at higher β_N in figure 5.7 shows typical behaviour for the RFA measurement as it reaches the ideal no-wall β limit allowing RWMs to become unstable. This is a well established practice to measure the β threshold. However, an interesting observation is that a peak in the RFA can be seen at lower β_N, well below the ideal no-wall β limit where the RWMs will be stable. This occurs just before the first ELM or after a long ELM free period. Using `MARS-F` it has been numerically shown that a marginally stable $n = 1$ peeling mode gives a response with an amplitude matching the experimental data from JET at the first ELM peak [154]. This shows that an $n = 1$ mode can indeed be the driving mode behind an ELM event, as the model states. The peeling mode, in this instance could be coupling with an internal mode creating a kink in the plasma, lowering the stability limit and thus increasing the value of RFA. After this event, as the β_N continues to rise to the ideal no-wall β limit, the RWMs take over as the dominant mode affecting the RFA. It is common to see different characteristics at the first ELM, which is often a larger event than the following steady state ELMs. It is possible that further peeling modes could be affecting the RFA during the steady state phase although this would be indistinguishable from the RWMs effect.

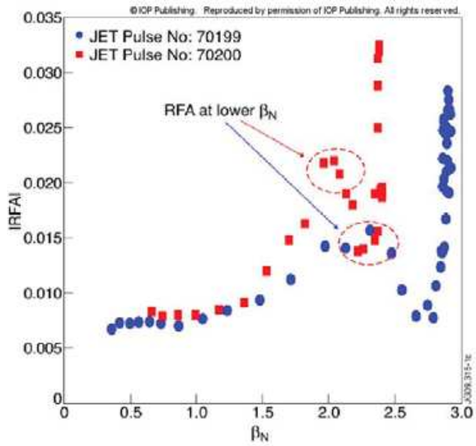

Figure 5.7: *Reconstructed RFA measurements using the* `MARS-F` *code. Two consecutive JET shots are presented, each showing an early peak in the RFA associated with the first ELM event followed by a threshold indicating the* $\beta^{no-wall}$ *limit [154].*

The addition of extra gas, as the plasma enters H-mode, has frequently been used in attempts to control the initial stages of the H-mode. On JET it was observed that a correlation between the extra gas puffing and the suppression of the RFA peak associated with the first ELM existed, as seen in figure 5.8.

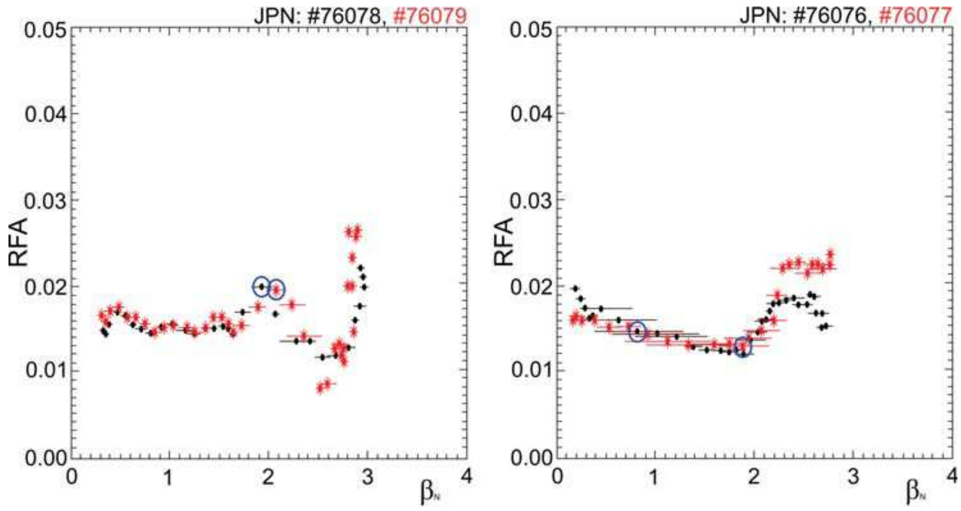

Figure 5.8: *Direct RFA measurements for four consecutive shots from JET. (left) Without, and (right) with additional gas puffing at the first ELM. The time of the first ELM event is highlighted by the blue circles.*

It should be noted that the data shown was taken from four adjacent shots in order to be valid for comparison and that only data with a strong correlation to the frequency of the EFCCs applied is plotted as the noise level is high.

The extra puffing at the first ELM is probing the low n peeling mode stability. One possible mechanism for this comes through increased convective losses at the plasma edge due to the additional gas. This would lead to a decrease in the pedestal mostly through the temperature gradient. The edge collisionality would then be increased and thus the resistivity goes up causing a decrease in the edge current density. This would then directly increase the multi-resonant nature of the peeling mode allowing higher toroidal mode numbers to become the dominant unstable mode. As RFA is a response from modes with the same toroidal mode number and frequency as the applied fields i.e. $n = 1$ or 2, then an increase of the dominant unstable mode number would decrease the value of RFA as, observed. This is strong evidence that not only are peeling modes one of the dominant drivers, but also that their dominant n can be affected by changes to the plasma edge conditions.

Edge Safety Factor Dependence on TEXTOR

Since the simple model has seen such a high level of agreement with results from JET, it is interesting to compare against another tokamak to see if these effects are seen across multiple machines. As TEXTOR is a medium sized device, and the limiter H-mode has a lower confinement than divertor H-modes, then the value of the edge current density should also be lower. The TEXTOR ELMs are also believed to be closer to type-III than type-I with a smaller pressure drive, and so have a much larger peeling contribution to the ELM stability than on JET. Thus the multi-resonance could be apparent on the TEXTOR tokamak without having to apply RMP fields. TEXTOR is also more suited to be compared against the current relaxation model as it has a definite value of q_a and can be described in the cylindrical approximation as it has no shaping effects.

The edge safety factor is especially relevant when dealing with plasma features driven at the edge, such as ELMs. The density of low to medium n rational magnetic surfaces, which are mainly responsible for driving ELMs, in the plasma is characterised by the magnetic shear, $s = \frac{r}{q}\frac{dq}{dr}$ which is clearly dependent on the q profile and thus q_a. A simple expression for q_a in a cylindrical approximation can be found in [62],

$$q_a = \frac{2\pi a^2 B_T}{\mu_0 I_P R}. \tag{5.4}$$

As q_a depends on both I_p and B_t it is important to establish the relation these quantities have on the ELMs. For TEXTOR, two q_a scans were performed for comparison, by changing either I_p or B_t whilst holding the other constant, seen in figure 5.9.

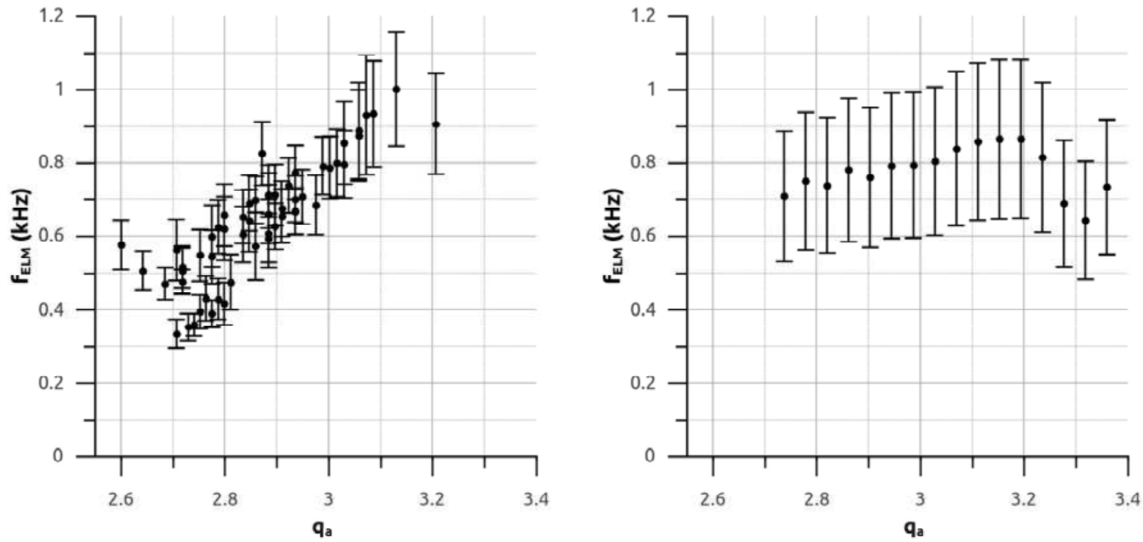

(a) *(b)*

Figure 5.9: The dependence of f_{ELM} on q_a through (*a*) *a plasma current scan between* 250 *and* 190 kA *at a constant magnetic field of* 1.3 T *taken over several shots with the same plasma density, and* (*b*) *a magnetic field scan between* 1.3 *and* 1.6 T *at a constant plasma current of* 230 kA *from shot* #115604.

If the stability of the ELMs only depended on the value of q_a then these two scans should show the same dependence, however, clearly the I_p scan has a much greater effect. One possibility is that this is due to the observed trend stated for figure 5.5 that as the I_a decreases the f_{ELM} increases. A change in the value of I_p does not necessarily mean a direct change in I_a, however here a large sensitivity of the value of I_a to I_p would be required. On JET, both I_p and B_t scans were conducted showing similar trends, although the B_t scan is rarely used as this has an effect on the effective perturbation field and so usually q_a is varied through I_p only. The relative insensitivity to the changing I_p on JET is due to the large bootstrap current, created by the pressure gradient, keeping the value of the current at the edge constant. This suggests that the bootstrap current on TEXTOR should be small which would make sense due to the relatively low pressure at the plasma edge.

An approximation of the bootstrap current is made on TEXTOR using the formulas set out in [7]. These are valid when the effective nuclear charge, Z_{eff}, is close to unity. On TEXTOR, Z_{eff} is usually ~ 1.5 however, for the limiter H-mode with low density and a large inward shift, the value becomes very close to 1 as calculated from the neoclassical conductivity of the plasma. The bootstrap current is then calculated using the density and temperature profiles from Thomson scattering with a trapped particle fraction of 0.7.

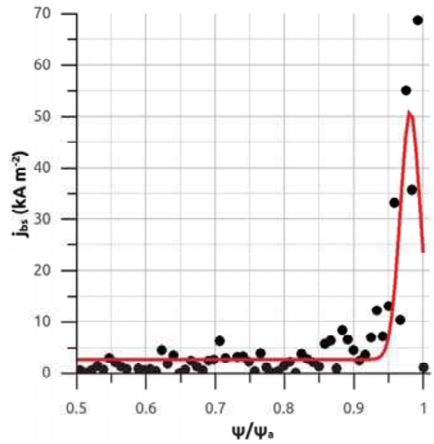

Figure 5.10: *The calculated bootstrap current density profile for TEXTOR limiter H-mode shot* #115594. *This is highly localized and quite small representing the weak pedestal formed in the limiter H-mode. A Gaussian fit* ($f(x) = y_0 + Ae^{\frac{-(x-x_c)^2}{2w^2}}$ *where* x_c *is the centre of the peak and* w *is the width) has been overlaid as the red line.*

A modelled current density profile without the bootstrap contribution, created through the DIVA code, gives a core current density of $I_0 = 1.13\,\mathrm{MAm^{-2}}$ for TEXTOR shot #107315. Comparing this with the bootstrap current calculated in figure 5.10, a normalised current density $I_a \sim 0.04$, is found.

An extremely low value of I_a is also backed up by measurements of the density dependence. During the early experiments undertaken on TEXTOR it was clear that the plasma density has a large effect on the f_{ELM}. Figure 5.11 shows the density dependence while keeping the other parameters constant.

A higher density will increase the collisionality causing high resistivity at the edge thus decreasing the current at the edge. Clearly the density needs to be well controlled to gain accurate dependencies from the other parameters. This has proved difficult in TEXTOR H-modes due to changing wall conditions and faulty electronics, often rendering large sets of results unacceptable.

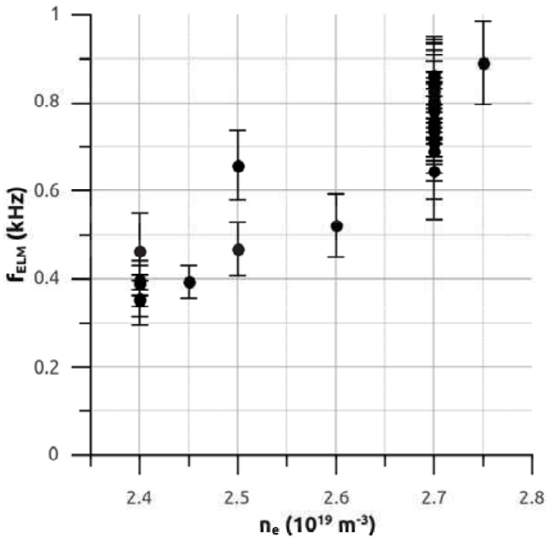

(a)

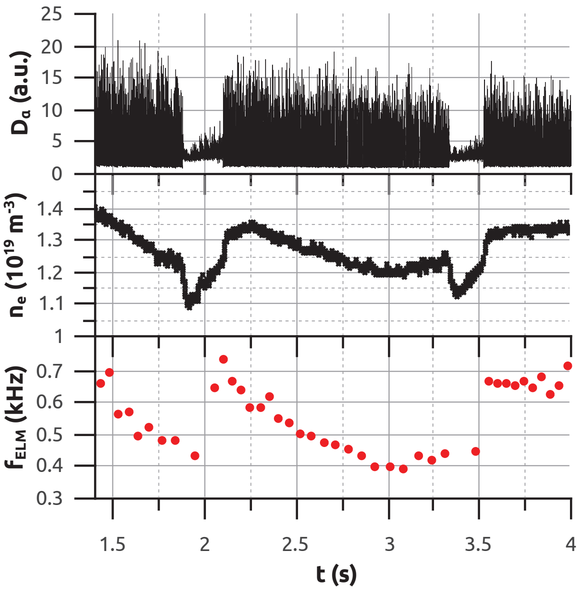

(b)

Figure 5.11: (*a*) *The dependence of f_{ELM} on the plasma density, holding all other plasma parameters constant (I_P = 245 kA, B_T = 1.3 T). An increase of* 1.0 $\times 10^{18}$m^{-3} *in the density increases the f_{ELM} by around* 0.1 kHz. (*b*) *A TEXTOR shot showing (top) D_α traces, (middle) line averaged density, and (bottom) average f_{ELM} behaviour for three regions of H-mode. The first two have changing density which shows a strong and clear effect in the f_{ELM}, whereas the last period has a constant density and so little change to the ELMs.*

To understand what could be occurring on TEXTOR, an extreme case is investigated by setting the model to its operational lower limit of $I_a = 0.01$. Below this value a high proportion of f_{ELM} calculated result in ∞. For the extreme case, the multi-resonant structures become distorted and appear chaotic and noisy. Figure 5.12 compares the model prediction of ELM frequencies (left) to a TEXTOR shot with a smooth q_a scan.

The model now suggests a general increase in the ELM frequencies as q_a increases, apart from a sudden drop directly before the integer value. The spread in frequencies changes non-uniformly. These features can be seen in the experimental data, although not as clearly, but this would be expected when comparing such an ideal model to real experiments, especially if the value of q_a is not perfectly controlled.

A closer look at the character of TEXTOR ELMs was conducted in order to establish the distribution of the ELM frequencies over a shot [155]. If a linear dependence is present between the plasma current and the f_{ELM} then the distribution would also be linear. However, this is rarely seen and instead it is suggested that a more complicated situation is at hand.

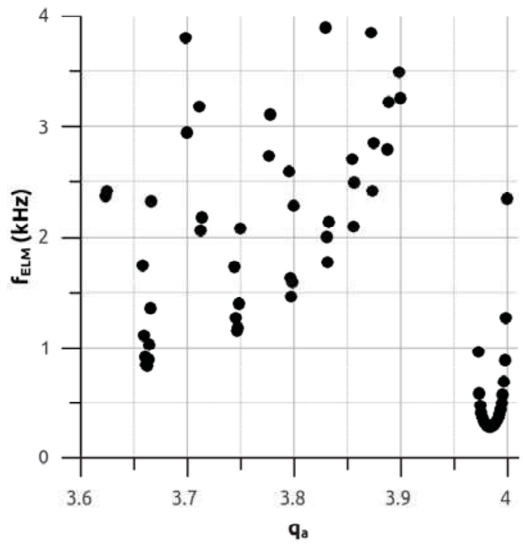

(a)

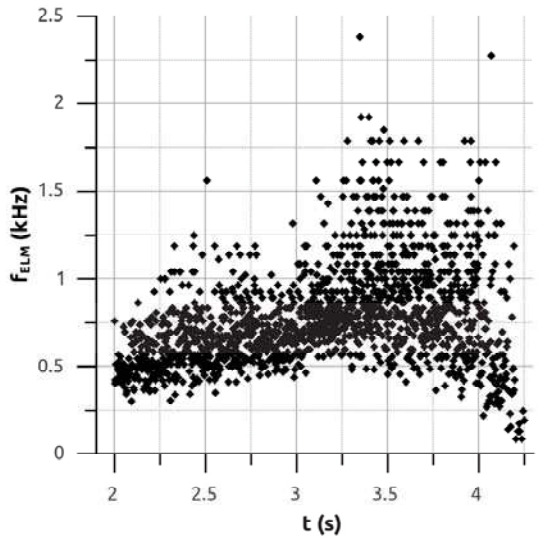

(b)

Figure 5.12: (a) *Predictions of f_{ELM} from the current relaxation model when the normalised edge current density is set to* 0.01. (b) *The f_{ELM} spread over time for TEXTOR shot* #115597 *where the I_{p} was slowly decreases thus increasing the value of q_a.*

Figure 5.13 shows four different time periods from shot #115597 compared with a modelled linear distribution. In this shot a current scan was performed in order to slowly increase q_a allowing the change in ELM distribution to be observed. All the cases have an overall Maxwellian distribution although certain artefacts are observed which indicate a multi-resonance nature. A linear distribution would have a constantly increasing broadness and amplitude as the f_{ELM} increases. Instead, sudden changes in broadness and amplitude of the distribution as well as secondary peaks can be seen.
Periods 2 and 3 show distributions most associated with the modelled linear case and would appear if the plasma was at point A with a small variation in q_a due to experimental fluctuations. In period 1 an additional peak in the distribution spectrum can be seen at a higher frequency. This secondary peak would be made if the value of q_a is near to two resonances, as for case C in figure 5.13 (right). This suggests that the non-linear dependence associated with the multi-resonant effect could be present although clearly a linear dependence is dominating.

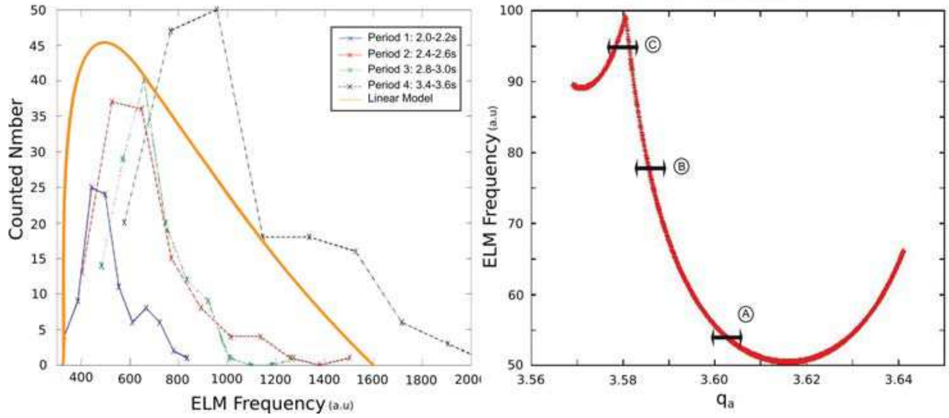

Figure 5.13: *(left) The distribution on measured frequencies. The solid orange line represents a modelled linear distribution. This is compared with four different time periods, each of* 0.2 s *from the shot* #115597*. (right) A focused view of the f_{ELM} dependence on q_a from the current relaxation model with three highlighted regions representing possible reasons for the additional features and non-linear behaviour observed in experiment [155].*

To summarise this chapter, the explanation of the multi-resonance effect observed on JET, by the current relaxation model, has been put forward. This relies upon changes to the peeling mode stability having a large effect on f_{ELM} which has been seen to be the case for at least the first ELM through RFA measurements. The observed pump-out effect when RMPs are applied, described earlier, also suggests that α decreases, and so the plasma would shift closer to the peeling dominated part of the stability boundary (seen in figure 2.6) increasing the peeling effects. The RFA measurements show that the peeling modes with $n = 1$ can be marginally unstable when the first ELM event takes place and that the n of the dominant peeling mode can be altered by changing the edge current density, through increasing the collisonality. On TEXTOR, a q_a scan was completed with the expectation of seeing the multi-resonance nature. However, instead a linear dependence on the plasma current with a noisy distribution was seen, which the model agrees with only if the edge current density is further decreased to $I_a = 0.01$. This indicates that different mechanisms are dominant on the two tokamaks.

6 Discussion and Conclusions

The two questions set out in the introduction are now discussed to see where progress has been made.

Do the resonant magnetic perturbations affect the edge localized modes through changes in the transport or stability?

There are two ways in which the frequency of the ELM cycle can be influenced: either, an alteration in the transport through a change in the edge confinement, so that the pedestal pressure takes a different time to build back up to the crash threshold; or a change in the stability boundary so that the crash occurs with a different pedestal pressure threshold. These two mechanisms and their interactions are represented in figure 6.1.

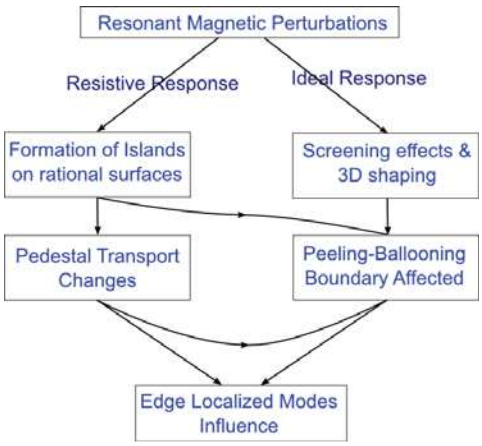

Figure 6.1: *The effects and interaction of how the ELMs are influenced by applied RMPs.*

The transport over the edge of the plasma depends primarily on the magnetic field structure, which as discussed, could form an ergodized region due to the creation and interaction of magnetic islands, induced by the plasma response to the externally applied fields. Any affect on the transport will show up when analysing the edge profiles such as measured through Thomson scattering.

Direct changes to the stability of the plasma edge or the dominant driving mode are difficult to model and measure due to the complex interplay of many different effects. Apart from coupling of the RMPs to the driving mode, there are many different ways that the mode stability could be being affected through coupling of the RMPs to low n or m features in the plasma such as: the $m = 1$ Shafranov shift, the $m = 2$ and $m = 3$ modes caused by the elongation and triangularity, respectively, the natural $n = 1$, $m = 1$ internal kink in the core of the plasma, the highly unstable $n = 1$, $m = 2$ tearing mode, and the $n = 0$, $m \neq 0$ shaping effects. Alternatively, the driving mode for the ELM could be altered through increasing the stability of the original driving mode until another mode becomes dominant or through some direct effect of the external fields enhancing a previously dormant mode.

The density pump-out effect observed on JET and other tokamaks, clearly indicates a decrease in the pedestal height. However, this does not necessarily mean that the transport has increased, as a closer look at the rate that the pedestal pressure grows after an ELM event, with and without RMPs, shows similar trends for both cases. This suggests that although the pedestal height has been decreased, which subsequently decreases the total stored energy, the pedestal growth rate is still the same and so the stability has been affected rather than the transport.
Further evidence comes when looking at the type of ELMs observed with RMPs on JET. If a large increase in transport occurred then either a back transition to the L-mode or a change to type-III ELMs would be expected. Before the application of RMPs, regular type-I ELMs are present. During the application of RMPs in low collisionality plasma with the CFC wall, the f_{ELM} has increased but the power dependence still suggests type-I ELMs [31]. This therefore indicates that similar peeling-ballooning modes to those before the RMPs have become more unstable causing the increase in f_{ELM}.

The drop of the pedestal pressure would also decrease α, moving the plasma stability down towards the peeling dominated regime seen in figure 2.6 and so peeling effects could become more prominent whilst still being coupled with ballooning modes.
The RFA modelling predicts that the peeling mode can indeed be the dominant mode behind an ELM event, as seen for the increase in RFA at the first ELM. The observation of suppressing the RFA peak, associated with the first ELM, with additional gas puffing, whilst leaving the ELM itself unaffected, indicates that a similar driving mode is still present but with conditions which would not appear in the RFA measurements, i.e. an increased toroidal mode number. The current relaxation model gives a path to achieve this through increasing collisionality by the gas puffing thereby changing the edge current density allowing peeling modes with higher toroidal mode numbers to become the dominant driver.

Thus, on JET it has been shown that the peeling mode effects are increasing when RMPs are applied, decreasing the current density and/or allowing the sensitive Δ_a term to play an important role in the f_{ELM} dependence on q_a. This is through the stability changing, allowing higher n to become unstable earlier than without the applied RMPs, by coupling of the plasma edge with the RMPs. This is likely to be mostly through changes in the shaping of the plasma, as discussed for the observations of manifold structures when RMPs are applied on MAST [92]; unfortunately the three-dimensional modelling required is beyond this study.

The dependence of f_{ELM} on q_a on TEXTOR is quite different although it is still suggested to be mainly due to stability effects. Evidence for this is seen when comparing the scans of f_{ELM} for I_{DED} and q_a in figures 4.14(a) and (b). Increasing the DED amplitude at a single value of q_a shows little change for any DED phase at both the densities presented. If the DED was degrading the edge confinement then an increase would be expected here. This suggests the I_{DED} is too small to be having large transport effects. Instead, the observation of a linear increase of f_{ELM} as q_a increases for ± 1 kHz and $+5$ kHz shows the importance of the distance from the plasma edge to the rational surface. As a rational surface comes closer to the plasma edge the stability of a limiter H-mode ELM decreases.
The special case of the -5 kHz DED, with the strong behaviour change when the $q = 3$ surface enters the plasma, is then due to a stabilising interaction with the rational surface, seen through the 3/1 mode locking, and thus the plasma becomes unstable earlier above $q_a = 3$.

Which parameters are key for the ELM control?

Throughout this study it has been made clear that the stability of the ELMs on any tokamak is dependent on a large variety of parameters and can be affected through different mechanisms which additionally couple with one another. Following on from the previous discussion the position of the rational surface, relative to the plasma edge characterised by the value of q_a, is clearly an important parameter due to the interaction of the magnetic islands formed on the surfaces.

The current relaxation model shows the importance of the values of J_a and Δ_a, and the balance between them on the f_{ELM}. The plasma response on JET was seen to saturate even as the amplitude of the external fields increased [149]. The ELM frequency stayed the same after the saturation level indicating that the mechanism changing the ELM stability is associated with the plasma response. There is no reason why the change in J_a should stop at a certain amplitude of the applied fields and thus the enhancement of the effect of having a rational surface near the edge is a more likely candidate as this could saturate as screening increases.

The effect of I_p on the L/H transition density threshold seen on TEXTOR with DED is a new observation showing that the transition into the H-mode can be made easier depending on the phases of the applied RMPs.

The difference in the q_a scans with the four different phases of DED investigated, shows the importance of the DED phase on the ELM behaviour. As pointed out this is due to the relative velocity of the electron fluid across the rational surfaces which is higher for the -5 kHz case.
The screening of the plasma to the different phases has been shown in this study to be different, even showing a possible change from field penetration to screening when entering the H-mode for the $+5$ kHz case although not in the -5 kHz case. That the saturation of the plasma response for the -5 kHz case is not seen for the $+5$ kHz case is interesting, as it suggests that the screening reaches a maximum value depending on the plasma current when the RMPs are applied in the co-current direction; above this value the DED has little effect.

Thus, when answering the two questions in short, it seems the effect of the RMPs on the ELMs is mainly through stability boundary changes and especially for the peeling mode depends on the interplay between the edge current density and the position of the rational surface nearest the edge which depends on q_a. The strength of the RMP influence can be optimised through knowing the plasma response to different applied phases, but unfortunately this is highly dependent on the individual tokamak making predictions for future devices difficult.

Outlook

Turning the focus to the future, the first thing to say is on TEXTOR. As the currently oldest operating machine it is worth remembering its long list of achievements before it shutdown in November of 2013. For this study TEXTOR was particularly useful due to its cylindrical nature, current driven type-III ELMs, and definite edge safety factor. This then also means that studies of the dynamic ergodic divertor will soon cease. In this study, the usefulness of applying helical rotating or AC resonant magnetic perturbations to the plasma has been widely discussed and strongly suggested for future devices. However, according to present research, in-vessel coils will not be feasible for future large devices due to the material strains and so such techniques as lower hybrid current driven resonant magnetic perturbations are of high interest and will be an expanding area of research over the next few years.

Studies of the effect on the edge localized modes on JET when resonant magnetic perturbations are applied through the error field correction coils will continue focusing on the difference between the ITER-like wall to the previous carbon fibre composite wall and on the strike point splitting effects on the divertor plates. As well as this a set of in-vessel coils are currently being designed and tested with the aim to have combined operation of the error field correction coils and the new in-vessel coils within the next couple of years.

As for the current relaxation model, the author believes that this has gone as far as it can go in its current state and new understanding in this area will come through full three dimensional modelling of the plasma edge which would require a full reformation of the boundary conditions for the peeling mode energy principle and a large analytical model. However, the model in its current form has been an essential tool to show just how strong the peeling effects are on the edge localized modes and will need to be considered in the future models.

7 Summary

To summarise, the effect of resonant magnetic perturbations on the edge localized mode control has been studied through both modelling, using a current relaxation model, and experiments on JET and TEXTOR. A wide range of physical effects and observed results have been outlined showing the complex dependencies in this area of research. The main new findings presented in this thesis are the following.

Firstly, it has been shown that the current relaxation model can explain certain features of edge localized mode control including the multi-resonant dependence observed on JET between the edge localized mode frequency and the edge safety factor. The agreement comes when the edge current density is decreased allowing the term associated with the distance from the plasma edge to the nearest rational surface to play an active role in the peeling mode stability. This leads to a new interpretation of the edge localized mode frequency dependence on the value of the edge safety factor. Three regimes are considered depending on the two parameters that drive a peeling mode i.e. the edge current density, I_a, and the distance of the rational surface to the plasma edge, Δ_a. If I_a is large, this will dominated the ELM frequency dependence on the edge safety factor producing a linear trend, such as seen on JET when no RMPs were applied. However, if I_a is decreased then Δ_a starts to have an equal effect and the interplay between these two driving terms creates the observed multi-resonant features seen when RMPs were applied on JET. Alternatively, if I_a is so small that all the peeling drive comes through the Δ_a term, then a chaotic structure appears and the random nature observed on TEXTOR forms. Clearly, this dependence is being largely influenced by the application of RMPs. This is backed up through measurements of resonant field amplification indicating that the peeling mode stability can be directly influenced through additional gas puffing by allowing modes with a higher toroidal mode number to become dominant.

Secondly, the large differences seen between the effects of resonant magnetic perturbations on JET and TEXTOR edge localized modes are interpreted. Type-I edge localized modes on the JET tokamak are influenced through their stability. This is affected through many channels including enhancing the effect of proximity of the nearest rational surface to the plasma edge, changes in the shape of the plasma edge, and coupling of the applied fields to features in the plasma. The effect on TEXTOR appears to be mainly from changes in the stability, dependent on the distance of the rational surface to the edge. This is especially prevalent on the TEXTOR limiter high confinement mode as it sits so close to the transition between the low and high confinement modes, so that slight changes can have a mixed effect on edge localized modes and the high confinement mode stability. When the resonant magnetic perturbations are applied on TEXTOR with a $-5\,\mathrm{kHz}$ phase the dependence of the edge localized mode frequency on the plasma current disappears due to a large interaction of the $q = 3$ surface.

Thirdly, the unique feature on TEXTOR of being able to apply rotating perturbations to the plasma has been further utilised and investigated in order to see if the plasma is sensitive to the frequency and direction of the applied perturbations. For the case where the perturbations were applied in the same direction, a higher sensitivity on the plasma was seen with occasional 3/1 locked modes. The transition from low to high confinement was also seen to be influenced suggesting that the formation of the pedestal in the plasma edge may be being helped by the perturbations when applied in the same direction as the current. The plasma response was measured for each of the different applied fields and was found to be dependent on the plasma current as this directly influences the position of the rational surface which will be giving the majority of the plasma response. For the $+5\,\mathrm{kHz}$ case a phase jump associated with field penetration was observed as the plasma entered high confinement mode, thought to be due to field penetration occurring in the $+5\,\mathrm{kHz}$ case in the L-mode. When the amplitude of the magnetic perturbations was ramped the plasma response was seen to saturate at a level dependent on the plasma current again emphasising the effect of the rational surface position.

In conclusion, the change in edge localized mode behaviour comes through an alteration of the stability of the plasma edge rather than through an effect on the pedestal transport. The perturbation spectrum and phase of the applied fields have been shown to be of high importance showing a dependence of the L/H power threshold on the phase. Optimised ELM control needs to consider not only the coil setup and perturbation spectrum applied, but also the relative velocity of the applied perturbations to the electron fluid on the rational surfaces resonant with the applied magnetic perturbations. For future studies it should be made clear that peeling mode effects are enhanced when applying RMPs through the effect of the proximity of the rational surface to the plasma edge, allowing modes with higher toroidal mode numbers to become unstable earlier than the original mode, causing the observed increase in ELM frequency.

Zusammenfassung

Der Effekt von resonanten magnetischen Störungen (RMP) auf die Kontrolle von Edge Localized Modes wurde sowohl durch Modellierung, mittels eines Strom-Relaxations-Models, als auch experimentell an JET und TEXTOR untersucht. Ein weiter Bereich von physikalischen Effekten und beobachteten Ergebnissen wurden herausgestellt, welche die komplexen Abhängigkeiten in diesem Feld der Forschung zeigen. Die neuen Hauptentdeckungen, die in dieser Arbeit präsentiert wurden, sind die folgenden.

1. Es wurde gezeigt, dass das Strom-Relaxations-Model gewisse Eigenschaften der Edge Localized Mode Kontrolle erklären kann, inklusive der multi-resonanten Abhängigkeiten, die an JET zwischen der Edge Localized Mode Frequenz und dem Sicherheitsfaktor am Rand beobachtet wurden. Die Übereinstimmung wird gefunden, sobald die Stromdichte am Rand soweit reduziert wird, dass der Term, der den Abstand des Plasmarandes zur nächsten rationalen Fläche beschreibt, eine aktive Rolle in der Peeling-Stabilität spielt. Dies führt zu einer neuen Interpretation der Abhängigkeit der Edge Localized Mode Frequenz von dem Wert des Sicherheitsfaktors am Rand. Drei Regime wurden berücksichtigt, abhängig von den zwei Peeling Antriebsmechanismen: Der Stromdichte am Rand und dem Abstand der rationalen Fläche vom Plasmarand. Wenn die Stromdichte am Rand groβ ist, dann ist die Abhängigkeit dominiert von diesem Term und verhält sich linear, so wie an JET gesehen, wenn keine RMPs verwendet werden. Im Gegensatz dazu, wenn die Stromdichte am Rand reduziert wird, beginnt der Term, der den Abstand der rationalen Fläche zum Plasmarand beschreibt, einen vergleichbaren Einfluss zu haben und das Wechselspiel zwischen diesen beiden Termen erzeugt die beobachteten multi-resonanten Eigenschaften. Alternativ, wenn die Stromdichte am Rand so gering ist, dass der gesamte Antrieb für die Peeling-Instabilität aufgrund des Abstands der rationalen Fläche zum Plasmarand auftritt, entsteht eine chaotische Struktur und ein zufälliges Verhalten, wie an TEXTOR beobachtet, tritt auf. Messungen der resonanten Feldverstärkung indizieren, dass die Peeling-Stabilität direkt von einem zusätzlichen Gaseinlass beeinflusst wird indem Moden mit höheren toroidalen Modennummern dominant werden können.

2. Die groβen Unterschiede, die zwischen den Effekten von resonanten magnetischen Störungen an JET und TEXTOR Edge Localized Modes gesehen wurden, wurden interpretiert. Typ-I Edge Localized Modes am JET Tokamak sind durch ihre Stabilität beeinflusst. Dies kann durch viele verschiedene Mechanismen geschehen wie zum Beispiel die Verstärkung des Effekts der Nähe der nächsten rationalen Flächen zum Plasmarand, Veränderung in der Form des Plasmarandes und Kopplung des verwendeten Feldes zu Eigenschaften im Plasma. Der Effekt an TEXTOR tritt je nach Abstand der rationalen Fläche vom Rand hauptsächlich durch die Veränderung in der Stabilität auf. Dies ist besonders vorherrschend bei H-Mode-Betrieb an TEXTOR, da dieser so nahe am Übergang zwischen schwachem und hohem Einschluss liegt, dass leichte Veränderungen einen gemischte Effekt auf Edge Localized Modes und die Stabilität

des hohen Einschlusses haben. Wenn die resonanten magnetischen Störfelder in einem -5 kHz Betrieb an TEXTOR angewendet werden, verschwindet die Abhängigkeit der Edge Localized Mode Frequenz vom Plasmastrom aufgrund der starken Wechselwirkung mit der $q = 3$ Fläche.

3. Die einzigartige Eigenschaft an TEXTOR, rotierende Störfelder auf das Plasma anzuwenden, wurde weiter verwenden und untersucht, um herauszufinden ob das Plasma sensitiv für Frequenz und Rotationsrichtung der Störfelder ist. Im Falle von in Plasmastromrichtung angelegten Störfeldern, wurde eine hohe Sensitivität auf das Plasma zum Auftreten von 3/1 gelockte Moden beobachtet. Es wurde ebenso gesehen, dass der Übergang vom schwachen zum hohen Einschluss beeinflusst wird, was darauf hindeutet, dass die Formation des Podestes am Plasmarand vielleicht von den Störfeldern unterstützt wird, wenn diese in dieselbe Richtung wie der Plasmastrom angewendet werden. Die Plasmareaktion wurde für jedes der unterschiedlichen Störfelder gemessen und es wurde eine Abhängigkeit vom Plasmastrom gefunden, da dieser direkt die Position der rationalen Flächen beeinflusst was den Haupteffekt auf die Plasmareaktion ausmacht. Für die $+5$ kHz Fälle wurde ein Phasensprung verbunden mit einer Feldpenetration beobachtet, sobald das Plasma in den hohen Einschluss überging. Bei Herauffahren der Amplitude der magnetischen Störung wurde ein Saturieren in der Plasmareaktion gesehen, wobei ihre Höhe vom Plasmastrom abhängt, was erneut den Effekt der Position der rationalen Fläche hervorhebt.

Schlussfolgernd kann gesagt werden, dass die Veränderung im Verhalten der Edge Localized Modes eher durch eine Ãnderung der Stabilität des Plasmarandes als durch einen Effekt des Transports im Podest kommt. Es wurde gezeigt, dass das Spektrum der Störung und die Phase der verwendeten Felder besonders wichtig sind, da diese eine Abhängigkeit des L/H Leistungsgrenzwerts von der Phase zeigen. Für die Optimierung der ELM-Kontrolle müssen nicht nur die Spulenkonfiguration und das Störfeldspektrum berücksichtigt werden, sondern auch die relative Geschwindigkeit der angewendeten Störungen zum Elektronenfluid auf den rationalen Flächen, die resonant mit den resonanten magnetischen Störungen sind. Für zukünftige Studien soll klargestellt werden, dass Peeling Effekte vergröβert werden, wenn RMPs angewendet werden. Dies ist bedingt durch den Effekt der Nähe von rationalen Flächen zum Plasmarand, was Moden mit höheren toroidalen Modennummern erlaubt früher instabil zu werden als die eigentliche Mode, was zum beobachteten Anstieg der ELM Frequenz führt.

Bibliography

[1] H. A. Bethe. *Energy Production in Stars.* Phys. Rev. **55**, (1939), 434

[2] J. D. Lawson. *Some Criteria for a Power Producing Thermonuclear Reactor.* Proc. Phys. Soc. **B70**, (1957), 6

[3] I. E. Tamm and A. D. Sakharov. *Plasma Physics and the Problem of Controlled Thermonuclear Reactions.* Pergamon, Oxford (1961)

[4] L. Spitzer Jr. *The Stellarator Concept.* Phys. Fluids **1**, (1958), 253

[5] R. J. Bickerton, J. W. Connor and J. B. Taylor. *Diffusion Driven Plasma Currents and Bootstrap Tokamak.* Nature Physical Science **229**, (1971), 110

[6] C. E. Kessel. *Bootstrap Current in a Tokamak.* Nucl. Fusion **34**, (1994), 1221

[7] O. Sauter, C. Angioni and Y. R. Lin-Liu. *Neoclassical Conductivity and Bootstrap Current Formulas for General Axisymmetric Equilibria and Arbitrary Collisionality Regime.* Phys. Plasmas **6**, (1999), 2834

[8] C. S. Pitcher and P. C. Strangeby. *Experimental divertor Physics.* Plasma. Phys. Control. Fusion **39**, (1997), 779

[9] D. D. Ryutov. *Geometrical Properties of a "Snowflake" Divertor.* Phys. Plasmas **14**, (2007), 064502

[10] F. Wagner *et al.* *Regime of Improved Confinement and High Beta in Neutral-Beam-Heated Divertor Discharges of the ASDEX Tokamak.* Phys. Rev. Lett. **49**, (1982), 1408

[11] M. Keilhacker *et al.* *Confinement Studies in L and H Type ASDEX Discharges.* Plasma Phys. Control. Fusion **26**, (1984), 49

[12] A. Loarte *et al.* *Characteristics of Type-I ELM Energy and Particle Losses in Existing Devices and their Extrapolation to ITER.* Plasma Phys. Control. Fusion **45**, (2003), 1549

[13] P. T. Lang *et al.* *ELM Pace Making and Mitigation by Pellet Injection in ASDEX Upgrade.* Nucl. Fusion **44**, (2004), 665. 665

[14] A. W. Degeling *et al.* *Magnetic Triggering of ELMs in TCV.* Plasma Phys. Control. Fusion **45**, (2003), 1637

[15] T. C. Hender *et al.* *Effect of Resonant Magnetic Perturbations on COMPASS C Tokamak Discharges.* Nucl. Fusion **32**, (1992), 12

[16] T. N. Todd and the COMPASS Team. *MHD Control and ECCD in COMPASS-D.* Plasma Phys. Control. Fusion **35**, (1993), B231

[17] T. E. Evans *et al.* *Suppression of Large Edge-Localized Modes in High-Confinement DIII-D Plasmas with a Stochastic Magnetic Boundary.* Phys. Rev. Lett. **92**, (2004), 23

[18] V. Parail *et al.* *Effect of Ripple-Induced Ion Thermal Transport on H-mode Performance.* Proc. 32nd EPS conf. on Plasma Physics (Tarragona, Spain) **29C**, (2005), O

[19] P. T. Lang *et al.* *ELM Control Strategies and Tools: Status and Potential for ITER.* Nucl. Fusion **53**, (2013), 043004

[20] Y. Liang *et al.* *Magnetic Topology Changes Induced by Lower Hybrid Waves and their Profound Effect on Edge-Localized Modes in the EAST Tokamak.* Phys. Rev. Lett. **110**, (2013), 235002

[21] T. E. Evans *et al.* *RMP ELM Suppression in DIII-D Plasmas with ITER Similar Shapes and Collisionalities.* Nucl. Fusion **48**, (2008), 024002

[22] B. Hudson *et al.* *ELM Suppression be Resonant Magentic Perturbation in High-Perfomance Stationary Plasmas.* Nucl. Fusion **50**, (2010), 045006

[23] Y. M. Jeon *et al.* *Suppression of Edge-Localized Modes in High-Confinement KSTAR Plasmas by Non-Axisymmetric Magnetic Perturbations.* Phys. Rev. Lett. **109**, (2012), 035004

[24] W. Suttrop *et al.* *First Observation of Edge-Localized Mode Mitigation with Resonant and Non-Resonant Magnetic Perturbations in ASDEX Upgrade.* Phys. Rev. Lett. **106**, (2011), 225004

[25] S. J. Fielding *et al.* *ELM Control in COMPASS-D.* 28th EPS Conference on Contr. Fusion and Plasma Phys. (Funchal) **25A**, (2001), 1825

[26] M. Mori *et al.* *Plasma Improvement with Erogic Magnetic Fields in JFT-2M.* Proc. 14th Int. Conf. on Plasma Physics and Controlled Nuclear Fusion Research (Würzburg) **2**, (1992), 567

[27] J. M. Canik *et al.* *On Demand Triggering of Edge-Localized Instabilities Using External Non-Axisymmetric Magnetic Perturbations in Toroidal Plasmas.* Phys. Rev. Lett. **104**, (2010), 045001

[28] J. M. Canik *et al.* *ELM Destabilization by Externally Applied Non-axisymmetric Magnetic Perturbations in NSTX.* Nucl. Fusion **50**, (2010), 034012

[29] Y. Liang *et al. Active Control of Type-I Edge-Localized Modes with n = 1 Perturbation Fields in the JET Tokamak*. Phys. Rev. Letts. **98**, (2007), 065001

[30] Y. Liang *et al. Active Control of Type-I Edge-Localized Modes on JET*. Plasma Phys. Control. Fusion **49**, (2007), B581

[31] Y. Liang *et al. Active Control of Type-I Edge-Localized Modes with n = 1 and n = 2 Fields on JET*. Nucl. Fusion **50**, (2010), 025013

[32] S. Saarelma *et al. Density Pump-Out Compensation During Type-I Edge-Localized Mode Control Experiments with n = 1 Perturbation Fields on JET*. Plasma Phys. Control. Fusion **53**, (2011), 085009

[33] A. Kirk *et al. Resonant Magnetic Perturbation Experiments on MAST Using External and Internal Coils for ELM Control*. Nucl. Fusion **50**, (2010), 034008

[34] A. Kirk *et al. Magentic Perturbation Experiments on MAST L- and H-mode Plasmas Using Internal Coils*. Plasma Phys. Control. Fusion **53**, (2011), 065011

[35] A. Kirk *et al. Effect of Resonant Magnetic Perturbations with Toroidal Mode Numbers of 4 and 6 on Edge-Localized Modes in Single Null H-mode Plasmas in MAST*. Plasma Phys. Control. Fusion **55**, (2013), 015006

[36] A. Kirk *et al. Understanding Edge-Localized Mode Mitigation by Resonant Magnetic Perturbations on MAST*. Nucl. Fusion **53**, (2013), 043007

[37] Y. Liang *et al. Multiresonance Effect in Type-I Edge-Localized Mode Control With Low n Fields on JET*. Phys. Rev. Letts. **105**, (2010), 065001

[38] J. A. Snipes *et al. ELMs and Fast Edge Fluctuations in Alcator C-Mode*. Plasma Phys. Control. Fusion **40**, (1998), 765

[39] W. Suttrop *et al. Characteristics of Edge Localized Modes in ASDEX Upgrade*. Plasma Phys. Control. Fusion **38**, (1996), 1407

[40] R. J. Buttery *et al. Proc. 22nd EPS Conf. on Controlled Fusion and Plasma Physics (Bournrmouth)*. In *Vol 19C Page 273* (1995)

[41] P. Gohil *et al. Study of Giant Edge-Localized Modes in DIII-D and Comparison with Ballooning Theory*. Phys. Rev. Lett. **61**, (1988), 14

[42] M. Jiang *et al. Characteristics of Edge-Localized Modes in the Experimental Advanced Superconducting Tokamak (EAST)*. Plasma Phys. Control. Fusion **54**, (2012), 095003

[43] D. C. McDonald *et al. Chapter 3. ELMy H-Mode Operation in JET*. Fusion Science and Technology **53**, (2008), 891

[44] K. Hagashima, T. Shoji and Y. Miura. *Investigation of Edge-Localized Mode in the JFT-2M Tokamak.* Nucl. Fusion **36**, (1996), 335

[45] N. Oyama *et al. Fast Dynamics of Type-I ELMs and Transport of the ELM Pulse in JT-60U.* Nucl. Fusion **44**, (2004), 582

[46] N. Oyama *et al. Energy Loss for Grassy ELMs and Effects of Plasma Rotation on the ELM Characteristics in JT-60U.* Nucl. Fusion **45**, (2005), 871

[47] J. W. Kirk, A. abd Ahn, G. F. Counsell and the MAST team. *The Influence of the Divertor Magnetic Configuration and of ELM Frequency on Target Heat Fluxes in MAST.* Journal of Nuclear Materials **313**, (2003), 1081

[48] R. Maingi *et al. H-mode Pedestal, ELM and Power Threshold Studies in NSTX.* Nucl. Fusion **45**, (2005), 1066

[49] H. Reimerdes *et al. Proc. 24th EPS Conf. on Controlled Fusion and Plasma Physics (Berchtesgaden).* In *vol 21A pp 533* (1997)

[50] S. Soldatov *et al. Turbulence, Flows and Edge-Localized Mode (ELM) Dynamics in Limiter H-mode Plasmas in TEXTOR.* Plasma Phys. Control. Fusion **52**, (2010), 085001

[51] J. W. Connor. *A Review of Models for ELMs.* Plasma Phys. Control. Fusion **40**, (1998), 191

[52] W. Suttrop. *The Physics of Large and Small Edge-Localized Modes.* Plasma Phys. Control. Fusion **42**, (2000), A1

[53] H. Zohm. *Edge-Localized Modes (ELMs).* Plasma. Phys. Control. Fusion **38**, (1996), 105

[54] A. Kirk *et al. Spatial and Temporal Structure of Edge-Localized Modes.* Phys. Rev. Lett. **92**, (2004), 245002

[55] A. Kirk *et al. Structure of ELMs in MAST and the Implications for Energy Deposition.* Plasma Phys. Control. Fusion **47**, (2005), 315

[56] J. W. Connor *et al. Magneto-Hydrodynamic Stability of Tokamak Edge Plasmas.* Phys. Plasmas **5**, (1998), 2687

[57] E. A. Frieman *et al. Toroidal Effects on Magneto-Hydrodynamic Modes in Tokamaks.* Phys. Fluids **16**, (1973), 1108

[58] H. R. Wilson *et al. Ideal Magneto-Hydrodynamic Stability of the Tokamak High-Confinement-Mode Edge Region.* Phys. Plasmas **6**, (1999), 1925

[59] H. R. Wilson *et al. Magneto-Hydrodynamic Stability of the H-mode Transport Barrier as a Model for Edge-Localized Modes: An Overview.* Plasma Phys. Control. Fusion **48**, (2006), A71

[60] O. A. Hurricane, B. H. Fong and S. C. Cowley. *Non-Linear Magneto- Hydrodynamic Detonation: Part I.* Phys. Plasmas **4**, (1997), 3565

[61] H. R. Wilson and S. C. Cowley. *Theory for Explosive Ideal Magneto-Hydrodynamic Instabilities in Plasmas.* Phys. Rev. Lett. **92**, (2004), 175006

[62] J. A. Wesson. *Tokamaks.* Oxford University Press (1997)

[63] D. Lortz and J. Nührenberg. *Ballooning Stability Boundaries for the Large-Aspect-Ratio Tokamak.* Phys. Letts. **68A**, (1978), 49

[64] J. W. Connor, R. J. Hastie and J. B. Taylor. *High Mode Number Stability of an Axisymmetric Toroidal Plasma.* Proc. of the Royal Society of London. Series A, Mathematical and Physical Sciences **365**, (1979), 1720

[65] A. Kirk *et al. ELM Characteristics in MAST.* Plasma. Phys. Control. Fusion **46**, (2004), 551

[66] A. Schmid *et al. Experimental Observation of the Radial Propagation of ELM Induced Filaments on ASDEX Upgrade.* Plasma Phys. Control. Fusion **50**, (2008), 045007

[67] J. Pearson. *The Explosive Nature of Edge Localized Modes.* University of York (2010)

[68] J. Manickam. *The Role of Edge Current Density on Kink Mode Stability and its Implication for Magneto-Hydrodynamic Activity Associated with Edge-Localized Modes.* Phys. Fluids B **4**, (1992), 1901

[69] S. M. Kaye *et al. Characteristics of High Frequency ELM Precursors and Edge Stability in the PBX-M Tokamak.* Nucl. Fusion **30**, (1990), 2621

[70] D. M. Thomas *et al. Measurement of Pressure-Gradient-Driven Currents in Tokamak Edge Plasmas.* Phys. Rev. Lett. **93**, (2004), 065003

[71] N. Vianello *et al. Direct Observation of Current in Type-I Edge-Localized Mode Filaments on the ASDEX Upgrade Tokamak.* Phys. Rev. Lett. **106**, (2011), 125002

[72] M. W. Bongard *et al. Measurement of Peeling Mode Edge Current Profile Dynamics.* Phys. Rev. Lett. **107**, (2011), 035003

[73] M. G. Dunne *et al. Measurement of Neoclassically Predicted Edge Current Density at ASDEX Upgrade.* Nucl. Fusion **52**, (2012), 123014

[74] A. J. Webster and C. G. Gimblett. *Magneto-Hydrodynamic Stability of a Toroidal Plasma's Separatrix.* Phys. Rev. Lett. **102**, (2009), 035003

[75] A. J. Webster and C. G. Gimblett. *Magneto-Hydrodynamic Stability at a Separatrix. I. Toroidal Peeling Modes and the Energy Principle.* Phys. Plasmas **16**, (2009), 082502

[76] G. T. A. Huysmans. *External Kink (Peeling) Modes in X-point Geometry.* Plasma Phys. Control. Fusion **47**, (2005), 2107

[77] S. Saarelma *et al.* *X point Effect on Edge Stability.* Plasma Phys. Control. Fusion **53**, (2011), 025011

[78] C. C. Hegna *et al.* *Toroidal Coupling of Ideal Magneto-Hydrodynamic Instabilities in Tokamak Plasmas.* Phys. Plasmas **3**, (1996), 584

[79] S. Saarelma *et al.* *MHD Stability Analysis of ELMs in MAST.* Plasma Phys. Control. Fusion **48**, (2007), 31

[80] G. Saibene *et al.* *Improved Performance of ELMy H-modes at High Density by Plasma Shaping in JET.* Plasma Phys. Control. Fusion **44**, (2002), 1769

[81] R. L. Miller and R. W. Moore. *Shape Optimization of Tokamak Plasmas to Localized Magneto-Hydrodynamic Modes.* Phys. Rev. Lett. **43**, (1979), 11

[82] P. B. Snyder *et al.* *Characterization of Peeling-Ballooning Stability Limits on the Pedestal.* Plasma Phys. Control. Fusion **46**, (2004), A131

[83] Y. Liang *et al.* *Observations of Multi-Resonance Effect in ELM Control with Magnetic Perturbation Fields on the JET Tokamak.* Nucl. Fusion **51**, (2011), 073001

[84] H. Stoschus *et al.* *Impact of Rotating Resonant Magnetic Perturbation Fields on Plasma Edge Electron Density and Temperature.* Nucl. Fusion **52**, (2012), 083002

[85] V. Rozhansky *et al.* *Modification of the Edge Transport Barrier by Resonant Magnetic Perturbations.* Nucl. Fusion **50**, (2010), 034005

[86] O. Schmitz *et al.* *Resonant Features of Energy and Particle Transport During Application of Resonant Magnetic Perturbation Fields at TEXTOR and DIII-D.* Nucl. Fusion **52**, (2012), 043005

[87] Q. Yu, S. Günter and K. H. Finken. *Effect of Resonant Helical Magnetic Fields on Plasma Rotation.* Physics of Plasmas **16**, (2009), 042301

[88] T. Eich *et al.* *Type-I ELM Substructure on the Divertor Target Plates in ASDEX Upgrade.* Plasma Phys. Control. Fusion **47**, (2005), 815

[89] M. Jakubowski *et al. Overview of the Results on Divertor Heat Loads in RMP Controlled H-mode Plasmas on DIII-D.* Nucl. Fusion **49**, (2009), 095013

[90] D. M. Harting *et al. Strike Point Spitting in the Heat and Particle Flux Profiles Compared with the Edge Magnetic Topology in a n=2 Resonant Magnetic Perturbation Field at JET.* Nucl. Fusion **52**, (2012), 054009

[91] A. Kirk *et al. Observation of Lobes Near the X Point in Resonant Perturbation Experiments on MAST.* Phys. Rev. Lett. **108**, (2012), 255003

[92] I. T. Chapman *et al. Towards Understanding ELM Mitigation: the Effect of Axisymmetric Lobe Structures Near the X-point on ELM Stability.* Nucl. Fusion **52**, (2012), 123006

[93] T. E. Evans *et al. Homoclinic Tangles, Bifurcations and Edge Stochasticity in Diverted Tokamaks.* Contirib. Plasma Phys. **44**, (2004), 235

[94] T. E. Evans *et al. A Conceptual Model of the Magnetic Topology and Nonlinear Dynamics of ELMs.* Journal of Nuclear Materials **390**, (2009), 789

[95] A. Wingen *et al. Traces of Stable and Unstable Manifolds in Heat Flux Patterns.* Phys. Plasmas **14**, (2007), 042502

[96] A. Wingen, T. E. Evans and K. H. Spatschek. *Footprint Structures due to Resonant Magnetic Perturbations in DIII-D.* Phys. Plasmas **16**, (2009), 142504

[97] A. Wingen *et al. Numerical Modelling of Edge-Localized Mode Filaments on Divertor Plates Based on Thermoelectric Currents.* Phys. Rev. Lett. **104**, (2010), 175001

[98] M. Rack *et al. Thermoelectric Currents and Their Role During ELM Formation in JET.* Nucl. Fusion **52**, (2012), 074012

[99] B. V. Chirikov. *A Universal Instability of Many-Dimensional Oscillator Systems.* Phys. Rep. **52**, (1979), 263

[100] J. M. Rax and R. B. White. *Effective Diffusion and Nonlocal Heat Transport in a Stochastic Magnetic Field.* Phys. Rev. Lett. **68**, (1992), 1523

[101] P. B. Snyder *et al. Development and Validation of a Predictive Model for the Pedestal Height.* Phys. Plasmas **16**, (2009), 056118

[102] P. B. Snyder *et al. The EPED Pedestal Model and Edge-Localized Mode-Suppressed Regimes: Studies of Quiescent H-mode and Development of a Model for Edge-Localized Mode Suppression via Resonant Magnetic Perturbations.* Phys. Plasmas **19**, (2012), 056115

[103] H. R. Wilson *et al. Numerical Studies of Edge-Localized Instabilities in Tokamaks.* Phys. Plasmas **9**, (2002), 1277

[104] A. B. Mikhailovskii *et al.* *Optimization of Computational MHD Normal-Mode Analysis for Tokamaks.* Plasma Phys. Rep. **23**, (1997), 884

[105] Y. Q. Liu, A. Kirk and E. Nardon. *Full Toroidal Plasma Response to Externally Applied Non-Axisymmetric Magnetic Fields.* Phys. Plasmas **17**, (2010), 122502

[106] Y. Q. Liu *et al.* *Modelling of Plasma Response to Resonant Magnetic Perturbation Fields in MAST and ITER.* Nucl. Fusion **51**, (2011), 083002

[107] Y. Q. Liu *et al.* *Toroidal Modelling of Plasma Response and Resonant Magnetic Perturbation Field Penetration.* Plasma Phys. Control. Fusion **54**, (2012), 124013

[108] X. Q. Xu *et al.* *Non-Linear Simulations of Peeling-Ballooning Modes with Anomalous Electron Viscosity and their Role in Edge-Localized Mode Crashes.* Phys. Rev. Lett. **105**, (2010), 175005

[109] X. Q. Xu *et al.* *Non-Linear ELM Simulations Based on a Non-Ideal Peeling-Ballooning Model Using the BOUT++ Code.* Nucl. Fusion **51**, (2011), 103040

[110] B. D. Dudson *et al.* *Simulation of Edge-Localized Modes Using BOUT++.* Plasma Phys. Control. Fusion **53**, (2011), 054005

[111] G. T. A. Huysmans and O. Czarny. *MHD Stability in X-point Geometry: Simulation of ELMs.* Nucl. Fusion **47**, (2007), 659

[112] E. Nardon *et al.* *Magneto-Hydrodynamics Modelling of H-mode Plasma Response to External Resonant Magnetic Perturbations.* Phys. Plasmas **14**, (2007), 092501

[113] M. Bécoulet *et al.* *Numerical Study of the Resonant Magnetic Perturbations for Type-I Edge-Localized Modes Control in ITER.* Nucl. Fusion **48**, (2008), 024003

[114] E. Nardon *et al.* *Quasi-linear MHD Modelling of H-mode Plasma Response to Resonant Magnetic Perturbations.* Nucl. Fusion **50**, (2010), 034002

[115] O. G. Spies, D. Lortz and R. Kaiser. *Relaxed Plasma-Vacuum Systems.* Phys. Plasmas **8**, (2001), 3652

[116] J. B. Taylor. *Relaxation of Toroidal Plasma and Generation of Reverse Magnetic Fields.* Phys. Rev. Lett. **33**, (1974), 1139

[117] J. B. Taylor. *Relaxation and Magnetic Reconnection in Plasmas.* Rev. Mod. Phys. **58**, (1986), 741

[118] C. G. Gimblett and R. J. Hastie. *Calculation of the Post-Crash State and 1.5 D Simulation of Sawtooth Cycles.* Plasma Phys. Control. Fusion **36**, (1994), 1439

[119] R. J. Hastie. *The Taylor Relaxed State in Tokamaks and the Sawtooth Collapse.* Nucl. Fusion **29**, (1989), 96

[120] S. R. Hudson *et al.* *Calculation of Multi-region Relaxed Magnetohydrodynamic Equlibria.* Physics of Plasmas **19**, (2012), 112502

[121] C. G. Gimblett, R. J. Hastie and P. Helander. *Model for Current Driven Edge-Localized Modes.* Phys. Rev. Lett. **96**, (2006), 035006

[122] C. G. Gimblett, R. J. Hastie and P. Helander. *The Role of Edge Current Driven Modes in ELM Activity.* Plasma Phys. Control. Fusion **48**, (2006), 1531

[123] I. B. Bernstein *et al.* *An Energy Principle for Hydromagnetic Stability Problems.* Proceedings of the Royal Society of London. Series A, Mathematical and Physical Sciences **244**, (1958), 1236

[124] J. P. Friedberg. *Ideal Magneto-Hydrodynamic Theory of Magnetic Fusion Systems.* Rev. Mod. Phys. **54**, (1982), 801

[125] D. Lortz. *The General "Peeling" Instability.* Nucl. Fusion **15**, (1975), 49

[126] C. Mercier. *A Necessary Condition for Hydromagnetic Stability of Plasma with Axial Symmetry.* Nucl. Fusion **1**, (1960), 47

[127] H. Furth, P. Rutherford and H. Selberg. *Tearing Mode in the Cylindrical Tokamak.* Phys. Fluids **16**, (1973), 7

[128] O. Neubauer *et al.* *Design Features of the Tokamak TEXTOR.* Fusion Science and Technology **47**, (2005), 76

[129] A. J. H. Donné *et al.* *Overview of Core Diagnostics for TEXTOR.* Fusion Science and Technology **47**, (2005), 220

[130] S. Brezinsek *et al.* *Plasma Edge Diagnostics for TEXTOR.* Fusion Science and Technology **47**, (2005), 209

[131] M. Rack *et al.* *A Rotating Directional Probe for Fast Ion Losses and Plasma Rotation Measurements at TEXTOR.* Rev. Scientific Instruments **84**, (2013), 083501

[132] M. Mitri. *Control of a Fast Reciprocating Probe for the TEXTOR Fusion Experiment. (Master's Thesis).* University Duisberg-Essen (2005)

[133] A. Kirk *et al.* *Comparison of the spatial and temporal structure of type-i elms.* Journal of Physics: Conference Series **123**, (2008), 012011

[134] Y. Yang *et al.* *Experimental Observations of Plasma Edge Magnetic Field Response to Resonant Magnetic Perturbations on the TEXTOR Tokamak.* Nucl. Fusion **52**, (2012), 074014

[135] O. Neubauer *et al.* *The Dynamic Ergodic Divertor in TEXTOR - A Novel Tool for Studying Magnetic Perturbation Field Effects.* Fusion Engineering and Design **75-79**, (2005), 495

[136] K. H. Finken *et al.* *Influence of the Dynamic Ergodic Divertor on Transport Properties in TEXTOR.* Nucl. Fusion **47**, (2007), 522

[137] B. Unterberg *et al.* *The Influence of Resonant Magnetic Perturbations on Edge Transport in Limiter H-mode Plasmas in TEXTOR.* Journal of Nuclear Materials **390-391**, 1, (2009), 351

[138] B. Unterberg *et al.* *The Impact of $n = 2$ Resonant Magnetic Perturbations on Limiter H-mode Plasmas in TEXTOR.* 34th EPS Conference on Plasma Phys. Warsaw, 2-6 July 2007 ECA **31F**, (2007), P

[139] K. H. Finken *et al.* *Improved Confinement due to Open Ergodic Field Lines Imposed by the Dynamic Ergodic Divertor in TEXTOR.* Phys. Rev. Lett. **98**, (2007), 065001

[140] T. N. Carlstrom *et al.* *JET/DIII-D Size Scaling of the H-mode Power Threshold.* Plasma Phys. Control. Fusion **38**, (1996), 1231

[141] Y. Ma *et al.* *Scaling of H-mode Threshold Power and L-H Edge Conditions with Favourable Ion Grad-B Drift in Alcator C-Mode Tokamak.* Nuclear Fusion **52**, (2012), 023010

[142] Y. R. Martin, T. Takizuka and I. C. H. mode Threshold Database Working Group. *Power Requirement for Accessing the H-mode in ITER.* Journal of Physics: Conference Series **123**, (2008), 012033

[143] H. Koslowski *et al.* *Dependence of the Threshold for Perturbation Field Generated $m/n = 2/1$ Tearing Modes on the Plasma Fluid Rotation.* Nucl. Fusion **46**, (2006), L1

[144] Y. Sun *et al.* *Neoclassical Toroidal Plasma Viscosity Torque in Collisionless Regimes in Tokamaks.* Phys. Rev. Lett. **105**, (2010), 145002

[145] Y. Sun *et al.* *Modelling of the Neoclassical Toroidal Plasma Viscosity Torque in Tokamaks.* Nucl. Fusion **51**, (2011), 053015

[146] R. Fitzpatrick. *Interaction of Tearing Modes with External Structures in Cylindrical Geometry.* Nucl. Fusion **33**, (1993), 1049

[147] M. Keilhacker *et al.* *High Fusion Performance from Deuterium-Tritium Plasmas in JET.* Nucl. Fusion **39**, (1999), 209

[148] I. Barlow *et al.* *The Error Field Correction Coils on the JET Machine.* Fusion Engineering and Design **58**, (2001), 189

[149] Y. Liang *et al. Mitigation of Type-I ELMs with n=2 Fields on JET with ITER-like Wall.* Nucl. Fusion **53**, (2013), 073036

[150] A. H. Boozer. *Physics of Magnetically Confined Plasmas.* Rev. Mod. Phys. **76**, (2004), 1071

[151] V. D. Pustovitov. *Error Field Amplification near the Stability Boundary of the Modes Interacting with a Conducting Wall.* Plasma Phys. Rep. **30**, (2003), 187

[152] M. P. Gryaznevich *et al. Experimental Studies of Stability and Beta Limit in JET.* Plasma Phys. Control. Fusion **50**, (2008), 124030

[153] M. P. Gryaznevich *et al. Determination of Plasma Stability Using Resonant Field Amplification in JET.* Nucl. Fusion **52**, (2012), 083018

[154] Y. Liu. *Modelling Resonant Field Amplification due to Low-n Peeling Modes in JET.* Plasma Phys. Control. Fusion **52**, (2010), 045011

[155] J. Pearson *et al. Modelling of Edge-Localized Modes with a Current Relaxation Model on JET and TEXTOR.* Nucl. Fusion **52**, (2012), 074011

Diagram courtesy of JET-EFDA- Enquiries about Copyright and reproduction should be addressed to the Publications Office, EFDA, Culham Science Centre, Abingdon, Oxon, OX14 3DB, UK.

Related Publications

First Author / Corresponding Author

1. P. Devoy, J. Pearson*, P.K. Browning, C.G. Gimblett and Y. Liang. *Bifurcation of Edge Localized Modes due to Current Distribution at the Plasma Edge.* Submitted to Plasma Physics and Controlled Fusion.

2. J. Pearson, Y. Liang, C.G. Gimblett, D. Reiser, Y. Sun, T. Zhang and Y. Yang. *Modelling of edge localized modes with a current relaxation model on JET and TEXTOR.* Nucl. Fusion **52** (2012) 074011.

Other Related Publications

3. M. Rack, Y. Liang, H. Jaegers, J. Aβmann, G. Satheeswaran, Y. Xu, J. Pearson, Y. Yang, P. Denner, L. Zeng and the TEXTOR team. *A Rotating Directional Probe for Fast Ion Losses and Plasma Rotation Measurements at TEXTOR.* Rev. Sci. Instrum. **84** (2013) 083501

4. L. Zeng, H.R. Koslowski, Y. Liang, A. Lvovskiy, M. Lehnen, D. Nicolai, J. Pearson, M. Rack, P. Denner, H. K. Finken, K. Wongrach and the TEXTOR team. *Experimental Observations of Hot Tail Runaway Electron Generation in TEXTOR Disruptions.* Phys. Rev. Lett. **110** (2013) 235003

5. Y. Liang, P. Lomas, I. Nunes, M. Gryaznevich, M.N.A. Beurskens, S. Brezinsek, J.W. Coenen, P. Denner, Th. Eich, L. Frassinetti, S. Gerasimov, D. Harting, S. Jachmich, A. Meigs, J. Pearson, M. Rack, S. Saarelma, B. Sieglin, Y. Yang, L. Zeng and JET-EFDA contributors. *Mitigation of type-I ELMs with* $n = 2$ *fields on JET with ITER-like wall.* Nucl. Fusion **53** (2013) 073036

6. M. Rack, B. Sieglin, T. Eich, J. Pearson, Y. Liang and JET-EFDA contributors. *Observations of ELM-Precursors in the Divertor Heat Load Patterns at JET.* Submitted to Physical Review Letters.

7. Y. Liang, X.Z. Gong, K.F. Gan, E. Gauthier, L. Wang, M. Rack, Y.M. Wang, L. Zeng, P. Denner, A. Wingen, B. Lv, B.J. Ding, R. Chen, L.Q. Hu, J.S. Hu, F.K. Liu, Y.X. Jie, J. Pearson, J.P. Qian, J.F. Shan, B. Shen, T.H. Shi, Y. Sun, F.D. Wang, H.Q. Wang, M. Wang, Z.W. Wu, S.B. Zhang, T. Zhang, X.J. Zhang, N. Yan, G.S. Xu, H.Y. Guo, B.N. Wan, J.G. Li, and the EAST team. *Magnetic Topology Changes Induced by Lower Hybrid Waves and their Profound Effect on Edge-Localized Modes in the EAST Tokamak.* Phys. Rev. Lett. **110** (2013) 235002.

8. L. Zeng, H. R. Koslowski, Y. Liang, A. Lvovskiy, M. Lehnen, D. Nicolai, J. Pearson, M. Rack, H. Jaegers, K. H. Finken, K. Wongrach, Y. Xu and the TEXTOR team. *Experimental Observation of Magnetic-Turbulence Threshold for Runaway-Electron Generation in the TEXTOR Tokamak.* Phys. Rev. Lett. 110 (2013) 235003.

9. Y. Yang, Y. Liang, Y. Sun, T. Zhang, J. Pearson, Y. Xu and TEXTOR Team. *Experimental observations of plasma edge magnetic field response to resonant magnetic perturbation on the TEXTOR Tokamak.* Nucl. Fusion **52** (2012) 074014.

10. T. Zhang, Y. Liang, Y. Sun, A. Kr amer-Flecken, S. Soldatov, E. Nardon, P. Tamain, F.L. Waelbroeck, Y. Yang, J. Pearson, H.R. Koslowski and the TEXTOR team. *Influence of Rotating Resonant Magnetic Perturbation on the Plasma Radial Electric Field on TEXTOR.* Nucl. Fusion **52** (2012) 074013.

11. Y. Liang, C.G. Gimblett, P.K. Browning, P. Devoy, A. Alfier, G. Calabró, C. Giroud, D. Harting, H.R. Koslowski, S. Jachmich, J. Pearson, Y. Sun, C. Wiegmann, T. Zhang and JET-EFDA contributors. *Observations of Multi-Resonance Effect in ELM Control with Magnetic Perturbation Fields on the JET Tokamak.* Nucl. Fusion **51** (2011) 073001.

Acknowledgments

Foremost, I would like to thank my supervisor Dr. Yunfeng Liang for granting me the opportunity to conduct my Ph.D. research as part of the Helmholtz Universität young investigators group VH-NG-410 and for the continuing support and guidance. I am also grateful for the large amount of opportunities and knowledge I have received from Dr. Liang which will be essential for my future career.

Numerous telephone and E-mail disscusions with Dr. Chris Gimblett have been invaluable to my understanding and success and I would like to offer my sincere gratitude to him. The opportunity to work on the resonant field amplification experiments and understanding of this field are due to Dr. Mikhail Grayaznevich. Thanks to Dr. Dirk Reiser and Dr. Rudi Koslowski for interesting conversations on both physics and life in general.

I would also like to thank Prof. Dr. Samm, Prof. Dr. Reiter, and my colleagues at IEK-4 for their guidance and advice. From the side of the Mathematisch-Naturwissenschaftlichen Fakultät der Heinrich-Heine-Universität Düsseldorf I would like to express my gratitude to Prof. Dr. Spatschek and Prof. Dr. Willi for their support and input from the academic side.

The other members of the young investigators group have my utmost thanks for their support over the past three years: Dr. Peter Denner, Dr. Youwen Sun, Dr. Yao Yang, Dr. Long Zeng, Dr. Tao Zhang and especially Michael Rack for his help with the graphical software and enjoyable disscusions. I have immensely enjoyed working with these colleagues.

The TEXTOR team need a large amount of recognition as without them the results would have been impossible to obtain. Special thanks go to Herr Nicolai and Herr Sauer for operating the tokamak, to Dr. Kantor for retrieving and calibrating the Thomson scattering data, and to Dr. Oliver Schmitz for the DIVA equilibrium.

Finally, I would like to thank the Jülich Wednesday group for keeping me sane, and last but by no means least, my family for their everlasting support and patience.

> “And I gave my heart to seek and search out by wisdom concerning all things that are done under heaven: this sore travail hath God given to the sons of man to be exercised therewith” - Ecclesiastes 1:13-17.

This work, supported by by the Helmholtz Association in the frame of the Helmholtz-University Young Investigators Group VH-NG-410, Graduiertenkolleg 1203. This work was also supported by the European Communities under the contract of Association between EURATOM and FZJ, was carried out within the framework of the European Fusion Development Agreement. The views and opinions expressed herein do not necessarily reflect those of the European Commission.

Erklärung

Die hier vorgelegte Dissertation habe ich eigenständig und ohne unerlaubte Hilfe angefertigt. Die Dissertation wurde in der vorgelegten oder einer ähnlichen Form noch bei keiner anderen Institution eingereicht. Ich habe bisher keine erfolglosen Promotionsversuche unternommen.

Düsseldorf, den 28.08.2013